AQUIFER STORAGE AND RECOVERY IN SALINE AQUIFERS

A Dissertation
Presented to
The Academic Faculty

by

Yiming Chen

In Partial Fulfillment
of the Requirements for the Degree
Doctor of Philosophy in the
School of Civil and Environmental Engineering

Georgia Institute of Technology
August 2014

AQUIFER STORAGE AND RECOVERY IN SALINE AQUIFERS

Approved by:

Dr. Jian Luo, Advisor
School of Civil and Environmental Engineering
Georgia Institute of Technology

Dr. Aris Georgakakos
School of Civil and Environmental Engineering
Georgia Institute of Technology

Dr. Jingfeng Wang
School of Civil and Environmental Engineering
Georgia Institute of Technology

Dr. Huaming Yao
School of Civil and Environmental Engineering
Georgia Institute of Technology

Dr. Yi Deng
School of Earth and Atmospheric Sciences
Georgia Institute of Technology

Date Approved: May 17, 2014

ACKNOWLEDGEMENTS

My life in pursuit of Ph.D. at Georgia Tech impressed, inspired and encouraged me in past five years. This kind of life is filled with five flavors- sourness, sweetness, bitterness, spiciness and saltiness, distinguishing from while interacting with each other. At this moment, I would like to thank all great people guiding, supporting and helping me. Because of you, I successfully came to the end of this life, and look forward to a new journey with full of confidence.

Firstly, I would like to thank my advisor Dr. Jian Luo with my sincere respect, for mentoring me with his comprehensive knowledge, strictly scientific attitude, and limitless enthusiasm to research. His kindness, diligence, patience, courage, wisdom is always an example in my life. I would never have finished this thesis without his encouragement, support, and guidance. There is never an over appreciation to my best advisor, Dr. Jian Luo. My sincere thanks also go to my committee, Dr. Aris Georgakakos, Dr. Jingfeng Wang, Dr. Huaming Yao, and Dr. Yi Deng. Each of them brought me many impressive ideas from distinct scientific fields. Their erudition and insights are always precious to me. Besides, I would also like to thank all my colleagues in our research groups — Chunhui Lu, Rulan Gong, and so on. That is my great honor to work with them, to share joyfulness and difficulties with them. Moreover, I also sincerely thank all my friends and others who offered me much help previously.

Finally, I would like to give my most significant appreciation and best love to my parents, Feng Wang and Peigang Chen, who gave birth to me and brought me up. Without their

care, love, trust, support, guidance, comprehension and encouragement, I would have never been myself today. Any words cannot definitely express my appreciation to them. I love them forever!

TABLE OF CONTENTS

LIST OF TABLES

LIST OF FIGURES

SUMMARY

Aquifer storage and recovery (ASR) is a particular scheme of artificial recharge of groundwater by injecting fresh water into aquifers and subsequently recovering the stored water during times of peak demand or extended drought. In the era of combating climate change, ASR, as an effective means for water reuse and sustainable management of water resources in concert with the natural environment, represents a huge opportunity for climate change adaptation to mitigate water availability stress. The success of an ASR scheme is quantified by the recovery efficiency (RE), defined as the volume of stored water that can be recovered for supply purposes divided by the total volume injected. It is not uncommon that RE may be significantly lower than 100% because of the water quality changes as a consequence of the mixing between the injected water and native groundwater and the interaction between injected water and soil. Thus, the key of a successful ASR scheme is (1) to select appropriate aquifers and (2) to design optimal operational processes to build up a bubble of injected water with minimized negative impact from such mixing and interaction.

To achieve this, this thesis develops an integrated knowledge base with sound interdisciplinary science and understanding of the mixing processes under operational ASR management in aquifers with various hydrogeological conditions. Analytical and numerical modeling are conducted to improve the scientific understanding of mixing processes involved in ASR schemes and to provide specific technical guidance for improving ASR efficiency under complex hydrogeological conditions. (1) An efficient

approach is developed to analytically evaluate solute transport in a horizontal radial flow field with a multistep pumping and examine the ASR performance in homogeneous, isotropic aquifer with advective and dispersive transport processes. (2) Numerical and analytical studies are conducted to investigate the efficiency of an ASR system in dual-domain aquifers with mass transfer limitations under various hydrogeological and operational conditions. Simple and effective relationships between transport parameters and ASR operational parameters are derived to quantify the effectiveness and ascertain the potential of ASR systems with mass transfer limitations. (3) Effects of hydrogeological and operational parameters on ASR efficiency are assessed in homogeneous/stratified, isotropic/anisotropic coastal aquifers. Effects of transverse dispersion are particularly investigated in such aquifers. (4) Finally, we test and study an innovative ASR scheme for improving the RE in brackish aquifers: injection through a fully-penetrated well and recovery through a partially-penetrated well.

CHAPTER 1

INTRODUCTION

Groundwater is a vital resource providing water supplies for public potable water, agriculture and industry. This usage is concentrated around fast growing and densely populated areas, of which are coastal areas where 70% of the world's population dwell. In the face of growing water scarcity and stress from climate change, there is an imperative need to developing strategies and techniques for sustainable groundwater management in coastal regions.

Aquifer storage and recovery (ASR) is a particular scheme of artificial recharge of groundwater by injecting fresh water into aquifers and subsequently recovering the stored water during times of peak demand or extended drought (***Figure 1.1***). In the era of combating climate change, ASR, as an effective means for water reuse and sustainable management of water resources in concert with the natural environment, represents a huge opportunity for climate change adaptation to mitigate water availability stress (Pyne, 1995; Yang et al., 2010). ASR can also be operated for other utilization such as maintaining the groundwater levels, storing the thermal differences to controlling the seasonal heat transfers, extracting recharged water for agriculture, preventing seawater intrusion in coastal aquifers, and so on.

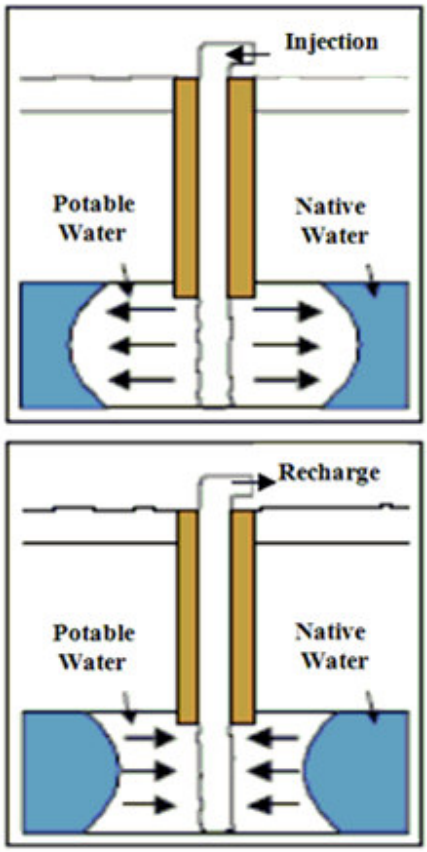

Figure 1.1 Schematic plot of an ASR scheme with a fully-penetrating well in a confined aquifer (CH2MHILL, Inc).

The success of an ASR scheme is quantified by the recovery efficiency (RE), defined as the volume of stored water that can be recovered for supply purposes divided by the total volume injected (Kimbler et al., 1975). It is not uncommon that RE may be significantly lower than 100% because of the water quality change as a consequence of the mixing between the injected water and native groundwater and the interaction between injected water and soil, such as dispersion, mass transfer and density effects (e.g., Eastwood and

Stanfield, 2001; Lowry and Anderson, 2006; Culkin et al., 2008; Lu et al., 2009; Lu and Luo, 2010). For example, the first full scale ASR trial in the UK failed because of the RE less than 15% after a 2 year programme of injection and recovery cycles (Eastwood and Stanfield, 2001). Thus, the key for an ASR scheme to successfully serve as a viable option of long-term water storage is to improve the RE by appropriately selecting storage aquifers and designing optimal operational processes.

1.1 Research Objectives

Designing a successful ASR scheme requires an integrated knowledge base of sound interdisciplinary science and understanding of the subsurface mixing processes under various ASR operational processes in aquifers with various hydrogeological conditions. Such a knowledge base is currently unavailable (Pyne, 2005). Development of such an integrated knowledge base with associated operational guidance for successful ASR schemes is the main theme of this thesis research.

Two primary, fundamental questions will be addressed:

(1) How to select the aquifer appropriate for ASR?

(2) Given a selected site, how to design ASR operations?

To answer the first question, we will conduct a comprehensive analysis of ASR performance in freshwater and saline aquifers by investigating the effects of hydrogeological conditions on ASR performance. Such hydrogeological conditions include aquifer thickness, hydraulic conductivity, stratification, anisotropy and mixing processes (dispersion, rate-limited mass transfer and density-driven convection). To

answer the second question, we will examine the effects of ASR operational parameters, including pumping rates and durations, on ASR performance. In particular, we will investigate a technique using partially-penetrating wells for improving the RE of ASR schemes in coastal aquifers

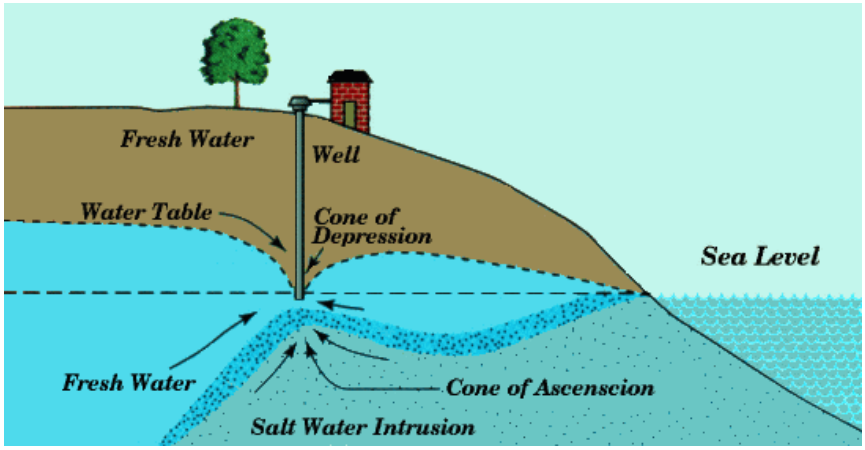

Figure 1.2 Pumping from a partially-penetrating well (Source: http://www.lenntech.com/groundwater/seawater-intrusions.htm).

The research topic of partially-penetrating wells is motivated by the most important feature in coastal aquifers: seawater is heavier than freshwater, and partially-penetrating wells are common practice. Compared with the traditional fully-penetrating wells, the use of partially-penetrating well appreciates the tilted freshwater-seawater interface with underlying heavier seawater. For example, for fully-penetrating wells, pumping or recovery during an ASR has to be terminated as soon as the interface toe reaches the well, while the toe can be further pulled up to the partially-penetrating well for pumping or

recovery termination (***Figure 1.2***), resulting in later breakthrough of salt water into the pumping well, more recoverable water extracted from the shallow layers, and a higher RE for an ASR.

1.2 Research Questions and Impacts

This research will establish an integrated knowledge base with associated technical guidance for successful applications of ASR in coastal aquifers. More importantly, this research will investigate the performance of both fully and partially penetrating wells in complex hydrogelogical conditions that have not been examined in previous research. The following specific scientific questions will be answered:

- How do hydrogeological conditions (e.g., aquifer thickness and hydraulic conductivity), mixing processes (dispersion, mass transfer and density-driven convection) and ASR operational processes (e.g., well pumping rates and durations) affect the design of ASR schemes?
- What are the effects of aquifer stratification and anisotropy on the RE of ASR in coastal aquifers?
- How does the transverse dispersivity affect ASR performance in stratified coastal aquifers?
- How significant will the RE of be improved by partially-penetrating wells compared with fully-penetrating wells?

Results will include new knowledge, numerical tools and critical insights into the hydraulics of both fully-penetrating and partially-penetrating wells and associated transport processes in coastal aquifers with different heterogeneities and anisotropies, as

well as specific technical recommendations and guidance for improving groundwater management in coastal aquifers.

1.3 Dissertation Organization

The dissertation is organized as follows.

Chapter 2 reviews previous studies on the ASR performance, fully-penetrating wells in coastal aquifers, partially-penetrating wells and modeling techniques.

Chapter 3 develops an efficient approach to analytically evaluate solute transport in a horizontal radial flow field with a multistep pumping and examine the ASR performance in homogeneous, isotropic aquifer with advective and dispersive transport processes (published in *Water Resour. Res.*, 48, W02510, doi:10.1029/2011WR010692).

Chapter 4 investigates ASR efficiency under various mass transfer limitations (published in *Water Resour. Res.*, 47, W08529, doi:10.1029/2011WR010605).

Chapter 5 discusses the effects of hydrogeological and operational parameters on ASR efficiency in homogeneous, isotropic coastal aquifers.

Chapter 6 investigates ASR performance in stratified, anisotropic coastal aquifers and the influence of transverse dispersivity.

Chapter 7 evaluates the effectiveness of partially-penetrating wells for ASR in coastal aquifers, and discusses the RE improvement by partially-penetrating wells in comparison with fully-penetrating wells.

Chapter 8 summarizes the dissertation and suggests the future work.

CHAPTER 2

LITERATURE REVIEW

This chapter summarizes the literature relevant to the proposed research. It begins with a summary of previous studies on applications of ASR schemes; then followed by a review of the utilization of conventional fully-penetrating wells in coastal aquifers with the focus on pumping optimization for preventing seawater intrusion and applications of partially-penetrating wells; finally, modeling techniques for investigating ASR and pumping in coastal aquifers are reviewed.

2.1 Seawater Intrusion in Coastal Aquifers

Coastal aquifers are distinguished from inland aquifers in terms of complex hydrogeological and variable-density transport characteristics.

Excessive groundwater withdrawals have upset the long established balance between freshwater and seawater potentials, causing encroachment of salty seawater into the freshwater aquifer, resulting in the well-known seawater intrusion problem (***Figure 2.1***, Bear, et al., 1999). In the United States, aquifer overdrafts are more than 25% higher than replacement rates on average (USWRC, 1979; Hutson et al., 2004). Once seawater has intruded into the coastal aquifer to an intolerable distance, the deterioration of the groundwater quality significantly threatens the sustainability of coastal communities and further development of coastal regions. For example, water that is high in salt content is detrimental to most plants. A relatively small quantity of seawater (about 1%) is sufficient to render freshwater non-compliant with secondary drinking-water standards

(250 mg/L for chloride). As seawater intrusion progresses, those wells pumping close to the coast become saline and have to be abandoned. Also, the area above the intruding seawater wedge is lost as a source of natural recharge to the aquifer.

Prevention is considered the most cost-effective approach from the perspective of implementing an integrative groundwater management strategy because restoration of groundwater quality in the invaded zones and contaminated near shore environments is generally an expensive and ineffective proposition.

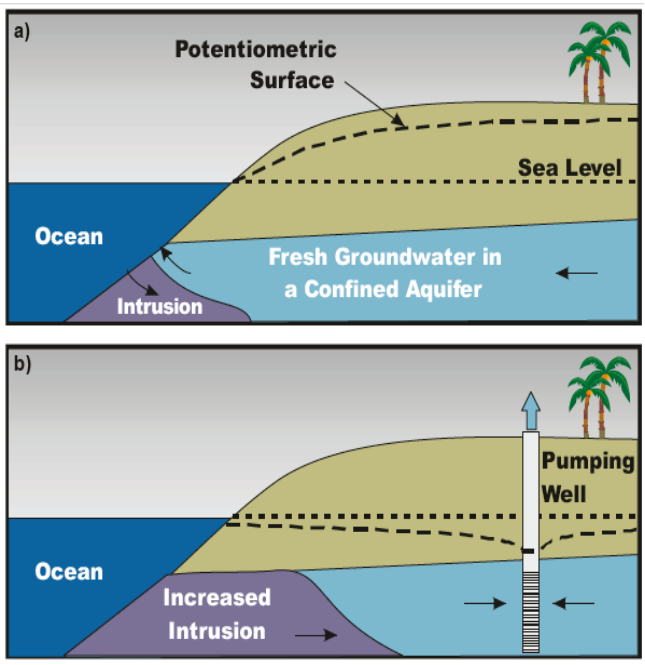

Figure 2.1 Seawater intrusion induced by groundwater withdrawal. a) Natural aquifer condition; b) Seawater intrusion caused by groundwater withdrawal (Johnson, 2007).

2.2 Aquifer Storage and Recovery Performance and Mixing Processes

Aquifer storage recovery (ASR) is a proven cost-effective powerful technology for environmental protection and water resources optimization, whose cycle comprises three steps related to water injection, storage and recovery. ASR can prevent declining groundwater levels, ground subsidence and decreasing seawater intrusion in the coastal and offshore area, and can alleviate water contaminant in the subsurface and increase water supply and desalinization of groundwater and keep the balance upon aquatic and terrestrial ecosystems (e.g., Pyne, 1995; Mirecki et al., 1998; Eastwood and Stanfield, 2001; Gaus et al., 2002; Pyne and Howard, 2004; Almulla et al., 2005; Lowry and Anderson, 2006; Maliva et al., 2006; Brown and Misut, 2010; Izbicki et al., 2010; Missimer et al., 2012). Moreover, ASR can be a very useful hydrogeological method to identify the occurrence of fracture flow in aquifers where there is a measurable concentration difference between the injected water and ambient groundwater (Miotlinski, et al., 2011).

An ASR scheme displaces the native groundwater and develops an interface or mixing zone between the injected and native water, which delineates the subsurface flow domain into regions with distinctive fluid physical and chemical properties. To evaluate the operation of ASR system, the concept of RE is outlined and defined as the ratio of the volume of recovered freshwater to the volume of injected freshwater (Kimbler et al., 1975). The recovery efficiency (RE) is widely recognized in the assessment of an ASR system (e.g., Mirecki et al., 1998; Konikow et al., 2001; Pavelic et al., 2006(a), 2006(b); Ward et al., 2007, 2008, 2009; Bakker, 2010; Lu et al., 2011). It is hardly to reach the completely recovered status (i.e. RE=100%) owing to the complex subsurface

mechanisms. The RE of an ASR system can be greatly affected by many parameters. Peters (1983), Pavelic et al. (2002), Ward et al. (2007) and Lu et al. (2011) provided key factors governing the RE, which includes the hydrogeological variables such as hydraulic conductivity, porosity, aquifer thickness, aquifer dispersivity, molecular diffusion, the rate-limited mass transfer, the density difference and background hydraulic gradient, and operational variables such as mixed convection ratio, the ratio of extraction and injection pumping rates, injected volume, the storage duration and the total duration for one ASR cycle.

Rate-Limited Mass Transfer

In geologic formations exhibiting dual-porosity behavior, e.g., mobile and relatively immobile domains such as media consisting of fractures and matrices (e.g., Fleming and Haggerty 2001; Haggerty et al. 2001), preferential flow paths and low permeability zones (e.g., Coats and Smith, 1964; van Genuchten and Wierenga 1976; Rao et al. 1980), native water in the immobile domain serves as a contaminant source for the injected water through rate-limited mass transfer between domains. Our recent research indicated that a much wider mixing (or buffer) zone will be created in dual-porosity aquifers and significantly influence the RE of an ASR scheme because mass transfer influences the water quality for the entire injected water body whenever there is a concentration gradient, not just at the interfaces (Lu et al., 2011). In addition, dissolution and desorption of chemical constituents from matrices and rocks caused by the water displacement behaves similarly as rate-limited mass transfer (Jones, 1983; Jones et al., 1998, 1999). Culkin et al. (2008) observed significant salinity rebounds during the storage phase in ASR field experiments in Charleston, South Carolina, USA, which was characterized by

the dual-domain mass transfer conceptualization. British Geological Survey (BGS, 2002) reported that dual-porosity mixing processes are dominant in the Chalk aquifer in the UK (Jones et al., 1998, 1999). The failure of the first full scale ASR trial in the UK was mainly attributed to the dual-porosity mechanism and associated geochemical reactions (CH2MHILL, 1999, 2000; Eastwood et al., 1998; Gaus et al., 2001; Eastwood and Stanfield, 2001).

Although the prevalent existence of mass transfer or dual-porosity behavior has been recognized in natural aquifers (e.g., Coats and Smith, 1964; van Genuchten and Wierenga, 1976; Chen, 1985, 1986; Goltz and Oxley, 1991; Moench, 1995), the effectiveness and efficiency of ASR subject to mass transfer limitations remain unknown. Particularly, there is no knowledge base to determine the likelihood of ASR being successful with mass transfer limitations and no technical guidance to optimize ASR operations to overcome the negative impact from mass transfer processes.

Density-Gradient Driven Mixing

In brackish aquifers, the density gradient between the injected and native water tends to tilt the freshwater-saltwater interface during the storage phase, resulting in a conical rather than a cylindrical water bubble. Because of the fast movement of the interface toe during the recovery phase, the titling interface significantly reduces the volume of recoverable water, resulting in a low RE (shown in ***Figure 2.2***). Previous studies of ASR in brackish aquifers mostly focused on evaluating the RE and investigating the effects of density gradients and other hydrogeological conditions (Ward et al., 2007). Few have proposed specific ASR schemes to improve the ASR performance in brackish aquifers.

Esmail and Kimbler (1967), Moulder (1970), Kumar and Kimbler (1970), Grove and Konikow (1976), Merritt (1985, 1986), Pavelic et al. (2006, b) and Ward et al. (2007, 2008) described the feasibility of developing the multi-cycle ASR system to improve the RE. The previous successful discussion about the RE of ASR systems has represented exhaustive and comprehensive views, which include not only numerical simulations but also actual field experiments (e.g., Mirecki et al., 1998; Konikow et al., 2001; Pavelic et al., 2006(a); Ward et al., 2007, 2008; Goyal et al., 2008; Culkin et al., 2008; Bakker, 2010; Lu et al., 2011; Miotlinski et al., 2011). Nonetheless, the detailed and convenient operation method for ASR systems concentrating on the extraction phase has not been set up.

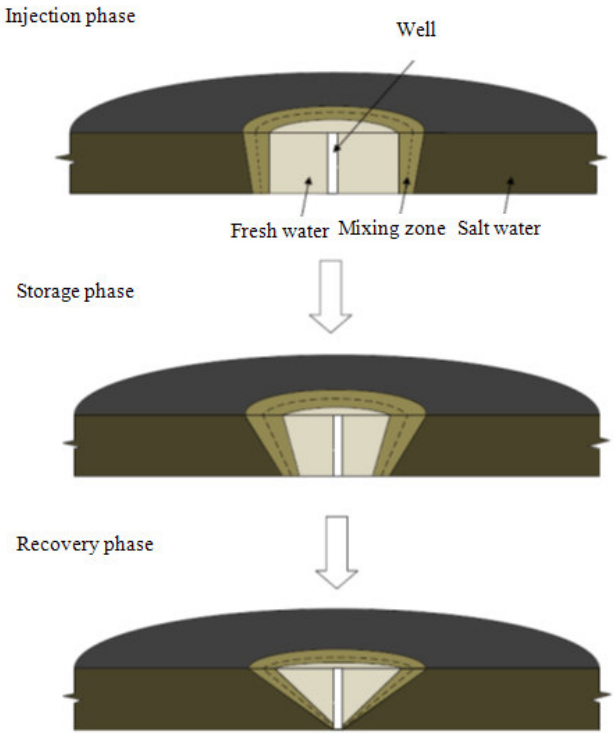

Figure 2.2 Schematic tilting interface of an ASR scheme in brackish aquifers. (modified from Ward et al., 2007)

Furthermore, the issues of realistic heterogeneous and anisotropic aquifers were discussed to investigate the ASR system (e.g., Diersch and Kolditz, 2002; Maliva et al., 2006; Ward et al., 2008). Hydrogeophysical methods and multiscale tracer testing were applied to analyze the ASR system in different types of heterogeneous aquifers (e.g., Pavelic et al., 2006; Minsley et al., 2011). But they did not address the RE. Diersch and Kolditz (2002) reviewed the state in modeling of variable-density flow and transport in porous media, and showed examples of field applications to demonstrate the importance of considering heterogeneities and large scales. It has been shown that aquifer heterogeneity can greatly affect ASR system performance by reducing the recoverable volume of low-salinity water (Pavelic et al., 2006 and Maliva et al., 2006). Maliva et al. (2006) presented the modeling results and field investigations to emphasize the pressing need for more sophisticated data collection and solute-transport modeling to predict how stored water migrates in heterogeneous aquifers. Ward et al. (2008) discussed the change of RE in different types of stratified heterogeneous aquifers. They concluded that the RE of a simulated ASR operation is sensitive to density gradients and anisotropic ratio, but relatively insensitive to the hydraulic conductivity distribution in stratified aquifers. They found that the RE in a stratified heterogeneous medium can be approximated well by the RE in an equivalent homogeneous (anisotropic) medium. However, their finding was based on only one type of layer placement and it is not clear that how the RE varies in different types of aquifer layer placement with different hydraulic conductivity ratios of horizontal structured layers. Moreover, it is doubtful whether the stratified aquifers can be simplistically replaced by the equivalent homogenized aquifers under complex hydrogeological circumstances in the evaluation of ASR performance.

Thus, our study will aim to explore the main effects of various anisotropy ratios and hydraulic conductivity contrasts on ASR systems in stratified aquifers, and discuss the RE variation in the stratified aquifers. In particular, we will examine the homogenization feasibility of stratified aquifers.

2.3 Well Pumping Optimization in Coastal Aquifers

Seawater intrusion is the most noteworthy issue in coastal aquifers. The impact of density differences between seawater and freshwater promotes the movement of saline water into groundwater aquifers, which is especially intensified by activities of pumping groundwater from coastal wells. Once salt water has intruded into coastal aquifer to an intolerable distance, the deterioration of the groundwater quality significantly threatens the sustainability of coastal communities and further development of coastal areas. Restoration of groundwater quality in the invaded zones is generally an expensive and ineffective proposition (Bear et al. 1999). It is generally admitted that the effective prevention is the optimal groundwater management strategy in coastal areas. Many researchers focus on setting up hydraulic barriers to avoid seawater intrusion (e.g., Todd, 1980; Abarca et al., 2006; Bray and Yeh, 2008; Pool and Carrera, 2010). Also many subsurface barriers can be installed to retain the groundwater while inhibiting seawater intrusion (e.g., Sugio et al., 1987; Dror et al., 2004; Luyun et al., 2011). The other cost-effective prevention strategy is to optimize withdrawal rates, that is, the management of groundwater extraction in coastal aquifers to maximize the water supply while avoiding seawater intrusion (Lu et al., 2012). To achieve the goal of maximizing freshwater pumping rates in coastal aquifers, the sharp-interface seawater intrusion approximation model combining with the potential flow theory is usually applied for simplicity,

especially when deriving analytical solutions (e.g., Bear and Dagan, 1964; Ozturk, 1970; Dagan and Zeitoun, 1998; Naji et al., 1998; Bakker, 2000, 2006; Kacimov and Obnosov, 2001; Kacimov and Sherif, 2006; Pool and Carrera, 2011). As one of the representatives, Strack (1976) presented a single potential analytical formulation for solving three-dimensional interface problems in confined or unconfined coastal aquifers, whose results analytically and graphically revealed the location of stagnation point and the critical maximum pumping rate for the fully-penetrating well in coastal aquifers. On the basis of the single-potential formulation of Strack (1976), Cheng et al. (2000) derived analytical solutions for maximum discharge for one-well, two-well, and one-well-with-recharge-canal problems, and applied a structured messy genetic algorithm for solving multiple pumping wells optimization. To better simulate the reality, many researchers grouped the variable density-flow and the advection-dispersion equations together to model the maximum groundwater pumping rates based on miscible-flow assumptions (e.g., Henry, 1964; Voss and Souza, 1987; Galeati et al., 1992; Croucher and O'sullivan, 1995; Ackerer et al., 1999; Diersch and Kolditz, 2002; Simpson and Clement, 2003; Simmons, 2005; Langevin and Guo, 2006; Lu et al., 2012).

In addition, some researchers concentrated on applying a range of mathematical optimization methods by fully-penetrating wells in coastal aquifers. Werner et al. (2013) summarized that the common techniques include: linear programming (e.g., Mantoglou, 2003); non-linear programming (e.g., Mantoglou and Papantoniou, 2008) and evolutionary algorithms (e.g., Kourakos and Mantoglou, 2009; Dhar and Datta, 2009; Ataie-Ashtiani and Ketabchi, 2011). Nicklow et al. (2010) provided a comprehensive review of evolutionary algorithms methods and their applications in the field of water

resources planning and management, and particularly emphasized the significance and popularity of genetic algorithms among evolutionary algorithms approaches. Genetic algorithms are welcomed for the search of optimum for the management of multiple pumping wells. A plenty of researches employed genetic algorithms in optimizing groundwater extraction in coastal aquifers using numerical and analytical solutions (e.g., Park and Aral, 2004; Bhattacharjya and Datta, 2005; Qahman et al., 2005; Dhar and Datta, 2009; Sreekanth and Datta, 2010; Javadi et al., 2012).

Besides, many groundwater optimization topics focused on the proven cost-effective ASR system by applying the fully-penetrating wells (e.g., Mirecki et al., 1998; Konikow et al., 2001; Pavelic et al., 2006(a), 2006(b); Ward et al., 2007, 2008, 2009; Bakker, 2010; Lu et al., 2011). The RE of an ASR system can be greatly affected by many parameters. Peters (1983), Pavelic et al. (2002), Ward et al. (2007) and Lu et al. (2011) provided key factors governing the RE, which includes both hydrogeological and operational variables. The fully-penetrating extraction wells were widely applied in the groundwater optimization management. But, there is not a comprehensive study of key hydrogeological and operational parameters on the ASR by fully-penetrating wells in coastal aquifers.

In this study, our focus of groundwater optimization management is on the application of ASR systems. We aim to conduct a comprehensive research on the influence of key hydrogeological and operational parameters on ASR systems in coastal aquifers.

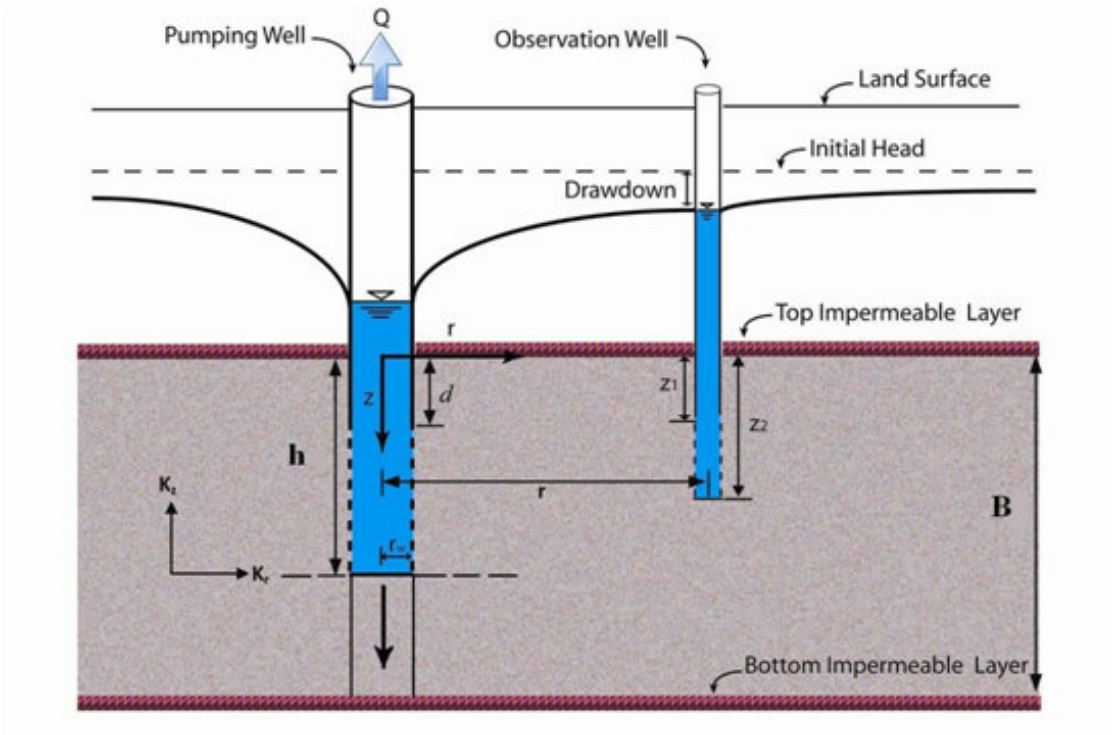

Figure 2.3 Configuration of partially-penetrating wells. (Source: http://www.midwestgeo.com/webinars/archived/aquiferpumping-04032013.php?item=WArc0075).

A well with its well screen length of water entry less than the aquifer thickness is known as a partially penetrating well (***Figure 2.3***). Partially penetrating wells are common in practice, particularly in areas where the aquifer is relatively thick. Previous studies of partially-penetrating wells include analytical solutions of well drawdown and numerical modeling of capturing contaminant plumes in aquifers. This idea of using partially-penetrating wells for ASR appreciates the tilting shape of the interface with underlying heavier salt water. The use of partially-penetrated well is similar to the well-known saltwater upconing problem. For fully-penetrated wells, recovery has to be terminated as

soon as the interface toe reaches the well, while the toe can be further pulled up to the partially-penetrated well for recovery termination, resulting in later breakthrough of salt water into the pumping well, more recoverable water extracted from the shallow layers, and a higher RE (***Figure 2.3***). The technique to pumping water from one part of a fully-penetrated well is mature in practice (e.g., Fienen et al., 2006). One may also simply install two adjacent wells, one fully-penetrated for injection and the other partially-penetrated for recovery.

2.4 Modeling Techniques for Well Pumping in Coastal Aquifers

Based upon those earlier studies during the 50's and the 60's, analytical solutions can be reached from simplified conceptual models for flow and transport in coastal aquifers, which usually assumed a steady flow in a hydrologically homogeneous porous medium, as well as a sharp interface between the freshwater and the seawater. The potential-flow theory was applied to describe the propagation of the freshwater-seawater interface (e.g., Strack, 1976). The rough, analytical solutions developed at that time provided the following two fundamental relationships that assisted the engineers to effectively operate subsurface barrier systems: (1) The rate of freshwater flow to the sea vs. the length of the intruding seawater wedge; and (2) The water table elevations in the vicinity of the coast vs. the length of the intruding seawater wedge. The second modeling approach is more realistic in that it contains a system of variable-density flow equations and the advection-dispersion equation (e.g., Henry, 1964; Voss and Souza, 1987; Herbert et al., 1988; Galeati et al., 1992; Fan and Kahawita, 1994; Croucher and O'Sullivan, 1995; Kolditz et al., 1998; Ackerer et al., 1999; Paniconi et al., 2001; Diersch and Kolditz, 2002; Gotovac et al., 2003; Simpson and Clement, 2003; Simmons, 2005; Langevin and Guo, 2006). In

this context, a variable-density mixing zone with a certain thickness, rather than a sharp interface, can be generated, consistent with field observations in coastal aquifers (Barlow, 2003; Cherry, 2006). However, none of these models consider the mobility of gas phase. To simulate and predict the gas injection strategy, the model is required to include both variable density effects and multiphase mass exchange and transport. Two types coupling relationships need to be incorporated into the model: concentration and density, and permeability and multiphase saturation. All these models need to calibrated and validated by experimental data. In addition, uncertainty and sensitivity analysis is required to identify key parameters and hydrogeologic conditions.

Analytical Solution

Groundwater flow in general is a three-dimensional (3D) problem. Nonetheless, researchers and engineers prefer simplifying the 3D problem to 2D or even 1D. However, this simplification certainly does not work for coastal aquifers because of the seaward boundary and density gradients. In addition, it may be appropriate for fully-penetrating wells to apply the well-known Dupuit-Forchheimer assumption of horizontal flow in modeling groundwater flow on a regional scale (Strack, 1984). However, such an assumption is invalid near 3D flow features, such as flow to a partially penetrating well (e.g., Luther and Haitjema., 1999; Bakker, 2001). Various analytical and semi-analytical solutions have been derived for a diversity of hydrogeological conditions based on reasonable assumptions.

Flow toward a partially penetrating well has usually been treated as a uniform radial flux along the well screen for the development of analytical solutions (Perina and Lee, 2006).

For example, Hantush (1961) presented an analytical solution of the drawdown distribution around a partially penetrating well. Neuman (1974) accounted for the effect of a well partially penetrating in a homogeneous anisotropic unconfined aquifer. Unlike making the assumption of uniform flow, many researchers focused on the non-uniform radial flux along the pumping well screen. Cassiani and Kabala (1998) derived a semi-analytic solution for well response to the pumping test and slug test performed on a partially penetrating well for the mixed-type boundary condition in a confined aquifer. Chang and Chen (2003) supplied an analytical solution of a partially penetrating well for a constant drawdown and no-flux condition pumping test in a finite thickness confined aquifer. Perina and Lee (2006) showed a general well function for groundwater flow toward a pumping well with non-uniform radial flux along the screen when it partially penetrates a confined or unconfined leaky aquifer. Furthermore, the seepage face and the decrease in saturated thickness of the aquifer were usually neglected when deriving flow analytical solutions to partially-penetrating wells in an unconfined aquifer (e.g., Neuman, 1972, 1974; Zlotnik et al., 1998; Perina and Lee, 2006).

The aquifer size is an important concern in deriving analytical solutions. In fact, inland aquifers with partially penetrating wells are usually assumed infinite (e.g., Muskat, 1937; Haitjema and Kraemer, 1988; Faybishenko et al., 1995), while coastal aquifers may only be considered as semi-infinite because of the seaward boundary. Thus, the method of linear superposition needs to be applied for the coastal pumping issues when seeking analytic expressions of flow (e.g., Strack, 1976). Javandel and Witherspoon (1983) presented an analytic solution to the problem of transient flow to a partially penetrating well that is open in either finite thickness layer of a two-layer system. Bakker (2001)

developed an analytic approximate solution for three-dimensional flow to a partially penetrating well by dividing the aquifer into many local layers. Yeh et al. (2008) presented a semi-analytical solution for a slug test in a constant-flux pumping well partially penetrating a radial two-zone confined aquifer with the consideration of the skin effect. Furthermore, Yang and Yeh (2012) developed a general mathematical model for describing the hydraulic head as a result of the constant-head, constant-flux, and slug tests at a partially penetrating well in a radial confined aquifer. By laying the stress on the anisotropy, the capture zone of a partially penetrating well in an anisotropic aquifer was delineated by different analytical solutions (e.g. Zlotnik, 1997; Chen et al., 2010; Mishra et al., 2012). We can see that the applications of analytical solutions are limited because each is expected to apply under a specific qualification, although many researchers developed various analytical solutions. It is so hard to develop a general analytical solution for the varying complex hydrogeological conditions.

Numerical Solution

Compared with analytic expressions, numerical explorations of flow to partially penetrating wells are more straightforward. Moreover, the combination of numerical simulations (for more realistic, complex systems) and analytical solutions (for simplified systems) can provide a comprehensive systematic perception for the invisible complex subsurface problem. Harmsen et al. (1991) conducted a numerical observation for flow to a partially penetrating well in an unconfined aquifer by using a particle-tracking model. Tiedeman and Gorelick (1993) suggested a three dimensional groundwater management model for a shallow unconfined aquifer. Bair and Lahm (1996) numerically demonstrated how the partial penetration, regional hydraulic gradient and anisotropy affect the

geometry of capture zones of wells pumping from unconfined aquifers. Hvilshoj et al. (1999) applied an inverse numerical model to analyze the data from pumping tests of partially penetrating wells carried out in an unconfined aquifer at the Vejen field site in Demark. Behrooz-Koohenjani et al. (2011) numerically simulated the steady unconfined flow to fully screened partially-penetrating wells by using MODFLOW 2000, taking into account the seepage face in the well and decrease in saturated thickness of the aquifer towards the well. Barua and Bora (2010) developed a steady/quasi-steady model for predicting flow into a partially penetrating well with skin zone in a confined aquifer overlying an impervious layer by considering flow through the bottom of the wellbore, finite skin thickness and finite horizontal and vertical extent of the aquifer.

The previous discussions about the applications of partially-penetrating wells were exhaustive. However, a systematic study focusing on the application of partially-penetrating wells for the ASR system has not been set up. The traditional common extraction method for ASR is based on fully-penetrating extraction wells, which implies that water is pumped out from the entire aquifer including the bottom. This method is inefficient and uneconomical in brackish aquifers because seawater is heavier. Can the RE of an ASR scheme be well improved by applying our proposed partially-penetrating wells? How will the hydrogeological and operational parameters affect the ASR system by applying partially-penetrating wells? Besides, it is also necessary to explore the performance of partially-penetrating wells in stratified costal aquifers.

To sum up, our study firstly focuses on key operational and mixing parameters which affect the RE of an ASR system in the absence of density gradients. Secondly, we investigate how the RE varies with the hydraulic conductivity ratios of structured layers

in heterogeneous and anisotropic coastal aquifers. Thirdly, we plan to propose an operation method on the basis of fully-penetrating injection wells and partially-penetrating extraction wells for ASR systems. This method is expected to greatly enhance the RE compared with fully-penetrating extraction wells in most coastal aquifers. The interests in how hydrogeological and operational key parameter variables affect the operation of partially-penetrating wells will be explored. Accordingly, key RE controlling factors will be determined by sensitivity analysis. To the best of our knowledge, there is no research on investigating the application of partially-penetrating wells for the ASR system in coastal aquifers. This is an unexplored, very promising area because of the unique variable-density feature in coastal aquifers. In addition, no systematic study on ASR performance in stratified coastal aquifers has been investigated.

CHAPTER 3

SOLUTE TRANSPORT IN DIVERGENT RADIAL FLOW WITH MULTISTEP PUMPING

Significant contributions have been made to evaluate analytical solutions to the problem of advection and dispersion in a homogeneous aquifer due to well injection or extraction in a horizontal, radially divergent or convergent flow field (e.g., Ogata, 1958; Tang and Babu, 1979; Moench and Ogata, 1981; Chen, 1985, 1986, 1987; Hsieh, 1986; Chen and Woodside, 1988; Moench, 1989, 1995; Goltz and Oxley, 1991; Tomasko et al., 2001; Huang and Goltz, 2006; Huang et al., 2010). Such solutions have important applications in groundwater practice whenever well pumping is involved, such as tracer tests in convergent and divergent radial flow fields (e.g., Novakowski, 1992; Moench, 1995; Becker and Charbeneau, 2000), decontamination by pumping with rate-limited sorption or mass transfer (e.g., Goltz and Oxley, 1991; Harvey et al., 1994), and single-well push-pull tracer tests (Huang et al., 2010), etc. First-order analysis and macrodispersion theory have also been applied for solute transport in divergent radial flow in heterogeneous porous media (e.g., Indelman and Dagan, 1999; Neuweiler et al., 2001). One major assumption for these analytical solutions and analyses is that the radial flow field is steady state, i.e., the velocity field is a spatial function of the distance to the pumping well, but not a temporal function. In this work, we present a novel, efficient approach to evaluate solute transport in divergent radial flow fields created by multistep pumping with an arbitrarily time-dependent input concentration. The major assumption of this approach is that the transitional period between two pumping steps can be neglected.

Such an assumption was accepted in all the available analytical solutions, i.e., solute transport starts when the radial field reaches the steady state. This work also presents theoretical analyses to investigate the conditions for such an assumption to be valid.

3.1 Governing Equations

Consider a recharge well that fully penetrates a homogeneous, confined aquifer of uniform thickness and infinite lateral extent. The transport problem can be described by the radially advective-dispersive equation in cylindrical coordinates as the following by neglecting molecular diffusion (e.g., Hoopes and Harleman, 1967; Hsieh, 1986):

$$\theta \frac{\partial c}{\partial t} = -\theta v \frac{\partial c}{\partial r} + \frac{1}{r}\frac{\partial}{\partial r}\left(\theta r \alpha_L |v| \frac{\partial c}{\partial r}\right), \quad r > r_w \quad (3.1)$$

where t $[T]$ is the time; r $[L]$ is the radial distance from the well center; r_w $[L]$ is the well radius; c $[M/L^3]$ is the dissolved solute concentration; θ $[-]$ is the effective porosity; α_L $[L]$ is the longitudinal dispersivity; v $[L/T]$ is the pore fluid velocity; and $|v|$ represents the absolute magnitude of v.

When the well injection rate is constant, the steady-state velocity field is only a spatial function of r,

$$v(r) = \frac{q}{2\pi\theta r}, \quad r > r_w \quad (3.2)$$

where q $[L^2/T]$ is the specific injection rate, defined as the flow recharge rate per unit length of aquifer thickness, and r_w is the well radius. The initial condition is:

$$c(r, t = 0) = 0 \quad (3.3)$$

and the boundary condition with a constant injection concentration is:

$$c(r \to \infty, t) = 0, \quad c(r = r_w, t) = c_0 \quad (3.4)$$

The above equations represent a typical model setup for describing solute transport in a steady-state divergent radial flow field with a constant solute input concentration at the injection well. In practice, however, one may adjust the pumping rate and input concentration during experiments to create favorable subsurface flow fields and conditions, i.e., both the pumping rate q and input concentration c_0 may vary with time. For example, a multistep pumping strategy consisting of a series of rate increases may be applied to increase the sensitivity of drawdown to zonal properties and to estimate well loss parameters (e.g., Butler and McElwee, 1990; Singh, 2002), and mixing within the injection well may generate a gradually increasing input concentration history for a step injection (Luo et al., 2006).

For a multistep pumping rate $q(t)$, we assume that the velocity field varies with the well pumping rate and the velocity field is a function of both r and t, i.e.,

$$v(r, t) = \frac{q(t)}{2\pi\theta r}, \quad r > r_w \quad (3.5)$$

and for a time-dependent input concentration, the boundary condition is:

$$c(r \to \infty, t) = 0, \quad c(r = r_w, t) = c_0(t) \quad (3.6)$$

Equation (3.5) neglects the transitional period between two well pumping rates and assumes a steady-state velocity for each pumping rate. Such an assumption has been widely accepted in the summarized analytical solutions. Harvey et al. (1994) showed that velocities approach steady state rapidly (exponentially decay with the increase of time) for changing pumping rates. In a typical mixed-sand aquifer, velocities may take only minutes to couple of days to reach 99% of steady state for a scale up to 100 meters. Thus, Equation (3.5) approximates a piecewise steady-state velocity field in aquifers with short transitional periods to reach steady state. The conditions for such an assumption to be valid will be further discussed in later sections.

As indicated in the introduction, a series of analytical solutions were derived for solute transport in a steady-state divergent radial flow field with a constant input concentration. To evaluate solute transport in a piecewise steady-state radial flow field, we may discretize the time-dependent function, $q(t)$, into a number of small intervals, $q(t_0), q(t_1), \ldots$, and assume a steady-state flow field within each time interval $t_{n-1} \le t < t_n$. For the first time interval, the transport problem has a zero initial condition and can be conveniently solved by available analytical solutions. For all subsequent time intervals, the transport problem can be described by Equation (3.1) with a steady-state velocity field but with a non-zero initial condition. Laplace transform of such a problem leads to an inhomogeneous differential equation, which may be solved by the much more complicated Green's function approach (e.g., Chen and Woodside, 1988). Furthermore, such problems can also be solved numerically by taking the solution of the previous time step as the initial condition for the next time step. However, with an arbitrarily time-dependent input concentration history, these methods are computationally complicated

and the accuracy relies on the temporal discretization of both q and c_0 and the spatial discretization of travel distance. For example, for a multistep pumping profile and a continuous temporal function of input concentration history, a finer time discretization than the pumping steps is necessary to characterize both q and c_0. In addition, for analyzing tracer tests, one may be interested in concentration profiles at specific sampling locations for parameter estimation. However, numerical models have to solve the entire spatial domain to evaluate concentration profiles at certain locations, causing inefficient inverse modeling and parameter estimation. In the following, we present an efficient approach to solve transport in a multistep pumping field, which is completely based on the available analytical solutions and does not require advanced numerical methods.

3.2 Analytical Solutions

3.2.1 Steady-state Flow With A Constant Input Concentration

For the sake of completeness, we first summarize the analytical solution in a steady-state flow field with a constant input concentration, which will be used later to evaluate the solution in a transient flow field. We denote c_s as the solution in a steady-state flow field. By introducing the following dimensionless groups:

$$c_s^* = \frac{c_s}{c_0}, R = \frac{r}{\alpha_L}, R_0 = \frac{r_w}{\alpha_L}, \tau = \frac{qt}{2\pi\theta\alpha_L^2} \quad (3.7)$$

Equation (3.1) can be transformed into:

$$\frac{\partial c_s^*}{\partial \tau} = \frac{1}{R}\left(-\frac{\partial c_s^*}{\partial R} + \frac{\partial^2 c_s^*}{\partial R^2}\right) \quad (3.8)$$

The analytical solution on the Laplace domain is given by (Moench and Ogata, 1981):

$$\overline{c_s^*}(R,p)=\frac{1}{p}\exp\left(\frac{R-R_w}{2}\right)\frac{\mathrm{Ai}(Y)}{\mathrm{Ai}(Y_w)} \quad (3.9)$$

where p is the Laplace coordinate, $\mathrm{Ai}(z)$ is an Airy function, and

$$Y=\frac{4Rp+1}{4p^{2/3}} \quad (3.10)$$

$$Y_w=\frac{4R_wp+1}{4p^{2/3}} \quad (3.11)$$

The time-domain solution can be evaluated numerically by inverse Laplace algorithms (e.g., de Hoog et al., 1982) or analytically by (Moench and Ogata, 1981):

$$c_s^*(R,\tau)=1-\int_0^\infty F(\upsilon)\,d\upsilon \quad (3.12)$$

where

$$F(\upsilon)=\frac{2\exp\left[-\upsilon^2\tau+(R-R_w)/2\right]}{\pi\upsilon}\frac{\mathrm{Ai}(y)\mathrm{Bi}(y_w)-\mathrm{Ai}(y_w)\mathrm{Bi}(y)}{[\mathrm{Ai}(y_w)]^2+[\mathrm{Bi}(y_w)]^2} \quad (3.13)$$

$$y=\frac{1-4R\upsilon^2}{4\upsilon^{4/3}} \quad (3.14)$$

$$y_w=\frac{1-4R_w\upsilon^2}{4\upsilon^{4/3}} \quad (3.15)$$

and Ai and Bi are independent Airy functions of first and second order, respectively.

3.2.2 Steady-state Flow With A Time-dependent Input Concentration

For a steady-state divergent flow field with a time-dependent injection history at the pumping well, $c_0(t)$, the solution can be conveniently evaluated by linear convolution:

$$c(R,\tau) = \int_0^{\tau} c_0(\tau')\, g(\tau - \tau')\, d\tau' \quad (3.16)$$

where g is known as the transfer function or impulse response function corresponding to a unit impulse input function at the pumping well. g can be evaluated by taking inverse Laplace transform of:

$$\bar{g}(R,p) = \exp\left(\frac{R - R_w}{2}\right)\frac{\mathrm{Ai}(Y)}{\mathrm{Ai}(Y_w)} \quad (3.17)$$

or by taking the first derivative of Equation (3.12) with respect to τ :

$$g(R,\tau) = \int_0^{\infty} \upsilon^2 F(\upsilon)\, d\upsilon \quad (3.18)$$

Because there is a scaling factor between t and τ according to the definition of dimensionless groups, g on the time domain is given by:

$$g(r,t) = \frac{q}{2\pi\theta\alpha_L^2}\, g(R,\tau) \quad (3.19)$$

3.2.3 Multistep Pumping With A Constant Input Concentration

We notice that Equation (3.12) is a general solution on the transformed time domain τ for a steady-state flow field with an arbitrary well pumping rate. For the solution on the

regular time domain t, one only needs to scale τ according to the definition of dimensionless parameters, i.e.,

$$c^*(r,t) = c_s^*\left(\frac{r}{\alpha_L}, \frac{qt}{2\pi\theta\alpha_L^2}\right) \quad (3.20)$$

We define:

$$Q(t) = qt \quad (3.21)$$

which represents the cumulative amount of injected water. Equation (3.20) can then be written as:

$$c^*(r,t) = c_s^*\left(\frac{r}{\alpha_L}, \frac{Q(t)}{2\pi\theta\alpha_L^2}\right) \quad (3.22)$$

For any two steady-state flow fields with different well flow rates, q_1 and q_2, we have:

$$c_{s1}^*(r,Q;q_1) = c_{s2}^*(r,Q;q_2) \quad (3.23)$$

which implies that the concentration distribution is independent of specific flow rate q given a constant total injected flow Q.

Equation (3.23) leads to an efficient approach to transform a multistep pumping history $q(t)$ to a constant pumping rate by working on the Q domain instead of the regular time domain t. Consider a simple $q(t)$ with a two-step injection: $q_1(0 \le t < t_1)$ and $q_2(t_1 \le t < t_2)$. At the end of the first pumping period, the concentration is given by:

$$c^*(r,t_1;q_1) = c_s^*(r,Q_1;q_1) = c_s^*(r,Q_1;q_2) \quad (3.24)$$

where Q_1 is the total injected flow amount during the first injection period, i.e., $Q_1 = q_1 t_1$. Equation (3.24) implies that the initial concentration for the second period may be considered as a result of the pumping rate q_2 for a total injected flow of Q_1. Thus, the piecewise steady-state flow field created by a two-step injection can be transformed into a steady-state flow field with a constant injection rate. The solution at t_2 can then be conveniently evaluated by:

$$c^*(r, t_2; q_2) = c_s^*(r, Q_1 + Q_2; q_2) \quad (3.25)$$

Equation (3.25) can be generalized to an arbitrarily discretized pumping history, $q_1(t_1), q_2(t_2), ..., q_n(t_n)$:

$$c^*(r, t_i; q_i) = c_s^*\left(r, \sum_{j=1}^{i} Q_j; q_i\right) = c_s^*\left(r, \sum_{j=1}^{i} Q_j; q'\right) \quad (3.26)$$

where q' represents an arbitrary, constant specific flow rate.

Essentially, Equation (3.26) evaluates the solution on the domain of the cumulative injection flow volume, Q, instead of the time domain. Equation (3.22) may be considered as the solution for a unit step injection flow rate on the Q domain. Thus, the transient flow is transformed into the steady-state flow on the Q domain. To obtain the time-domain solution, one only needs to map the solution to the time domain according to the relation between t and $Q(t)$. The fundamental physical principle is that the concentration distribution is completely determined by the total volume of injected water but independent of specific flow rates. We shall notice that the cumulative flow or mass

concept has been widely used in analyzing column studies, in which the cumulative mass is usually expressed as pore volume (e.g., Shackelford, 1995). The general procedure to analytically evaluate the concentration solution in a divergent flow field with a multistep pumping history and a constant injection concentration can be summarized as follows:

1) Calculate the analytical solution for a steady-state flow field $c^*(R,\tau)$;

2) Transform $c^*(R,\tau)$ into $c^*(r,Q)$ according to the definition of dimensionless groups, i.e., $r = \alpha_L R$ and $Q = 2\pi\theta\alpha_L^2\tau$;

3) Evaluate the cumulative pumping function $Q(t) = \int_0^t q dt$;

4) Map $c^*(r,Q)$ onto the time domain, $c^*(r,t)$.

The above algorithm is essentially identical to defining the dimensionless time, τ, by:

$$\tau = \frac{1}{2\pi\theta\alpha_L^2}\int_0^t q(t')dt' \quad (3.27)$$

which removes $q(t)$ from the transport equation and results in the same dimensionless transport equation in a steady-state flow field. Analytical solutions can then be applied and the mapping between t and τ yields the solution on the time domain, similar to the mapping between t and Q. For a known $q(t)$, the mapping can be implemented by numerical methods with very fine discretization in time and linear interpolation. In addition, the developed approach is similar to the time transformation to evaluate concentrations in transient uniform flow fields (Carlier, 2008). However, our algorithm evaluates concentrations on the cumulative flow domain, and time mapping only applies

in the end to obtain the regular time solution. This algorithm is more efficient and straightforward and can be conveniently extended to cases with time-dependent input concentrations (section 3.2.4).

3.2.4 Multistep Pumping With A Time-dependent Input Concentration

For both a multistep well flow rate, $q(t)$, and a time-dependent input concentration, $c_0(t)$, we may discretize the functions into $q(t_0), q(t_1),...$ and $c_0(t_0), c_0(t_1),...$. Consider the simple case with the first two steps: $q_1(0 \le t < t_1), c_1(0 \le t < t_1)$ and $q_2(t_1 \le t < t_2), c_2(t_1 \le t < t_2)$. Following the procedure describe in the previous section, the solution at t_1 is given by:

$$c(r, t_1; q_1, c_1) = c_s(r, Q_1; q_1, c_1) = c_s(r, Q_1; q_2, c_1) \quad (3.28)$$

That is, the initial solution for the second period can be regarded as a result of the pumping rate q_2 for a total injected flow Q_1 at a constant input concentration c_1. Thus, for the second period, the problem becomes a steady-state flow with a time-dependent input history at the pumping well, which can be solved by linear convolution,

$$c(r, t_2; q_2, c_2) = g(r, Q_1 + Q_2)c_1 + g(r, Q_1)c_2 \quad (3.29)$$

where the transfer function $g(r, Q)$ is given by

$$g(r, Q) = \frac{g(r, t)}{2\pi\theta\alpha_L^2} \quad (3.30)$$

The general solution on the Q domain is given by:

$$c(r,Q;q(t),c_0(t))=\int_0^Q g(r,Q')c_0(Q-Q')dQ' \quad (3.31)$$

where the input concentration is written as a function of Q instead of t. Thus, the procedure to analytically evaluate solute transport in a multistep divergent flow field with a time-dependent input concentration can be summarized as follows:

1) Calculate the transfer function $g(r,t)$ in a steady-state flow field;

2) Transform $g(r,t)$ into $g(r,Q)$ according to the definition of dimensionless groups;

3) Evaluate the cumulative pumping function $Q(t)=\int_0^t qdt$;

4) Transform the input concentration history $c_0(t)$ into $c_0(Q)$;

5) Evaluate the linear convolution, Equation (3.31);

6) Map $c(r,Q)$ onto the time domain, $c(r,t)$.

3.2.5 An Alternative Approach

For an impulse or step concentration input function, the concentration distribution may be written as:

$$c(r,t;q(t))=c\left(r,\int_0^t qdt;q'\right)=c(r,t;\bar{q}) \quad (3.32)$$

where $\bar{q}$ is the mean pumping rate

$$\bar{q}(t) = \frac{1}{t}\int_0^t q\,dt \quad (3.33)$$

Thus, the concentration distribution at a time moment is the same to that created by the mean pumping rate within the same time frame. This means one can always assume an effective, constant pumping rate, i.e., the mean pumping rate, in the transport model to describe the spatial concentration distribution at a time moment. To describe concentration distributions at different time moments or concentration breakthrough curves at monitoring points, one needs to use the time-dependent mean flow rate. This provides an alternative approach to evaluate the transport problem: given the q function, one may first evaluate the time-dependent $\bar{q}$ function and the concentration at a time moment t can then be calculated using the analytical solutions by assuming the constant $\bar{q}(t)$. This approach is equivalent to the above approach on the cumulative flow domain because the mean flow rate function essentially reproduces the cumulative flow within the same time frame. In addition, this approach does not require time transformation or mapping because it deals with the problem in the original time frame. However, the alternative approach may not be as convenient as the proposed approach on the cumulative flow domain for a variable input concentration because the transfer function changes with time.

3.3 Case Study

In this section, we present two synthetic cases to validate the developed algorithms describe in the previous section. Consider a discrete function for $q(t)$:

$$q(t)=\begin{cases}10\,m^2/d, & 0\le t<20d\\ 8\,m^2/d, & 20d\le t<30d\\ 5\,m^2/d, & 30d\le t<40d\\ 2\,m^2/d, & 40d\le t<50d\\ 10\,m^2/d, & t\ge 50d\end{cases} \quad (3.34)$$

Associated with the well flow rate, we consider two input concentration profiles at the injection well: one has a discrete concentration history:

$$c_0^*(t)=\begin{cases}1, & 0\le t<20d\\ 0.5, & 20d\le t<30d\\ 0.2, & 30d\le t<40d\\ 1, & 40d\le t<50d\\ 0, & t\ge 50d\end{cases} \quad (3.35)$$

and the other has a continuous concentration history:

$$c_0^*(t)=1+0.1\sin\left(\frac{\pi t}{10}+\frac{\pi}{2}\right) \quad (3.36)$$

which represents an input concentration fluctuating around 1. Other parameters include: $r_w=0.5m$, $\alpha_L=1m$, and $\theta=0.3$.

Figure 3.1 shows the well flow rate history (***Figure 3.1a***) and the two input concentration profiles (***Figure 3.1b*** and ***3.1c***). ***Figure 3.1d*** shows the cumulative injected flow, Q, which is the integral function of the multistep pumping rate shown in ***Figure 3.1a***. ***Figures 3.1e*** and ***3.1f*** show the input concentration as a function of Q by mapping $c_0^*(t)$ shown in ***Figures 3.1b*** and ***3.1c*** onto the Q domain.

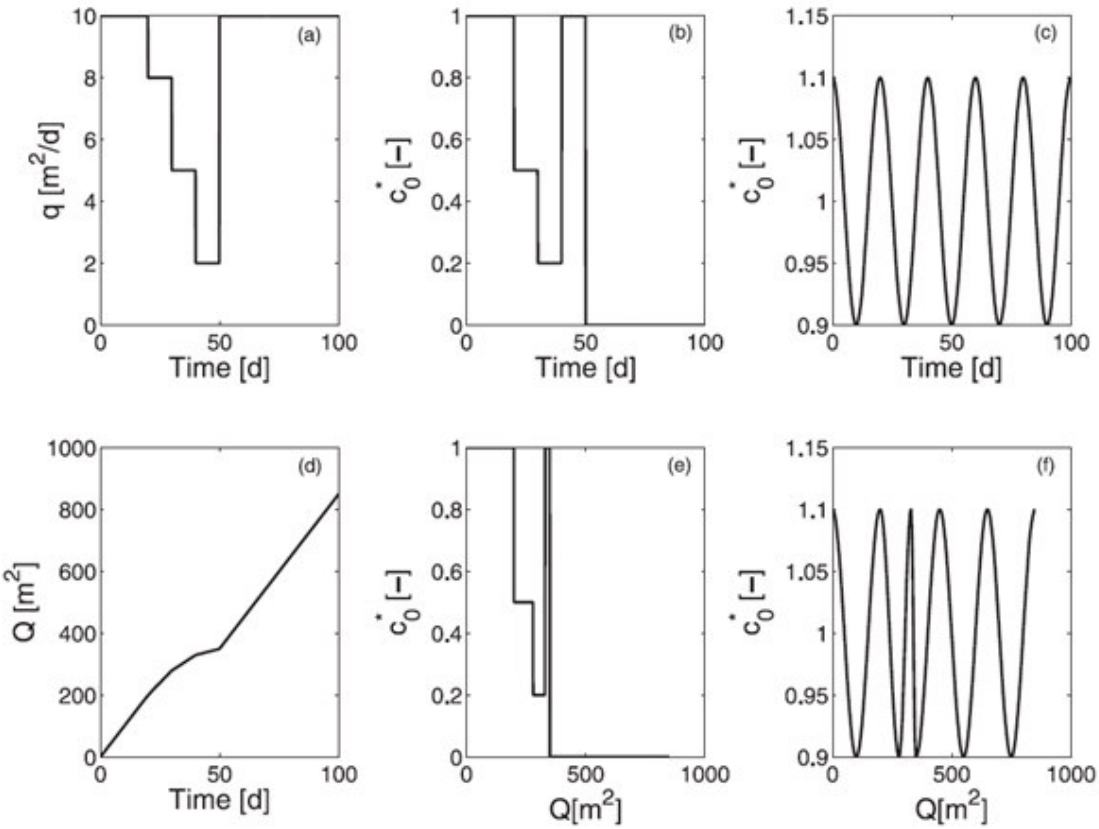

Figure 3.1 Numerical cases for testing developed algorithms for analytically evaluating solute transport in divergent radial flow with multistep pumping and time-dependent input concentrations. (a) well flow rate; (b) a discrete input concentration profile; (c) a continuous input concentration profile; (d) cumulative injected flow; (e) the discrete input concentration as a function of cumulative injected water; and (f) the continuous input concentration as a function of cumulative injected water.

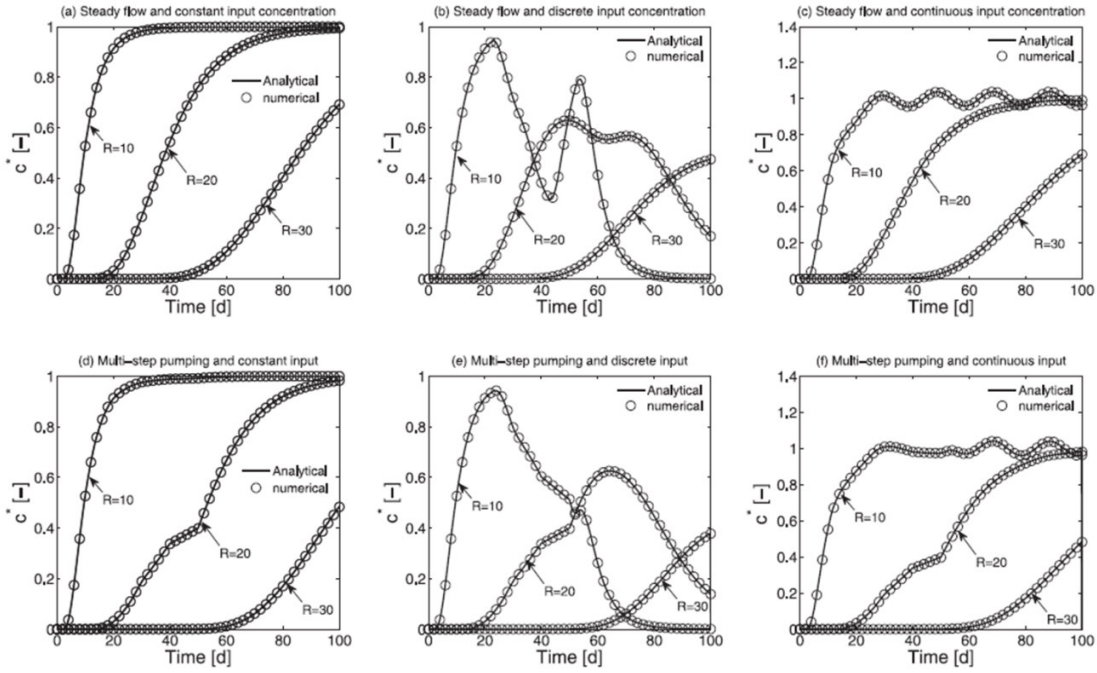

Figure 3.2 Comparison of analytical solutions with numerical solutions for multistep pumping and time-dependent input concentrations. (a) steady-state flow and a constant input concentration; (b) steady-state flow and discrete input concentrations; (c) steady-state flow and continuous input concentrations; (d) multistep pumping flow and a constant input concentration; (e) multistep pumping flow and discrete input concentrations; and (f) multistep pumping flow and continuous input concentrations.

Figure 3.2 compares the results of the proposed algorithms with numerical solutions evaluated by the MATLAB built-in ODE solver. The cases compared include: steady-state flow for a constant well injection rate, $q = 10m^2/d$, and a constant input concentration, $c_0^* = 1$, throughout the pumping history (***Figure 3.2a***); steady-state flow, $q = 10m^2/d$, and the discrete input concentration history described by Equation (3.35) (***Figure 3.2b***); steady-state flow, $q = 10m^2/d$, and the continuous input concentration history described by Equation (3.36) (***Figure 3.2c***); multistep pumping flow created by the pumping history, Equation (3.34), and a constant input concentration, $c_0^* = 1$ (***Figure 3.2d***); multistep pumping flow with the discrete input concentration history (***Figure 3.2e***); and multistep pumping flow with the continuous input concentration history (***Figure 3.2f***). For the discrete input concentration case, numerical methods may be conveniently applied by dividing the time into several time intervals with a step of 10 days so that within each time interval the problem becomes a steady-state flow with a constant input concentration. However, for the continuous input concentration, numerical methods are required to divide the time into much smaller intervals to reproduce the continuous function although there are only several steps of pumping. Thus, the continuous case requires more considerations in terms of the spatial and temporal discretization to satisfy the accuracy requirement and to characterize the continuous input function well. The developed algorithms on the basis of the analytical solutions have no such concerns and are much more efficient. ***Figure 3.2*** shows that the developed algorithms and numerical solutions match very well for all cases.

Figure 3.3 illustrates the developed algorithms using two cases presented above: one is the multistep pumping with a constant input concentration (***Figure 3.3a-3.3d***), and the other is the multistep pumping with the discrete input concentration described by Equation (3.35) (***Figure 3.3e-3.3i***). ***Figure 3.3a*** shows the analytical solution in a steady-state radial divergent flow field, i.e., Equation (3.9) or (3.12). Such a solution can be conveniently expressed a function of the cumulative injected water, Q, which is a linear function of time (***Figure 3.3b***). The solution for the multistep pumping (***Figure 3.3d***) is then evaluated by simply mapping ***Figure 3.3b*** from the Q domain to the time domain according to the function of the cumulative injected water (***Figure 3.3c***). We shall notice that ***Figure 3.3b*** works for any pumping strategy with a constant input concentration. One only needs to update the mapping function, i.e., Q (***Figure 3.3c***), for other pumping strategies. For the case with both time-dependent pumping and input concentrations, ***Figure 3.3e*** provides the transfer functions as a function of Q, which can be analytically evaluated by Equation (3.30) or numerically by taking the first derivative of ***Figure 3.1b***. The solution on the Q domain (***Figure 3.1g***) is evaluated by the convolution of the transfer function (***Figure 3.3e***) with the input concentration function on the Q domain (***Figure 3.3f***). The solution on the time domain (***Figure 3.3i***) is then evaluated by mapping ***Figure 3.1g*** to the time domain according to the Q function (***Figure 3.1h***). Unlike the constant input concentration case, ***Figure 3.1g*** changes with the pumping strategy because the input concentration profile (***Figure 3.1f***) changes. Thus, for different pumping strategies, one needs to update ***Figure 3.3f*** and the mapping function (***Figure 3.3h***). We can see from the presented case that the developed algorithms completely rely on the available analytical solutions and are very efficient and straightforward.

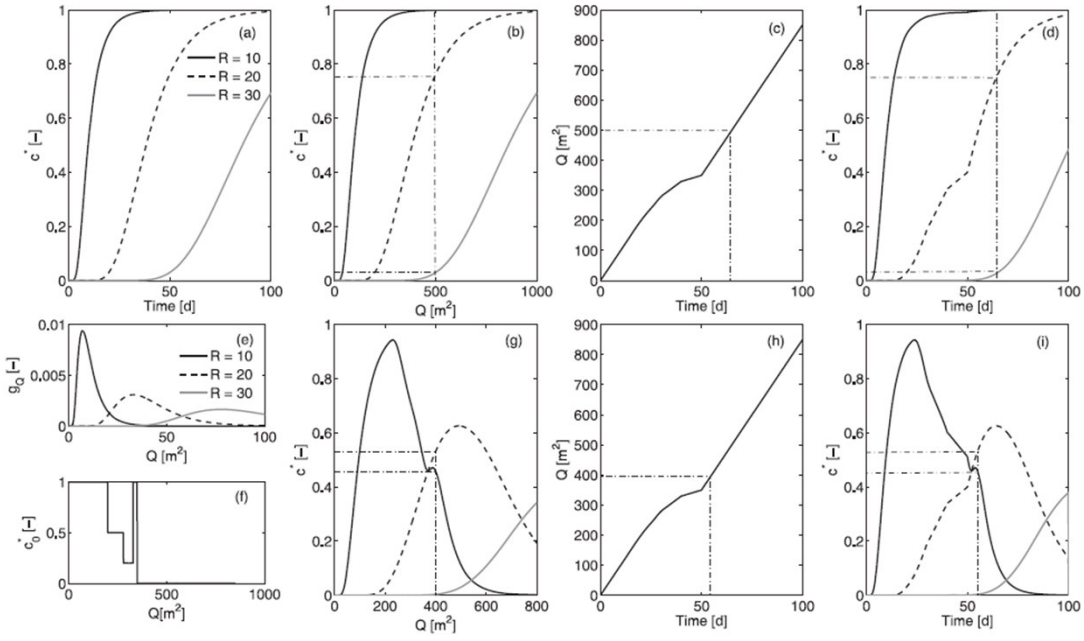

Figure 3.3 Illustration of developed algorithms: (a) - (d) multistep pumping with a constant input concentration; and (e) - (i) multistep pumping with the discrete input concentration history. (a) concentration profiles for a unit step pumping and a constant input concentration; (b) concentration profiles as a function of Q; (c) function of the cumulative injected water for the multistep pumping case; (d) concentration profiles mapped from (b) according to (c); (e) concentration transfer functions as a function of Q; (f) input concentration as a function of Q; (g) concentration profiles on the Q domain evaluated by the convolution of (e) and (f); (h) function of the cumulative injected water for the multistep pumping case, the same as (c); and (i) concentration profiles mapped from (g) according to (h).

3.4 Transitional Period

The major assumption for the developed approach is that the flow field created by multistep pumping is piecewise-steady state, i.e., the velocity field reaches steady state instantaneously with the pumping rate and the transitional period between two steady-state flow fields can be neglected. In the following, we discuss the conditions for this assumption to be valid from two aspects: one is the critical timescale to reach a "peudo-steady state condition", and the other is mean travel time from the pumping well to a certain point.

3.4.1 Critical Time Scale

The velocity $v(r,t)$ for an arbitrary pumping history $q(t)$ can be computed from the velocity $v_\delta(r,t)$, valid for instantaneous pumping of a unit volume, by convolution:

$$v(r,t)=\int_0^t v_\delta(r,t-t')q(t')dt' \quad (3.37)$$

In an infinite horizontal confined aquifer with an isotropic, homogeneous hydraulic conductivity, the Theis solution yields:

$$v_\delta(r,t)=\frac{rS}{8\pi\theta Tt^2}\exp\left(-\frac{r^2S}{4Tt}\right) \quad (3.38)$$

where S is the storage coefficient [-], and T is the aquifer transmissivity [L^2/T]. For a one-step pumping case from the static state, the transient velocity is given by:

$$v(r,t)=\frac{q}{2\pi\theta r}\exp\left(-\frac{r^2S}{4Tt}\right) \quad (3.39)$$

A "peudo-steady state condition" is defined when velocities reach 99% of their steady-state values, which requires $\left(r^2 S / 4Tt\right) \leq 0.01$ (Chen, 1985). We may define a critical timescale for velocities to reach the "peudo-steady state condition", t_c,

$$t_c(r) = \frac{25 r^2 S}{T} \quad (3.40)$$

which indicates that the critical timescale increases with the radial distance and storage coefficient and decreases with the transmissivity. In order to assume a steady-state flow field, the pumping duration must be longer than the critical timescale (Harvey et al., 1994).

For a multistep pumping profile, we consider the fundamental two-step pumping: $q_1(0 \leq t < t_1)$ and $q_2(t_1 \leq t)$. When $q_1 = 0$, the two-step pumping reduces to the single-step pumping presented above. The velocity field for the two-step pumping is given by:

$$v(r,t) = \begin{cases} q_1 \int_0^t v_\delta(r,t')dt', & 0 \leq t < t_1 \\ q_1 \int_0^t v_\delta(r,t')dt' + \Delta q \int_0^{t-t_1} v_\delta(r,t')dt', & t_1 \leq t \end{cases} \quad (3.41)$$

where $\Delta q = q_2 - q_1$ is the increment of the pumping rate. We assume at the end of the first pumping step the velocity has reached the peudo-steady state and can be approximated by the steady-state velocity, i.e., the pumping duration of the first step is longer than the critical timescale given by Equation (3.40). Thus, the velocity during the transitional period within the second pumping step is approximated by:

$$
\begin{aligned}
v(r,t) &= \frac{q_1}{2\pi\theta r} + \Delta q \int_0^{t-t_1} v_\delta(r,t')dt' \\
&= \frac{q_1}{2\pi\theta r} + \frac{\Delta q}{2\pi\theta r}\exp\left[-\frac{r^2 S}{4T(t-t_1)}\right], \quad t_1 \le t
\end{aligned}
\tag{3.42}
$$

We define the critical timescale of the "peuso-steady state condition" for the two-step pumping as the time required for the velocity field to accomplish 99% of the change between two steady-state flow fields, i.e.,

$$
\frac{\Delta q}{2\pi\theta r}\exp\left[-\frac{r^2 S}{4T(t-t_1)}\right] = 0.99\frac{\Delta q}{2\pi\theta r} \tag{3.43}
$$

which yields the same critical timescale given by Equation (3.40). Thus, a necessary condition for a multistep pumping field to assume the "peuso-steady state condition" is that the duration of each pumping step, t_p, must be greater than the critical timescale:

$$
t_p \ge t_c = \frac{25r^2 S}{T} \tag{3.44}
$$

which can be written as:

$$
r \le \sqrt{\frac{t_p T}{25S}} \text{ or } r_{\max} = \sqrt{\frac{t_p T}{25S}} \tag{3.45}
$$

Equation (3.45) defines the maximum spatial distance for a given pumping period or the maximum domain from the pumping well where the transitional period is possible to be neglected. In addition, we should notice that a very small constant time step or a variable time step may be required to characterize the transitional period within the critical

timescale at all locations because the critical timescale varies spatially and is very small near the pumping well.

3.4.2 Mean Travel Time

The above condition in terms of the critical timescale and pumping duration is not sufficient to assume the "peuso-steady state" for transport because it does not directly evaluate the error for solute transport. Here, we further examine the relative error of the mean travel time between the transient and steady-state case to quantify the impact of the transitional period on transport. For a tracer released in the injection well at the moment of pumping change, the relative error of the mean travel time for the tracer plume reaching a certain location is given by:

$$\varepsilon_\tau(r) = \frac{|\tau_t(r) - \tau_s(r)|}{\tau_t(r)} \quad (3.46)$$

where τ_t and τ_s represent the mean travel time for the transient and steady-state case, respectively. Consider the two-step pumping with pumping rates q_1 and q_2. By integrating the steady-state velocity, Equation (3.2), we have:

$$\tau_s(r) = \frac{\pi\theta r^2}{q_2} \quad (3.47)$$

For the transient case, we have:

$$\frac{dr}{dt} = \frac{q_1}{2\pi\theta r} + \frac{\Delta q}{2\pi\theta r}\exp\left(-\frac{r^2 S}{4Tt}\right) \quad (3.48)$$

which applies Equation (3.42) with the time reset at the end of the first pumping step, t_1. Integrating Equation (3.48) yields the mean travel time for the transient case:

$$\tau_t(r) = r^2 \left\{ \frac{q_1}{\pi\theta} + \frac{4T}{S} W\left[\frac{S\Delta q}{4\pi\theta T} \exp\left(-\frac{Sq_1}{4\pi\theta T} \right) \right] \right\}^{-1} \quad (3.49)$$

where $W(\cdot)$ is the Lambert W function (Corless et al., 1996). Substituting Equation (3.47) and (3.49) into (3.46), the relative error of the mean travel time, ε_τ, can be evaluated as:

$$\varepsilon_\tau = \frac{\left| \left\{ q_1 + \frac{4\pi\theta T}{S} W\left[\frac{S\Delta q}{4\pi\theta T} \exp\left(-\frac{Sq_1}{4\pi\theta T} \right) \right] \right\}^{-1} - q_2^{-1} \right|}{\left\{ q_1 + \frac{4T\pi\theta}{S} W\left[\frac{S\Delta q}{4\pi\theta T} \exp\left(-\frac{Sq_1}{4\pi\theta T} \right) \right] \right\}^{-1}} \quad (3.50)$$

which is not a function of r, indicating that the assumption of a steady-state velocity results in the same relative error of the mean travel time to any locations. Similar to the "peuso-steady state condition", we may require:

$$\varepsilon_\tau \le 0.01 \quad (3.51)$$

Figure 3.4 shows the relative error of the mean travel time as a function of transmissivity and storage coefficient for a single-step pumping with $q_1 = 0$, $\Delta q = q_2 = 1$ m^2/s and $\theta = 0.3$. The examined range for S is $[10^{-2}, 10^{-6}]$, and for T is $[10^{-2}, 10^{-6}]$. The contour line in ***Figure 3.4a*** delineates the ranges of T and S for $\varepsilon_\tau \le 0.01$. ***Figures 3.4b*** and ***3.4c*** show that ε_τ decreases with the increase of T and the decrease of S. Thus, to make the assumption of piecewise steady-state flow fields for a multistep pumping profile, the aquifer should have a large hydraulic conductivity and a small storage coefficient, which essentially decrease the critical timescale defined by Equation (3.40). In fact, for a very small S and a very large T, we have:

$$\lim_{S\to 0, T\to\infty} \varepsilon_\tau = \frac{\left| \left[q_1 + \frac{4\pi\theta T}{S} \left(\frac{S\Delta q}{4\pi\theta T} \right) \right]^{-1} - (q_1 + \Delta q)^{-1} \right|}{\left[q_1 + \frac{4T\pi\theta}{S} \frac{S\Delta q}{4\pi\theta T} \right]^{-1}} = 0 \quad (3.52)$$

Although Equation (3.50) and inequality (3.51) accurately define the conditions for the "peuso-steady state condition", they are not convenient to use. Here, we may compare the critical timescale and the mean travel time in the steady-state flow field to identify an empirical relation for the piecewise steady-state flow field to be valid:

$$\tau_s(r) \geq t_c(r) \quad (3.53)$$

which implies that the velocity at a certain travel distance has reached the "peudo-steady state condition" before the solute plume arrives at the point. Thus, the plume always moves with a nearly steady-state velocity from the pumping well. Because a multistep pumping profile may involve both positive and negative increment in pumping rates, we may use the maximum pumping rate to evaluate inequality (3.53):

$$\frac{\pi\theta r^2}{q_{\max}} \geq \frac{25 r^2 S}{T} \quad (3.54)$$

Because $q_{\max}$ corresponds to the minimum travel time, inequality (3.54) assures the validity of (3.53) for all pumping steps. Thus, we have:

$$\frac{T}{S} \geq \frac{25 q_{\max}}{\pi\theta} \quad (3.55)$$

Inequality (3.55) gives a simple relation to determine whether an aquifer appropriate or not for assuming the "peudo-steady state condition" with a given pumping strategy. We may write inequality (3.55) as:

$$q_{\max} \leq \frac{\pi\theta T}{25 S} \quad (3.56)$$

which defines the maximum well pumping rate allowed to satisfy the "peuso-steady state condition" at a given site, i.e., T and S are constant. A larger q implies a shorter travel time to a certain point, while the critical timescale does not change. Therefore, the piecewise-steady state assumption is not valid. Contrarily, a smaller q implies a longer travel time to a certain point than the critical timescale so that the "peuso-steady state condition" is always satisfied. The contour line in ***Figure 3.4a*** and the circles in the bottom of ***Figures 3.4b*** and ***3.4c*** show the critical cases with $T/S = 25q_2/\pi\theta$ and $\varepsilon_\tau \approx (1/0.99q_2 - 1/q_2)/(1/0.99q_2) = 0.01$. In addition, for a larger acceptable error, one may conveniently modify the critical timescale accordingly to identify appropriate conditions. For example, for a 5% error, $t_c(r) = 4.87r^2S/T$ and $q_{\max} \le \pi\theta T/4.87S$; and for a 10% error, $t_c(r) = 2.37r^2S/T$ and $q_{\max} \le \pi\theta T/2.37S$, which indicate that a larger error allowed, a shorter pumping duration or a larger domain and a larger pumping rate accepted, also shown in ***Figure 3.4***.

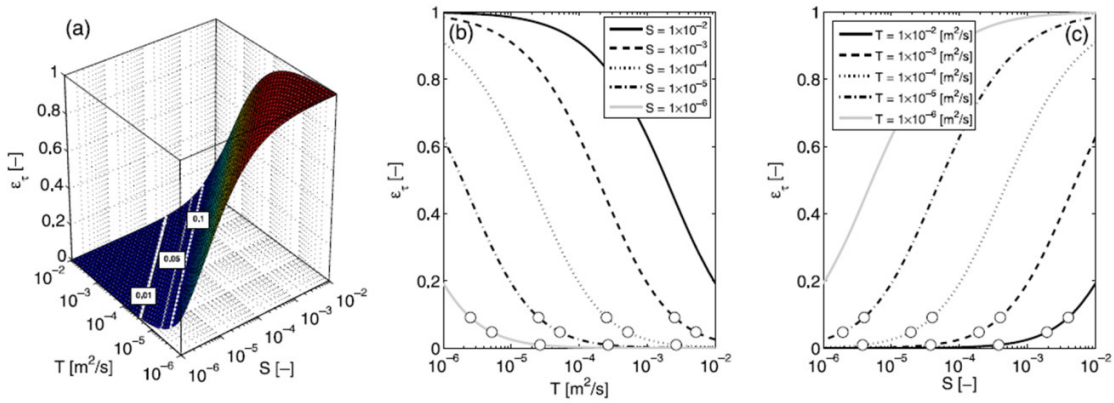

Figure 3.4 Relative error in the mean travel time, ε_τ, between the steady-state and transient flow field for a single-step pumping with a pumping rate of $1\text{m}^2/\text{s}$ and $\theta = 0.3$. (a) ε_τ as a function of both T and S and the contour lines of 0.01, 0.05 and 0.1; (b) ε_τ as a function of T for fixed S; and (c) ε_τ as a function of S for fixed T. The circles in (b) and (c) represent the cases with relative errors of 0.01, 0.05 and 0.1.

3.5 Conclusion

We develop a novel, efficient approach to evaluate solute transport in divergent radial flow fields created by multistep pumping and with an arbitrary input concentration function. By working on the cumulative injected flow domain, $Q(t) = \int_0^t q(t')\,dt'$, instead of the time domain, the transport problem with a temporally varying velocity field can be transformed into a steady-state flow problem. The fundamental physical principle is that the concentration distribution is completely determined by the total volume of injected water but independent of specific flow rates, i.e., given a constant total injection volume, the final concentration distribution does not change with different pumping strategies. By directly mapping the available analytical solutions in steady-state flow fields according to the relation between the cumulative injected flow and time, one can conveniently evaluate the solution in multistep pumping flow fields. For time-dependent input concentrations, linear convolution can be applied on the Q domain and the solution on the time domain can be obtained by direct mapping. The proposed algorithms are very efficient and accurate because they are completely based on analytical solutions and no spatial and temporal discretization is required. An alternative approach is also proposed by working with the time-dependent mean well pumping rate for an impulse and step input function, which does not require mapping between the cumulative flow and time.

The primary assumption of the developed approach is the piecewise steady-state flow for each pumping rate, i.e., the transitional period between two pumping rates is neglected. We derive important conditions accurately determining the appropriate aquifer properties and pumping operations for the assumption to be valid. The analysis uses the Theis

solution to evaluate the critical timescale of "peuso-steady state condition", defined when velocity changes reach 99% of their steady-state differences, and to evaluate the mean travel time of the solute plume from the pumping well for both steady and transient cases. Simplified but more practical conditions are obtained, which are:

1) $t_p \geq 25r^2 S/T$ or $r \leq \sqrt{t_p T/25S}$, where t_p is the pumping duration of a pumping step, r is the radial distance to the pumping well, S is the storage coefficient, and T is the transmissivity.

2) $q_{\max} \leq \pi\theta T/25S$, where θ is the effective porosity and $q_{\max}$ is the maximum well pumping rate.

The first condition yields the minimum pumping duration or the maximum problem domain, which essentially implies that the transitional period may be negligible when the pumping periods are much longer than the critical timescale to reach steady state or in the vicinity of the pumping well. The second condition defines the maximum pumping rate allowed in a site for a multistep pumping strategy. When both conditions are satisfied, one may neglect the transitional periods between pumping steps and assume a piecewise steady-state flow field. Furthermore, if one considers T as the single parameter that varies most in natural aquifers, the two conditions imply that the "peuso-steady state" is more likely to be satisfied in high-conductivity aquifers or more likely to fail in low-conductivity aquifers.

CHAPTER 4

RE OF ASR WITH MASS TRANSFER LIMITATION

The present study numerically and analytically investigates the efficiency of an ASR system in dual-domain aquifers with mass transfer limitations under various hydrogeological and operational conditions. Simple and effective relationships between transport parameters and ASR operational parameters are derived to quantify the effectiveness and ascertain the potential of ASR systems with mass transfer limitations. Specific questions to be answered by the present research are as follows: (1) how can we determine whether a site is appropriate or not for ASR with mass transfer limitations and identify when mass-transfer limitations are important; (2) what is the effect of mass transfer parameters and ASR operational parameters on ASR performance; and (3) how many cycles are needed for an ASR system to perform well?

4.1 Numerical Model

Figure 4.1 shows the conceptual model of a typical ASR system with a fully-penetrated pumping well installed in a confined, homogeneous, isotropic aquifer. The three-dimensional domain is modeled by a two-dimensional axisymmetric cross-section. The vertical axis of rotation is located at the pumping well. The medium consists of overlapped mobile and immobile domains, which have a uniform initial contaminant concentration of c_0. The mass transfer process between the mobile and immobile domain is described by a first-order mass transfer model. An ASR cycle consists of an injection, resting (storage) and extraction (recovery) phase. The groundwater velocity is assumed to

be steady state during each phase and the transition period between two phases is neglected (Harvey et al., 1994). During the injection phase, fresh water is injected into the aquifer and a concentration front moves away from the pumping well. During the storage phase, no flow occurs but the concentration profile may be altered by mass transfer between the mobile and immobile domain. During the recovery phase, stored water is extracted via the same pumping well and the concentration front moves toward the pumping well. For simplicity, we assume that the injection flow rate and the recovery rate are the same and the flow field is static during the storage phase. These assumptions are reasonable in practice and were adopted in many other studies (e.g., Ward et al., 2007, 2008). By neglecting regional flow and density effects, the problem can be described as one-dimensional transport in radial coordinates. It has been known that both regional flow and density effects may significantly influence the RE because regional flow may alter the shape of the water body in the subsurface during the storage phase and density effects may enhance solute mixing (e.g., Ward et al., 2007, 2008). However, these two mechanisms are not the focus of the present research. The RE is evaluated by setting a criterion of the average concentration of extracted water at the pumping well, such as the U.S. EPA potable-water standard. In the absence of dispersion and mass transfer, i.e., advection is the only transport process, the ASR system is completely reversible and the RE is 1. With dispersion and mass transfer, the mixing enhancement is not reversible, and hence the injection and extraction phase are not identically reversed and the RE is less than 1.

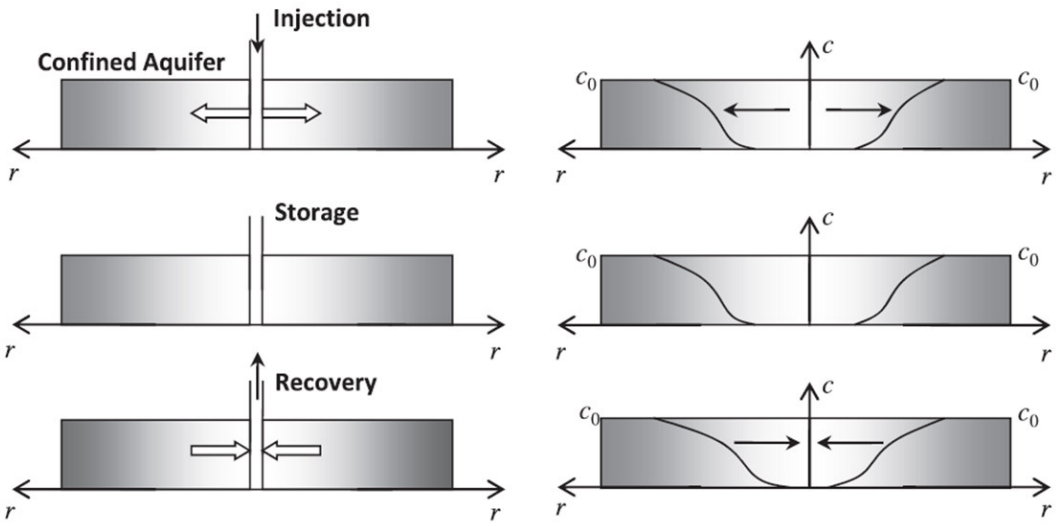

Figure 4.1 A schematic conceptual model of an ASR system with a fully-penetrating well in a confined aquifer in an axisymmetric coordinate system. The right panel is the concentration along the radial direction.

4.1.1 Governing Equations

In radial coordinates, the conceptual model can be described by one-dimensional dual-domain advective-dispersive transport and a first-order mass transfer model (e.g., Bear, 1979; Chen, 1985):

Mobile domain:

Injection and recovery phase:

$$\theta_m \frac{\partial c_m}{\partial t} + \theta_{im} \frac{\partial c_{im}}{\partial t} = -\theta_m v \frac{\partial c_m}{\partial r} + \frac{1}{r} \frac{\partial}{\partial r} \left(\theta_m r \alpha_L |v| \frac{\partial c_m}{\partial r} \right), \quad r > r_w \quad (4.1)$$

Storage phase:

$$\theta_m \frac{\partial c_m}{\partial t} + \theta_{im} \frac{\partial c_{im}}{\partial t} = 0, \quad r > r_w \quad (4.2)$$

Immobile domain:

$$\frac{\partial c_{im}}{\partial t} = \alpha(c_m - c_{im}), \quad r > r_w \quad (4.3)$$

where t [T] is the time; r [L] is the radial distance from the well center; r_w [L] is the well radius; θ_m [-] and θ_{im} [-] are porosities of the mobile and immobile domain, respectively; c_m [M/L^3] and c_{im} [M/L^3] are dissolved solute concentrations in the mobile and immobile domain, respectively; α_L [L] is the longitudinal dispersivity; v [L/T] is the pore fluid velocity; $|v|$ represents the absolute magnitude of v; and α [$1/T$] is the first-order mass transfer rate coefficient. Equations (4.1) and (4.2) assume that lateral mixing caused by molecular diffusion is negligible.

The steady-state velocity is given by:

Injection and recovery phase:

$$v = \pm \frac{q}{2\pi\theta_m r}, \quad r > r \quad (4.4a)$$

Storage phase:

$$v = 0 \quad (4.4b)$$

where q [L^2/T] is the specific pumping rate (positive sign for injection and negative for extraction), defined as the flow rate per unit length of aquifer thickness. Substituting Equation (4.4) into (4.1) yields:

Injection phase:

$$\theta_m \frac{\partial c_m}{\partial t} + \theta_{im} \frac{\partial c_{im}}{\partial t} = -\frac{q}{2\pi r} \frac{\partial c_m}{\partial r} + \frac{q\alpha_L}{2\pi r} \frac{\partial^2 c_m}{\partial r^2}, \quad r > r_w \quad (4.5)$$

Recovery phase:

$$\theta_m \frac{\partial c_m}{\partial t} + \theta_{im} \frac{\partial c_{im}}{\partial t} = \frac{q}{2\pi r} \frac{\partial c_m}{\partial r} + \frac{q\alpha_L}{2\pi r} \frac{\partial^2 c_m}{\partial r^2}, \quad r > r_w \quad (4.6)$$

The boundary conditions are given by:

Injection phase:

$$c_m(r \to \infty, t) = c_{im}(r \to \infty, t) = c_0, \quad \left(vc_m - \alpha_L |v| \frac{\partial c_m}{\partial r}\right)_{r=r_w} = 0 \quad (4.7a)$$

Recovery phase:

$$c_m(r \to \infty, t) = c_{im}(r \to \infty, t) = c_0, \quad \left.\frac{\partial c_m}{\partial r}\right|_{r=r_w} = 0 \quad (4.7b)$$

where c_0 [M/L^3] is the initial background concentration. For injection of fresh water, the boundary condition assumes zero mass flux during the injection phase. For ASR systems with stream water or reclaimed wastewater injection (e.g., Sheng, 2005), a non-zero input flux may be defined. Note the boundary conditions for the extraction phase are the same at the pumping well as previous radial pumping problems, but are different at the infinite distance (e.g., Chen and Woodside, 1988; Harvey et al., 1994), in which the

concentrations at the infinite distance are 0, representing a finite contaminant plume length. This is because such problems only involved extraction phases with or without storage phases, which resulted in a trivial solution of concentration c_0 for an infinite plume. However, for ASR systems, such a problem does not occur because extraction phases always follow injection and storage phases, which result in nonuniform concentration distributions at the beginning of extraction phases.

The final concentration distribution at the end of each cycle is used as the initial concentration distribution at the start of the subsequent cycle:

$$c_m(r, t = 0) = c_{m0}(r), \quad c_{im}(r, t = 0) = c_{im0}(r) \quad (4.8)$$

where the time is reset for each ASR cycle. $c_{m0}(r)$ and $c_{im0}(r)$ are not constant functions and vary for different phases and different ASR cycles. For the first injection phase, $c_{m0}(r)$ and $c_{im0}(r)$ are equal to c_0.

4.1.2 Dimensional Analysis

We introduce the following dimensionless groups:

Concentration:

$$c_m^* = \frac{c_m}{c_0}, c_{im}^* = \frac{c_{im}}{c_0} \quad (4.9)$$

Spatial distance:

$$R = \frac{r}{\alpha_L}, R_0 = \frac{r_w}{\alpha_L} \quad (4.10)$$

Mass transfer coefficients:

$$\text{Capacity ratio} : \beta = \frac{\theta_{im}}{\theta_m} \quad (4.11)$$

$$\text{Mass transfer timescale} : \tau_{im} = \frac{1}{\alpha} \quad (4.12)$$

where τ_{im} $[T]$ is a dimensional parameter.

ASR operational parameters:

$$\text{Time} : \tau = \frac{t}{\tau_{im}} \quad (4.13)$$

$$\text{Pumping rate} : \phi = \frac{q}{\theta_m \pi \alpha_L^2 \alpha} \quad (4.14)$$

$$\text{Injection duration} : T_i = \frac{t_i}{\tau_{im}} \quad (4.15)$$

$$\text{Storage duration} : T_s = \frac{t_s}{\tau_{im}} \quad (4.16)$$

$$\text{Recovery duration} : T_e = \frac{t_e}{\tau_{im}} \quad (4.17)$$

where t_i, t_s and t_e are the actual time periods of the injection, storage and extraction phase. All these time periods are normalized by the mass transfer timescale.

By substituting the velocity function given by Equation (4.4) and the defined dimensionless groups into Equation (4.1) and (4.2), the governing equations for an ASR system can be transformed into:

Mobile domain:

Injection phase:

$$\frac{\partial c_m^*}{\partial \tau} + \beta \frac{\partial c_{im}^*}{\partial \tau} = \frac{\phi}{2R}\left(-\frac{\partial c_m^*}{\partial R} + \frac{\partial^2 c_m^*}{\partial R^2} \right), \quad R > R_0 \;\&\; 0 < \tau \le T_i \quad (4.18)$$

Storage phase:

$$\frac{\partial c_m^*}{\partial \tau} + \beta \frac{\partial c_{im}^*}{\partial \tau} = 0, \quad R > R_0 \;\&\; T_i < \tau \le T_i + T_s \quad (4.19)$$

Recovery phase:

$$\frac{\partial c_m^*}{\partial \tau} + \beta \frac{\partial c_{im}^*}{\partial \tau} = \frac{\phi}{2R}\left(\frac{\partial c_m^*}{\partial R} + \frac{\partial^2 c_m^*}{\partial R^2} \right), R > R_0 \;\&\; T_i + T_s < \tau \le T_i + T_s + T_e \quad (4.20)$$

Immobile domain:

$$\frac{\partial c_{im}^*}{\partial \tau} = c_m^* - c_{im}^*, \qquad R > R_0 \quad (4.21)$$

Correspondingly, the boundary and initial conditions become:

$$\begin{aligned} &\text{Injection phase}: \quad c_m^*(R \to \infty, \tau) = c_{im}^*(R \to \infty, \tau) = 1, \quad \left(c_m^* - \frac{\partial c_m^*}{\partial R} \right)\Big|_{R=R_0} = 0 \\ &\text{Recovery phase}: \quad c_m^*(R \to \infty, \tau) = c_{im}^*(R \to \infty, \tau) = 1, \quad \frac{\partial c_m}{\partial R}\Big|_{R=R_0} = 0 \end{aligned} \quad (4.22)$$

and

$$c_{m0}^{*} = \frac{c_{m0}(r)}{c_0}, \quad c_{im0}^{*} = \frac{c_{im0}(r)}{c_0} \quad (4.23)$$

Our definition of dimensionless groups follows the previous study for intermittent extraction of contaminant plume (Harvey et al., 1994). Other dimensionless systems are also available for mass transfer models (e.g., van Genuchten and Wierenga, 1976; Goltz and Oxley, 1991). The advantage of the defined dimensionless parameters is that the time is normalized by the mass transfer timescale, which is particularly useful for studying the storage phase. In addition, Equations (18) - (21) are also valid for linear rate-limited sorption processes by modifying dimensionless groups accordingly (Harvey et al., 1994).

4.1.3 Numerical Solution

Analytical solutions in Laplace domain have been derived for radial injection and extraction problems (e.g., Chen, 1985, 1986, 1987; Chen and Woodside, 1988; Moench, 1989, 1995; Goltz and Oxley, 1991; Huang and Goltz, 2006; Huang et al., 2010). Such analytical solutions have been used to analyze tracer tests in convergent and divergent radial flow fields (e.g., Novakowski, 1992; Moench, 1995; Becker and Charbeneau, 2000), decontamination by pumping with rate-limited sorption or mass transfer (e.g., Goltz and Oxley, 1991; Harvey et al., 1994), and single-well push-pull tracer tests (Huang et al., 2010). For the injection and recovery phase, the proposed ASR model is a combination of radial dispersion in convergent and divergent flow fields and rate-limited mass transfer, which can be readily solved by modifying the available solutions. For the storage phase, analytical solutions in time domain are given by (Harvey et al., 1994):

$$c_m^*(\tau) = -\frac{c_{im0}^* - c_{m0}^*}{1+\beta}\beta \exp[-(1+\beta)\tau] + \frac{\beta c_{im0}^* + c_{m0}^*}{1+\beta} \quad (4.24)$$

$$c_{im}^*(\tau) = \frac{c_{im0}^* - c_{m0}^*}{1+\beta} \exp[-(1+\beta)\tau] + \frac{\beta c_{im0}^* + c_{m0}^*}{1+\beta} \quad (4.25)$$

where c_{m0}^* and c_{im0}^* are the initial concentrations at the beginning of the storage phase. In addition, numerical codes, such as MT3DMS and SUTRA, are also available for modeling axisymmetric solute transport by adjusting transport parameters to account for the cylindrical geometry (Langevin, 2008). In the present research, we use MATLAB built-in PDE and ODE solvers to solve Equations (18) - (21), which yield satisfactory results comparing with analytical solutions.

4.1.4 Evaluation of ASR Performance

The performance of an ASR system is evaluated by the RE, which is defined as (Kimbler et al., 1975):

$$RE = \frac{V_r\left(c_m^*(R_0) < c_{crit}^*\right)}{V_i} \quad (4.26)$$

where c_{crit}^* is the critical concentration normalized by c_0, V_r is the volume of recovered water through the pumping well that satisfies the predefined standard, and V_i is the total volume of injected fresh water. Certainly, RE increases with c_{crit}^*, i.e., more water can be recovered for lower-standard quality requirements. We here assume $c_{crit}^* = 0.1$, which represents that the initial contaminant concentration is 10 times of the criterion. During

the recovery phase, if the extracted concentration becomes greater than c^*_{crit}, the pumping will be terminated because the extracted water will need further aboveground treatment.

Other than the critical concentration c^*_{crit}, which is a function of the initial contaminant concentration and the predefined criterion, RE is affected by both transport parameters, including dispersion and mass transfer coefficients, and ASR operational parameters, including durations of injection, storage and extraction phase and well flow rates. At a selected site where transport parameters are fixed and are a function of the hydrogeology, the optimization of ASR operational parameters is the major problem. Furthermore, in regions of stable seasonal fluctuations in freshwater resources availability, the durations of injection, storage and extraction phase are relatively constant and well pumping rates are the most flexible parameter to control. For simplicity, we assume $t_i = t_s = t_e$, i.e., equal durations of injection, storage and extraction phase, representing a 4-month time period for each phase for a yearly-based ASR cycle. To analyze the ASR performance at different hypothetical sites, we vary three dimensionless parameters: β, T_i and ϕ, in which β is controlled by the mass transfer capacity or the size of the immobile domain, T_i is influenced by the mass transfer timescale, i.e., the first-order mass transfer rate coefficient and the immobile porosity, given constant pumping periods, and ϕ is influenced by the well pumping rate, mass transfer coefficients and dispersivity.

4.2 Results and Discussion

4.2.1 Single ASR Cycle

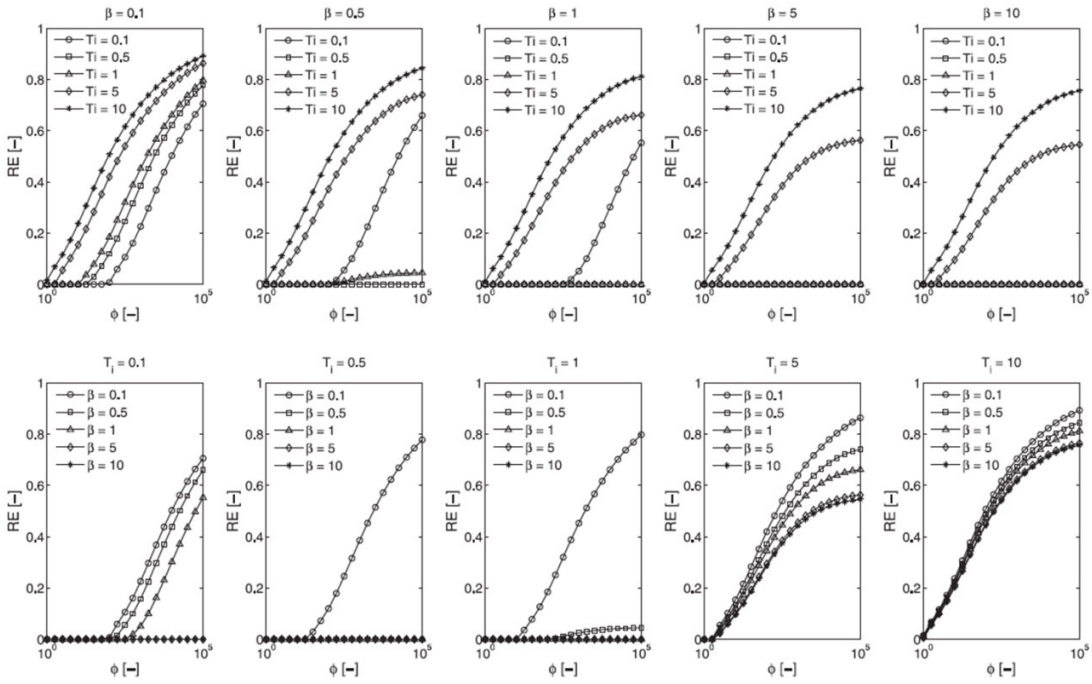

Figure 4.2 RE for a single ASR cycle at various mass transfer parameters and pumping operational parameters.

Figure 4.2 shows the RE of a single ASR cycle at different β, T_i and ϕ. The tested parameter ranges are: $\beta \sim 10^{-1} - 10^{1}$, $T_i \sim 10^{-1} - 10^{1}$, and $\phi \sim 10^{0} - 10^{5}$, in which $\beta = 0.1$ represents small portion of immobile domain (~9%) and $\beta = 10$ large portion of immobile domain (~91%) and $T_i = 0.1$ represents a large mass transfer timescale comparing with pumping periods and a small mass transfer rate coefficient and $T_i = 10$

represents a small mass transfer timescale and a large mass transfer rate coefficient. If we consider an aquifer thickness 20 m, $\alpha_L = 1$ m, and $\theta_m = 0.3$, the examined range of ϕ corresponds to the actual pumping rate $[0.0157\text{m}^3/\text{d},\ 1.57\times10^3\text{m}^3/\text{d}]$ for $T_i = 0.1$ and $[1.57\text{m}^3/\text{d},\ 1.57\times10^5\text{m}^3/\text{d}]$ for $T_i = 10$, respectively. The major information delivered by ***Figure 4.2*** is summarized in the following:

1) RE generally increases with the well pumping rate given β and T_i except for cases with zero RE.

2) In many combinations of β and T_i, RE remains zero, i.e., no recovered water satisfies the predefined standard, $c^*_{crit} = 0.1$, within the wide tested range of ϕ. However, no clear pattern of β and T_i can be observed for zero RE from ***Figure 4.2*** (the pattern will be explained in the next section).

3) At a small β, e.g., $\beta = 0.1$, RE increases with T_i at the same ϕ, implying a faster mass transfer rate yields a higher RE for a small immobile domain. However, such behavior is not consistent for all examined β. For example, at $\beta = 0.5$ and $\beta = 1$, the RE of $T_i = 0.1$ is greater than that of $T_i = 0.5$ and $T_i = 1$, indicating that the RE is not a monotonic function of T_i.

4) At a large T_i, e.g., $T_i = 10$, RE decreases with β, implying a larger immobile domain yields a lower RE for a fast mass transfer rate coefficient. At low T_is except those cases with zero RE, RE also decreases with β. However, at different low T_is, the cases of zero RE do not show a consistent pattern.

Zero and Non-zero RE

Understanding the pattern of cases with zero RE is an essential problem for ASR design because it identifies specific conditions inappropriate for ASR. According to the zero-gradient boundary condition at the well during the extraction phase, the concentration of extracted water is identical to the concentrations at adjacent locations. $RE = 0$ implies that after the storage phase the concentration at such adjacent locations are greater than c^*_{crit} so that no fresh water can be extracted. Consider such an adjacent point, R_0^+, with an infinitesimally small distance to the well boundary. During the injection phase, we assume that the concentration at this point will quickly change to zero as a result of fresh water flushing at a large flow rate. Thus, the immobile concentration history at this point during the injection phase is governed by the following equation:

$$\frac{\partial c^*_{im}\left(R_0^+\right)}{\partial \tau} = -c^*_{im} \quad (4.27)$$

which yields

$$c^*_{im}\left(R_0^+\right) = \exp(-\tau) \quad (4.28)$$

and the initial condition for the subsequent storage phase is:

$$c^*_{m0} = 0 \quad (4.29)$$

$$c^*_{im} = \exp\left(-T_i\right) \quad (4.30)$$

Substituting Equations (4.29) and (4.30) into (4.24) yields the concentration at the end of the storage phase:

$$c^*_m\left(R_0^+, T_i + T_s\right) = \frac{\beta}{1+\beta}\exp\left(-T_i\right)\left\{1 - \exp\left[-\left(1+\beta\right)T_s\right]\right\} \quad (4.31)$$

Thus, for a non-zero RE, the ASR system must satisfy

$$\frac{\beta}{1+\beta}\exp(-T_i)\{1-\exp[-(1+\beta)T_s]\} < c^*_{crit} \quad (4.32)$$

This is a simple relationship that can be applied to evaluate the applicability for a single ASR cycle. For the proposed case, $T_i = T_s$ and $c^*_{crit} = 0.1$, we have:

$$c^*_m(R_0^+, T_i + T_s) = \frac{\beta}{1+\beta}\exp(-T_i)\{1-\exp[-(1+\beta)T_i]\} < 0.1 \quad (4.33)$$

Figure 4.3 shows the contour lines of $c^*_m(T_s)$ as a function of β and T_i. The area contained by the thick contourline of 0.1 indicates the regions of β and T_i that will yield zero RE. All simulated cases in Figure 4.2 are shown by "+". There is no exception that all the cases with zero RE fall into the area contained by 0.1 contourline and all the cases with non-zero RE are located outside of this area. Thus, the simple inequality (4.32) provides an efficient approach for determining the likelihood of single ASR cycle being successful. Furthermore, inequality (4.32) gives operational guidance for ASR systems: (1) inequality (4.32) does not involve the well pumping rate, indicating that increasing the well pumping rate is not an effective way for improving the RE within a single ASR cycle at aquifers falling into the zero-RE area shown in Figure 4.3; and (2) there are two ways to convert a zero-RE case to a non-zero RE case by increasing the injection period, which yields a longer mass transfer duration to deplete contaminant in the immobile domain, and by decreasing the storage period, which yields a shorter mass transfer duration for the high concentration in the immobile domain entering the low-concentration mobile domain. Essentially, these approaches are to move the points vertically upward from inside the zero-RE area in Figure 4.3. In addition, if the

concentration at the end of the injection phase is greater than c^*_{crit}, decreasing the storage period is not effective. Finally, ***Figure 4.3*** also shows that a lower c^*_{crit} yields a larger zero-RE area. An aquifer with a fast mass transfer rate coefficient, i.e., a larger T_i, or a small immobile domain, i.e., a small β, is generally appropriate for ASR. Thus, for aquifers without mass transfer or with equilibrium (i.e., instantaneous) mass transfer, we can always have a positive RE.

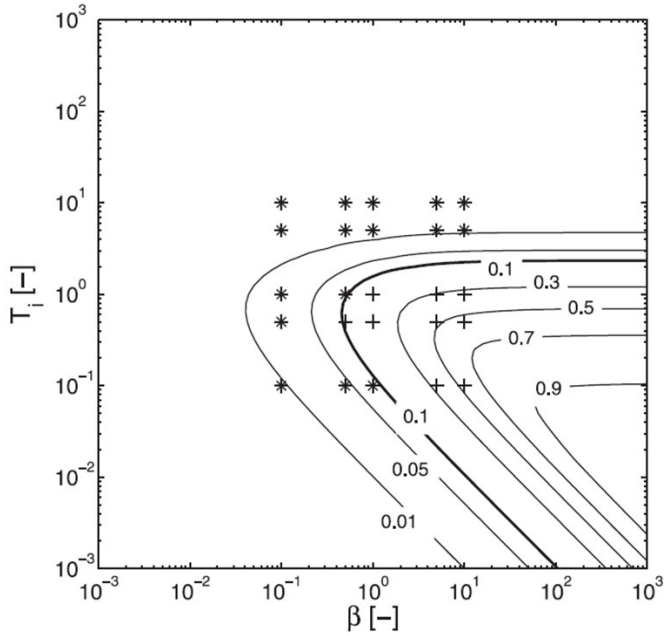

Figure 4.3 Concentration in the mobile domain after the storage phase for a single ASR cycle. Contour lines represent predefined concentration criteria. "+" indicates the numerical case with a zero RE and "*" indicates the case with a non-zero RE.

Effects of mass transfer parameters

Given the same ASR operational strategies, i.e., constant well flow rate q and phase durations (t_i, t_s and t_e), the RE is controlled by the mass transfer parameters, including capacity ratio β and mass transfer timescale τ_{im}, and the dispersivity α_L. According to the dimensionless groups, the effect of dispersivity is opposite to the well flow rate: a larger dispersivity yields a lower RE because more fresh water is contaminated due to enhanced mixing. In the following, we consider constant ASR operational parameters and dispersivity and examine the transferability of an ASR strategy to aquifers with different mass transfer parameters by varying β and T_i (Note T_i is controlled by τ_{im} for a constant t_i).

With the same flow rate and dispersivity, the RE is ultimately controlled by the mobile concentration at the adjacent points to the well boundary at the end of the storage phase, described by Equation (4.31). That is, a lower $c_m^*(T_s)$ yields a higher RE and a higher $c_m^*(T_s)$ a lower RE. Taking derivatives of Equation (4.33) with respect to β and T_i (We assume $T_i = T_s$), we have:

$$\frac{\partial c_m^*(R_0^+, T_i + T_s)}{\partial \beta} = \frac{1}{(1+\beta)^2}\exp(-T_i)\{1-\exp[-(1+\beta)T_i]\} + \frac{\beta T_i}{1+\beta}\exp(-T_i)\exp[-(1+\beta)T_i] > 0 \tag{4.34}$$

$$\frac{\partial c_m^*\left(R_0^+, T_i + T_s\right)}{\partial T_i} = \frac{\beta}{1+\beta}\{(2+\beta)\exp[-(2+\beta)T_i] - \exp(-T_i)\} \quad (4.35)$$

Thus, for a constant mass transfer timescale, $c_m^*\left(R_0^+, T_i + T_s\right)$ always increases with β, resulting in a decreasing RE as shown by ***Figure 4.2***. For a constant β, let $\frac{\partial c_m^*\left(R_0^+, T_s\right)}{\partial T_i} = 0$. We obtain a critical T_i,

$$T_{crit} = \frac{\ln(2+\beta)}{1+\beta} \quad (4.36)$$

And

$$\frac{\partial c_m^*\left(R_0^+, T_i + T_s\right)}{\partial T_i} > 0, \text{ if } T_i < T_{crit} \quad (4.37)$$

$$\frac{\partial c_m^*\left(R_0^+, T_i + T_s\right)}{\partial T_i} < 0, \text{ if } T_i > T_{crit} \quad (4.38)$$

Thus, the changing pattern of $c_m^*\left(R_0^+, T_i + T_s\right)$ with the mass transfer timescale or mass transfer rate coefficient is non-monotonic.

Figure 4.4 shows that T_{crit} decreases with β and the concentration gradient non-monotonically changes with T_i. ***Figure 4.4a*** identifies the specific cases shown in ***Figure 4.2***. For $\beta = 0.5$, $T_{crit} = 0.61$. Thus, ***Figure 4.2*** shows a decrease of RE from $T_i = 10$ to $T_i = 1$ (negative concentration gradient in ***Figure 4.4b***) and then an increase to $T_i = 0.1$ (positive concentration gradient in ***Figure 4.4b***). In fact, this non-monotonic behavior always occurs in the presence of mass transfer. Consider two limiting cases: one

with an extremely high T_i and the other nearly 0. The high T_i case represents a small mass transfer timescale or a very large mass transfer rate coefficient. Thus, the rate-limited mass transfer process becomes equilibrium and the transport problem may be described by an advection-dispersion equation with a retardation factor. On the other hand, the low T_i case implies a large mass transfer timescale or a very small mass transfer rate coefficient. In such cases, mass transfer may be neglected and the transport problem may be simplified into an advection-dispersion equation. Both limiting cases will yield high RE and T_{crit} is the turning point between them.

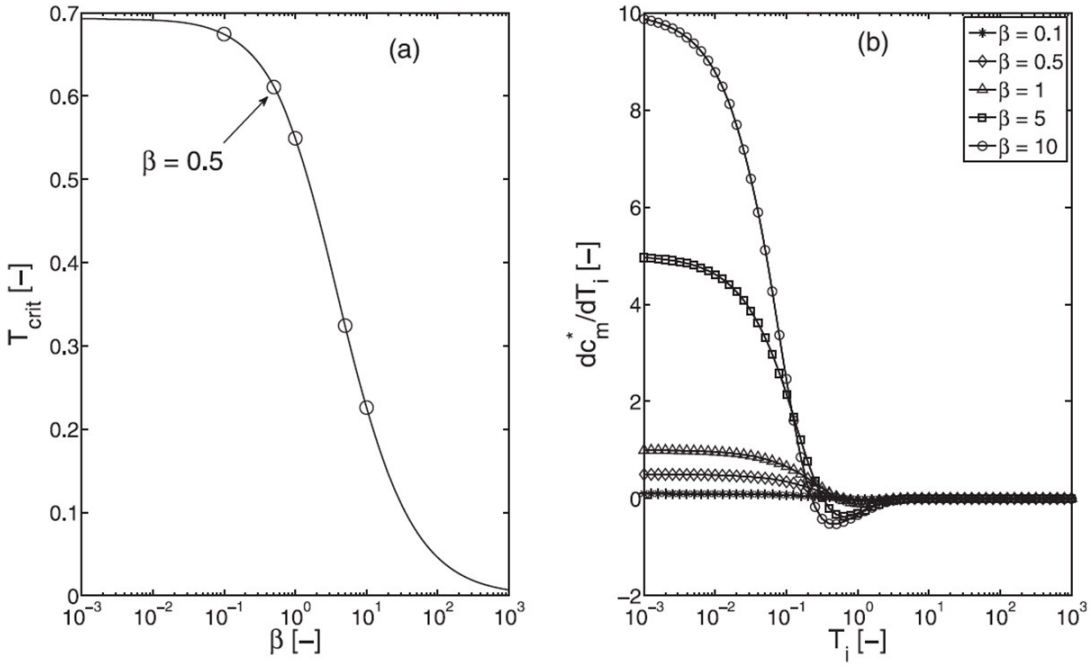

Figure 4.4 A critical timescale at different capacity ratio and sensitivity of concentration at the pumping well to the dimensionless timescale. (a) critical timescale; and (b) concentration gradient with respect to the injection duration.

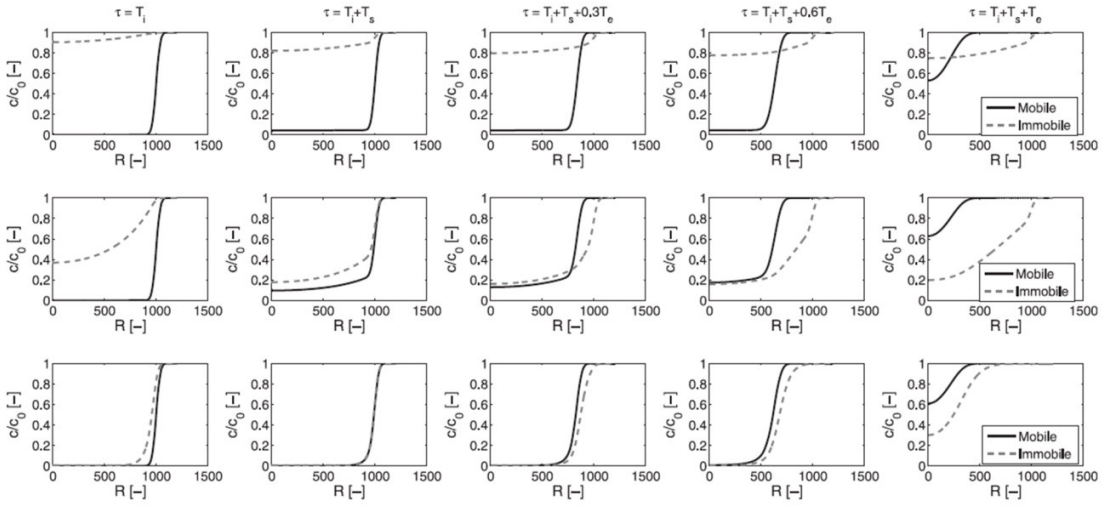

Figure 4.5 Concentration profiles during a single ASR cycle at different mass transfer timescale or injection duration.

Figure 4.5 shows the concentration profiles for the cases with $\beta = 0.5$ and different T_i at the same well flow rate and pumping durations. Here we do not terminate the recovery phase when the concentration is greater than the criterion in order to show the concentration profiles during a complete cycle. During the injection phase, the immobile domain serves as a contaminant source for all cases. However, immobile concentrations drop significantly for $T_i = 10$ due to fast mass transfer and remain high levels for $T_i = 0.1$ due to slow mass transfer. During the storage phase, the mobile concentration rebounds as a result of mass transfer from the immobile domain with higher

concentrations. By the end of the storage phase, mobile and immobile concentrations reach equilibrium for $T_i = 10$, while there remain small and significant concentration differences for $T_i = 1$ and $T_i = 0.1$, respectively. As a result of the equilibrium concentrations, the immobile domain always serves as a sink during the recovery phase for $T_i = 10$, which has positive impact on the RE. For $T_i = 1$, the immobile domain initially acts as a contaminant source and then as a sink after the plume front in the mobile domain passes. By contrast, the immobile domain mostly serves as a contaminant source near the pumping well for $T_i = 0.1$. However, such negative impact on the RE may not be significant because of slow mass transfer rates. That is, the overall effect on the RE is an integral result of both immobile domain functions and mass transfer rates. With the increase of T_i, the immobile domain transforms from a contaminant source to a sink, but the increased mass transfer rate may enhance the negative impact from the function as a contaminant source more than the positive impact from the function as a contaminant sink. The critical value of T_{crit} reflects a turning point when the immobile domain functions and mass transfer rate reach a certain balanced state.

Inequalities (4.37) and (4.38) also provide very useful operational guidance for ASR systems at sites where there is flexibility in injection times. At a site with $T_i > T_{crit}$, increasing the injection duration always improves the RE. However, if $T_i < T_{crit}$, one may need to increase the injection duration significantly in order to achieve an improved RE. A slight increase may even result in a lower RE. Furthermore, Equation (4.36) yields the range $(0, \ln 2)$ for T_{crit}, which implies that if the injection duration satisfies $t_i > \ln 2 \tau_{im}$ (or $t_i > 0.6931 \tau_{im}$), increasing pumping duration is an effective approach for improving RE.

$\ln 2\tau_{im}$ is known as the half life of mass transfer, i.e., the time period for the concentration to decay to one half of its initial value by assuming first-order decay. Thus, increasing pumping period is effective when the period is greater than the half life of mass transfer.

4.2.2 Multiple ASR Cycles

Figure 4.6 shows a typical concentration history at the pumping well during multiple ASR cycles for specified parameters. For injection phases, the concentration remains zero as a result of freshwater flushing. During the first three ASR cycles, no water can be recovered because at the end of the storage phase the concentration is greater than the predefined standard due to mass transfer from the immobile domain. Thus, recovery phases during the first three cycles actually function as storage phases. From the fourth cycle, the mobile concentration drops below the standard at the end of the storage phase so that fresh water can be extracted from the pumping well until the concentration rises to the standard. The withdrawal period during the recovery phase increases with the ASR cycle, representing that the RE increases with the ASR cycle. The immobile domain functions as a contaminant source at the early ASR cycles, and gradually transforms into a contaminant sink during the recovery phase. In general, the RE of an ASR system improves with ASR cycles and a zero-RE ASR system for a single cycle may eventually develop into an ASR system with a positive RE because multiple ASR cycles essentially increase the injection duration and total injected fresh water. Here, we are particularly interested in how many ASR cycles are necessary for such a transformation.

To determine the number of needed ASR cycles for a system to transform from a zero RE to a non-zero RE, we still focus on the adjacent points to the well boundary. Because no

water can be extracted for an ASR system with a zero RE, the actual storage duration is actually the sum of the designed storage phase and the recovery phase. By the end of such a cycle, the mobile and immobile concentrations are:

$$c^*_{m,n-1}\left(R_0^+, T_i + T_s + T_e\right) = c^*_{im0,n-1}\exp(-T_i)\frac{\beta}{1+\beta}\{1-\exp[-(1+\beta)(T_s+T_e)]\} \quad (4.39)$$

$$c^*_{im,n-1}\left(R_0^+, T_i + T_s + T_e\right) = c^*_{im0,n-1}\exp(-T_i)\frac{1}{1+\beta}\{\beta+\exp[-(1+\beta)(T_s+T_e)]\} \quad (4.40)$$

where $c^*_{m,n-1}$ and $c^*_{im,n-1}$ are the mobile and immobile concentrations during the $(n-1)$th ASR cycle, and $c^*_{im0,n-1}$ is the initial immobile concentration of the n th cycle. Thus, at the end of the storage phase of the n th cycle, we have:

$$\begin{aligned} c^*_{m,n}\left(R_0^+, T_i + T_s\right) &= \frac{\beta}{1+\beta}\exp(-T_i)\{1-\exp[-(1+\beta)T_s]\} \\ &\left\{\exp(-T_i)\frac{1}{1+\beta}\{\beta+\exp[-(1+\beta)(T_s+T_e)]\}\right\}^{n-1} \end{aligned} \quad (4.41)$$

A non-zero RE for the n th cycle requires:

$$c^*_{m,n}\left(R_0^+, T_i + T_s\right) < c^*_{crit} \quad (4.42)$$

By assuming $T_i = T_s = T_e$, we have:

$$\begin{aligned} c^*_{m,n}\left(R_0^+, T_i + T_s\right) &= \frac{\beta}{1+\beta}\exp(-T_i)\{1-\exp[-(1+\beta)T_i]\} \\ &\left\{\exp(-T_i)\frac{1}{1+\beta}\{\beta+\exp[-2(1+\beta)T_i]\}\right\}^{n-1} < c^*_{crit} \end{aligned} \quad (4.43)$$

which yields

$$n > 1 + \left\{ -T_i + \ln\left[\frac{1}{1+\beta} \left\{ \beta + \exp\left[-2(1+\beta)T_i \right] \right\} \right] \right\}^{-1} \qquad (4.44)$$
$$\ln\left\{ \frac{1+\beta}{\beta} \frac{\exp(T_i)}{1-\exp\left[-(1+\beta)T_i \right]} c^*_{crit} \right\}$$

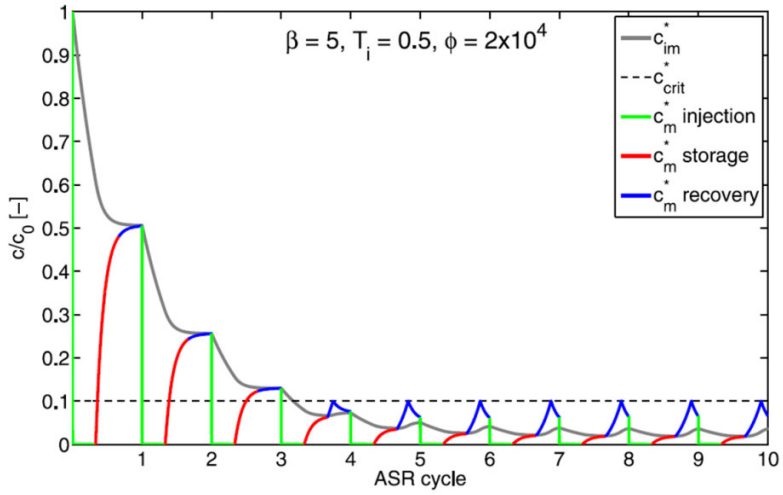

Figure 4.6 Concentration history at the pumping well for multiple ASR cycles.

Figure 4.7 shows the areas with zero RE and non-zero RE delineated by the contourlines of the mobile concentration at the end of the storage phase of the n th cycle. The subplot of cycle 1 is identical to ***Figure 4.3***. With the increase of ASR cycles, the area with zero RE, i.e., the area contained by the contourline of 0.1 becomes smaller and more tested cases, "+" symbols, fall outside of the area. At cycle 7, all the tested cases, except the one

with $\beta = 10$ and $T_i = 0.1$, should have non-zero RE at a large pumping rate. In addition, the area with zero RE shrinks with ASR cycles, but the shape of the contourlines remains similar, indicating that the effects of mass transfer and operational parameters on multiple ASR cycles may be similar to those identified in the single ASR cycle.

Actually, taking derivatives of Equation (4.43) with respect to n, β and T_i, respectively, we can also obtain $\frac{\partial c^*_{m,n}\left(R_0^+, T_i+T_s\right)}{\partial n} < 0$ for $n \geq 2$, $\frac{\partial c^*_{m,n}\left(R_0^+, T_i+T_s\right)}{\partial \beta} > 0$, and a critical value, $T_{crit}(n,\beta)$, by setting $\frac{\partial c^*_{m,n}\left(R_0^+, T_i+T_s\right)}{\partial T_i} = 0$. Thus, the RE improves with ASR cycles, decreases with capacity ratio, and exhibits non-monotonic behavior in terms of mass transfer timescale and the injection duration. ***Figure 4.8*** shows that the critical timescale decreases with ASR cycle and all cases with different β approach a low value of 0.0405 according to our numerical solution. In addition, T_{crit} is a monotonic, decreasing function of β at the first cycle, a non-monotonic function at intermediate cycles, and a monotonic, increasing function at late cycles.

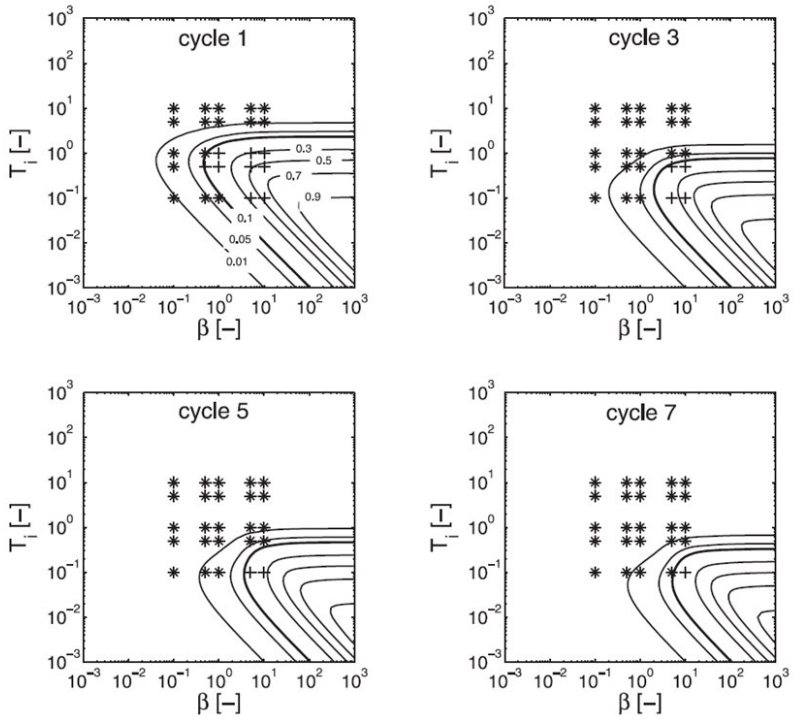

Figure 4.7 The evolution of zero-RE cases with ASR cycles as a function of mass transfer parameters.

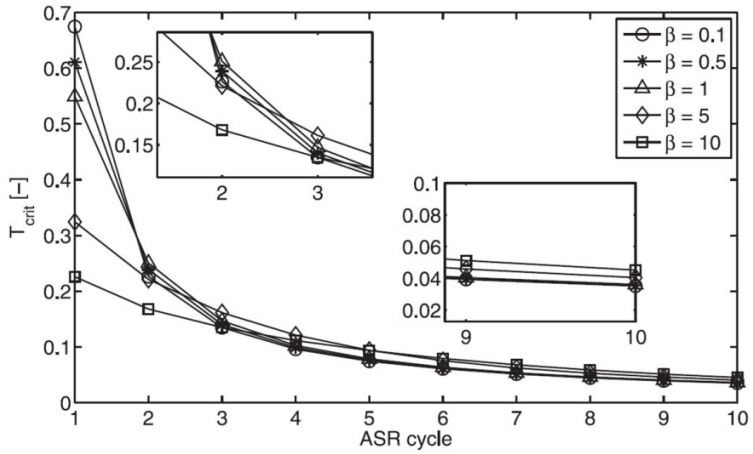

Figure 4.8 A critical timescale at multiple ASR cycles.

Figure 4.9 shows the contoured areas for the required cycles to achieve a non-zero RE. For $\beta \leq 1$ or $T_i > 1$, all the tested cases should expect a non-zero RE within two ASR cycles. For a large β and a small T_i, e.g., $\beta = 5$ and $T_i = 0.1$, more ASR cycles are required. In particular, the case with $\beta = 10$ and $T_i = 0.1$ requires more than 10 cycles.

Figure 4.10 shows the numerically-simulated RE for $\beta = 5$ at a constant ϕ. For large mass transfer rate coefficients, i.e., $T_i = 5$ and 10, the first ASR cycle has a non-zero RE. For $T_i = 1, 0.5, \text{and } 0.1$, it requires 2, 4, and 7 ASR cycles, respectively. The result is consistent with that shown by ***Figures 4.6, 4.7 and 4.9***.

The above analyses delineate between zero RE and non-zero RE and determine the number of ASR cycles required to sufficiently "flush" the subsurface and move from zero RE to non-zero RE. However, in practical ASR applications, a low RE of, say, 5% may be considered effectively a failure despite being non-zero. Thus, the number of ASR cycles determined here may serve as an indicator for broad comparisons between hydrogeological and operational combinations (i.e. those that are likely to be fairly quickly flushed versus those which are likely to require many flushing cycles), and may not be taken as a strict predictor of how many cycles/years before an operation becomes "viable".

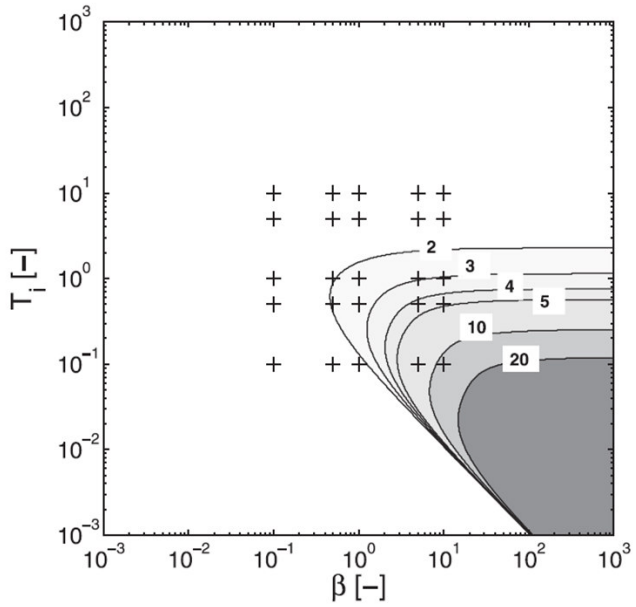

Figure 4.9 The required number of ASR cycles for achieving a nonzero RE.

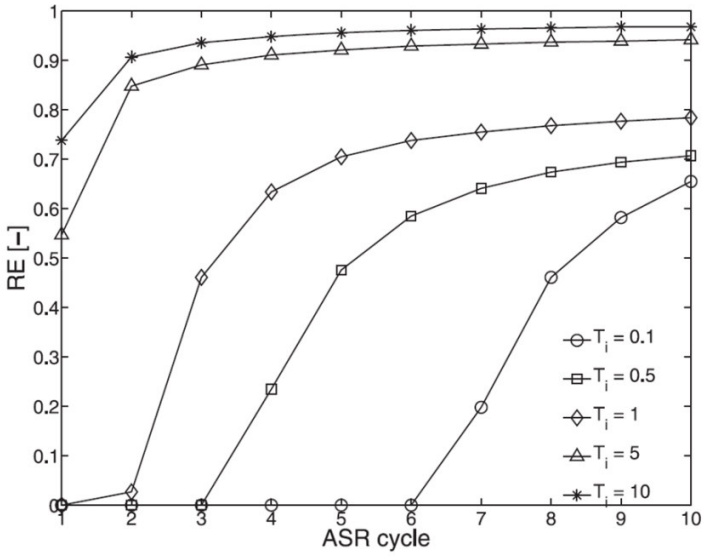

Figure 4.10 The RE improvement with ASR cycles for $\beta = 5$ and $\phi = 1 \times 10^5$.

4.3 Summary and Conclusion

ASR is an effective strategy for sustainable management of water resources, but its efficiency may be limited by kinetic mass transfer caused by contaminant sorption and dual-domain behavior of subsurface media. A numerical model is developed for simulating ASR performance by combining the convergent and divergent dispersion models with a first-order mass transfer model. More importantly, by analyzing the concentration history at the pumping well, simple relationships between mass transfer parameters and ASR operational parameters are derived for understanding ASR performance and improving its efficiency. Several practical and useful contour figures are generated based on such relationships for delineating the ranges of mass transfer parameters and the necessary ASR cycles that may yield effective and efficient ASR performance. The developed numerical model and analyzed results provide very useful and practical guidance for determining a potential ASR site with mass transfer limitations and optimizing ASR operations. The main conclusions drawn from the analysis are as follows:

Increasing well pumping rates may yield higher RE for a single ASR cycle, but usually does not transform an ASR system from zero RE to non-zero RE.

RE decreases with the mass transfer capacity ratio, i.e., a large immobile domain or sorption capacity often undermines the ASR efficiency.

The effect of mass transfer rate coefficients and the injection period on the ASR efficiency is non-monotonic. A critical value, T_{crit}, may be defined for both single and multiple ASR cases. When the injection period is greater than such a critical value,

increasing injection period results in a higher RE. Contrarily, when the injection period is less than the critical value, increasing the injection period may even yield a lower RE.

ASR efficiency improves with multiple ASR cycles and the required cycles for a zero-RE ASR in a single cycle to transform into a non-zero RE is derived as a function of mass transfer parameters and the durations of injection, storage and recovery phases.

The immobile domain may function as a contaminant source or sink or both during the recovery phase. In aquifers with large capacity ratio and slow mass transfer, the immobile domain may serve as a long-term contaminant source that causes negative impacts on ASR efficiency. By contrast, in aquifers with small capacity ratio and fast mass transfer, concentrations in the mobile and immobile domain may quickly reach equilibrium at the end of the storage phase so that the immobile domain mostly serves as a contaminant sink, which improves the RE. With the increase of ASR cycles, the immobile domain will eventually transform from a contaminant source to a sink.

Our analyses and results are based on the transport model with both a mobile and an immobile domain with adjustable mass transfer parameters, which may represent an aquifer with high and low permeability zones and mass transfer between these zones. As stated in the introduction and conceptual model, many other mechanisms may significantly influence the ASR performance, such as density effects and regional flow. Further modeling work is required to study the combined effects of these mechanisms and rate-limited mass transfer in more realistic geological settings.

CHAPTER 5

EFFECTS OF HYDROGEOLOGICAL AND OPERATIONAL PARAMETERS ON ASR RE IN HOMOGENEOUS ISOTROPIC SALINE AQUIFERS

This chapter will apply the numerical simulation to discuss the influence of key hydrogeological and operational parameters on the ASR system by conventional fully-penetrating wells in coastal aquifers. The investigation is based on one cycle ASR system. We assume a basic field-scale numerical model named as the base case (BC) to simulate the typical ASR system in a homogeneous, isotropic, confined aquifer. The parameters of the BC provide a comparison standard for various simulations when evaluating the RE. We assume the groundwater velocity is axisymmetric about the well, and promptly reaches the steady state during each phase (Harvey et al., 1994). It is well known that the typical one cycle ASR system includes three phases: injection, storage and extraction.

5.1 Numerical Methods

5.1.1 Conceptual Model

Lowry and Anderson (2006) proposed that ASR can be best simulated using coupled numerical ground water flow and transport models. In addition, Langevin (2008) proved that modified versions of common computer programs such as MODFLOW, MT3DMS, and SEAWAT that use Cartesian geometry can accurately simulate axially symmetric

ground water flow and solute transport by modifying several main input parameters to account for the increase in flow area with radial distance from the pumping well.

In this study, numerical models are solved by a graphic user interface software calling Groundwater Vista Version 5.20 (GWV). GWV is specialized to solve the three-dimensional groundwater flow and transport modeling problem. GWV is essentially a combination software including MODFLOW, MT3DMS, SEAWAT-2000 and so on contributed by USGS, whose goal is to make a simple visualized combined program to solve various numerical coupled flow and solute transport problems. It is proved that the axisymmetric model is much faster than an equivalent three-dimensional Cartesian model for some particular problems such as upconing problem (Langevin, 2008). It confirms that the axisymmetric model is suitable to solve the ASR problem analogous to the upconing problem. Therefore, we prefer the axisymmetric coordinate implementing the ASR numerical simulation.

Figure 5.1 shows the conceptual model of typical axisymmetric ASR systems with a fully-penetrating pumping well installed in a confined, homogeneous, isotropic coastal aquifer with a uniform thickness. By neglecting regional flow, the three-dimensional (3D) domain is modeled by a two-dimensional (2D) axisymmetric cross-section with the vertical axis of rotation located at the pumping well. The 3D Cartesian coordinate (x, y, z) is simplified to the 2D axisymmetric geometry (r, z). The radius r represents the distance to the pumping well. The pumping well (injection/extraction) is set at the left boundary while the constant seawater level is assumed at the right boundary. At the beginning, we suppose that the whole domain is full of seawater. For simplicity, we assume the injection flowrate is the same as the extraction flowrate. The RE is evaluated by setting a criterion

of the average concentration of extracted water at the pumping well, such as the U.S. EPA potable-water standard. In this research, we choose 1% of the original groundwater concentration as the threshold concentration.

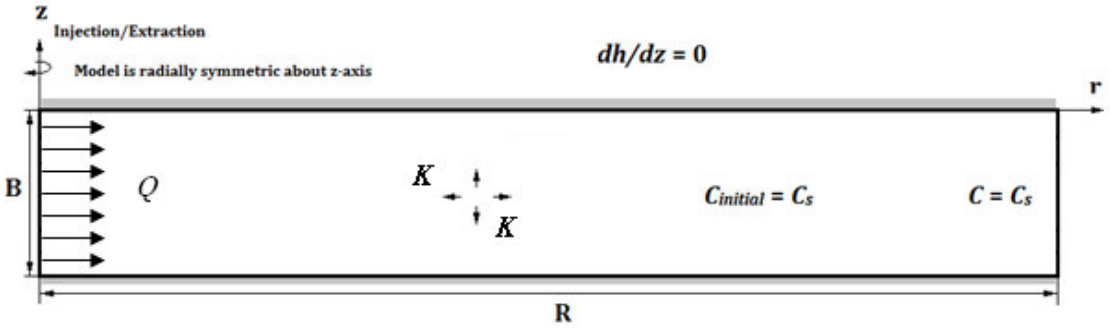

Figure 5.1 Conceptual model for axisymmetric ASR in coastal aquifers

5.1.2 Governing Equations

In a homogeneous, isotropic confined aquifer, the governing equation for the variable-density groundwater flow in terms of freshwater head is described by:

$$\rho S_f \frac{\partial h_f}{\partial t} + \theta \frac{\partial \rho}{\partial t} = \nabla \cdot \left[\rho K \left(\nabla \cdot h_f + \frac{\rho - \rho_f}{\rho_f} \nabla z \right) \right] \quad (5.1)$$

where t [T] is the time; z [L] is the vertical coordinate directing upward; S_f [L^{-1}] is the equivalent freshwater storage coefficient; θ [-] is the effective porosity; K [LT^{-1}] is the equivalent freshwater hydraulic conductivity; h_f [L] is the equivalent freshwater head; ρ [ML^{-3}] is the fluid density; and ρ_f [ML^{-3}] is the freshwater density.

The initial condition is a uniform hydraulic head distribution over the domain, i.e., no regional flow. The boundary condition at the well is determined by assuming that flow across the screen into the well is equal to the pumping rate :

$$2\pi r_w Kb\left(\frac{\partial h_f}{\partial r}\right)_{r=r_w} = Q \quad (5.2)$$

where r_w [L] is the well radius; b [L] is the well screen length. For a fully penetrating well, b is equal to the aquifer thickness.

The governing equation for solute transport is given by:

$$\frac{\partial c}{\partial t} = \nabla \cdot (\mathbf{D}\nabla \mathrm{c} - \mathbf{v}\mathrm{c}) \quad (5.3)$$

where c [ML^{-3}]is the dissolved solute concentration; **v** [LT^{-1}] is the pore water velocity; and **D** [L^2T^{-1}] is the hydrodynamic dispersion coefficient tensor. The domain has an initial salt concentration of the original groundwater; and the concentration gradient at the well boundary is zero.

Equations (5.1) and (5.3) are coupled by the relationship between the fluid density and salt concentration, which is described by a simple linear function:

$$\rho = \rho_f + \overline{\varepsilon} c \quad (5.4)$$

where $\overline{\varepsilon}$ [-] is a dimensionless constant with a value of 0.7143 for salt concentrations ranging from zero to that of sea water.

Equations (5.1) and (5.3) are solved in cylindrical coordinates using the density-dependent groundwater flow code, SEAWAT-2000 (Langevin et al., 2003). To simulate

the axisymmetric flow and transport, several input parameters are adjusted to account for the radial flow area change from the pumping well, which was successfully tested for push-pull and saltwater upconing problems (Langevin, 2008).

5.1.3 Evaluation of ASR Performance

The performance of an ASR system is evaluated by the RE, which is defined as:

$$RE = \frac{V_r(C^*_{r_w} < C^*_{crit})}{V_t} \quad (5.5)$$

where $C^*_{r_w}$ is the salt concentration at the extraction well normalized by C_s, $C^*_{r_w}$ is the critical concentration, V_r is the volume of recovered water through the pumping well that satisfies the predefined standard, and V_t is the total volume of injected fresh water. Certainly, RE increases with C^*_{crit}, i.e., more water can be recovered for lower-standard quality requirements. We here assume C^*_{crit} = 0.01, i.e., 1% of the seawater concentration. During the recovery phase, if the extracted concentration exceeds C^*_{crit}, the pumping will be terminated because the extracted water will need further aboveground treatment.

5.1.4 Model Parameters

Other than the critical concentration C^*_{crit}, which is a function of the initial salt concentration and the predefined criterion, RE is affected by both hydrogeological and transport parameters and ASR operational parameters. ***Table 5.1*** summarizes the hydrogeological, transport and operational parameters in a base case (BC) numerical model, which serves as the base model for the subsequent sensitivity analysis to

investigate the effects of various hydrogeological conditions, transport and operational parameters. The selected base model parameters are similar to the parameters used in previous studies (Ward et al., 2007). The ASR aquifer is considered as a coastal aquifer with the original salt concentration of the sea water. At a selected site, ASR operational parameters are the parameters to be varied, including the well pumping rates, injection, storage and extraction durations and the well penetration thickness for partially penetrating extraction wells. For the BC model, we consider the regions of stable seasonal fluctuations in freshwater resources availability. For simplicity, we assume a 3-month injection, 6-month storage and 3-month extraction durations, representing a yearly-based ASR cycle. To analyze the ASR performance at different hypothetical sites, we vary both hydrogeological and transport parameters.

5.1.5 Dimensional Analysis

The RE is influenced by almost all parameters listed in ***Table 5.1***. By defining the By defining the repeating variables, ρ_f, K and B. ***Table 5.2*** lists the primary dimensionless parameters that will be studied. To simplify the analysis, we focus on parameters that are more variable in reality in the following sensitivity analysis. For hydrogeological and transport parameters, we consider $\rho_s{}^*$, $\alpha_L{}^*$ and $\alpha_T{}^*$, which correspond to various original salt concentration and dispersivities. For ASR operational parameters, we vary Q^*, $T_i{}^*$, $T_s{}^*$ and b^*. Because of the relationship $V_t{}^* = Q^* \cdot T_i{}^*$, the total injection volume varies with the pumping rate and injection duration. Thus, the RE for one cycle ASR system can be expressed by a function consisted of 10 normalized dimensionless parameters,

$$RE = \int (\rho_s^*, \alpha_L^*, \alpha_T^*, S_s^*, Q_i^*, Q_e^*, T_i^*, T_s^*, V_t^*, h^*) \quad (5.6)$$

Table 5.1 Geometrical, hydrogeological and transport parameters used for BC model

BC Model Parameter	Variable	Value
Aquifer Thickness (m)	B	50
Domain Radius (m)	L	370
Seawater/Freshwater Level (m)	h_s / h_f	50
Initial Ambient/Salt Water Salinity (g kg^{-1})	C_i / C_s	35
Injected Water Salinity (g kg^{-1})	C_w	0
Effective Porosity (-)	θ	0.3
Molecular Diffusivity (m^2 d^{-1})	D_m	0
Specific Storage (m^{-1})	S_s	0.005
Hydraulic Conductivity (m d^{-1})	K	5
Longitudinal Dispersivity (m)	α_L	1
Transverse Dispersivity (m)	α_T	0.1
Freshwater Density (kg m^{-3})	ρ_f	1000
Seawater Density (kg m^{-3})	ρ_s	1025
Injection/Extraction Flowrate (m^3 d^{-1})	Q_i / Q_e	4000 / -4000
Injection Duration (day)	T_i	90
Storage Duration (day)	T_s	180
Total Injection Volume (m^3)	V_t	360000
Extraction Thickness (m)	h	50

Table 5.2 Primary dimensionless parameters

Dimensionless Parameter	Definition
Hydrogeological and transport parameters	
Saltwater density	$\rho_s^* = \frac{\rho_s}{\rho_f}$
Salt concentration	$c^* = \frac{c}{c_s}$
Specific Storage	$S_s^* = S_s B$
Longitudinal dispersivity	$\alpha_L^* = \frac{\alpha_L}{B}$
Transverse dispersivity	$\alpha_T^* = \frac{\alpha_T}{B}$
ASR operational parameters	
Injection/Extraction flow rate	$Q^* = \frac{Q}{KB^2}$
Injection duration	$T_i^* = \frac{T_i K}{B}$
Storage duration	$T_s^* = \frac{T_s K}{B}$
Total injection volume	$V_t^* = \frac{V_t}{B^3}$
Extraction well screen thickness	$b^* = \frac{b}{B}$

5.1.6 Test of Dimensionless Groups

To verify the flexibility and accuracy of dimensionless groups for the RE of one cycle ASR system, we can vary values of independent dimensions to observe the RE results.

According to Equation (5.6), the RE function consists of 10 dimensionless parameters in terms of 3 independent dimensions (i.e. B [L], K [L T^{-1}] and ρ_f [M L^{-3}]). In reality, the ratio of freshwater density ρ_f [M L^{-3}] and the seawater density ρ_s [M L^{-3}] keeps constant. As a result, it makes little sense to change ρ_f for testing the dimensionless groups due to its invariability. By applying the fully-penetrating well, the extraction thickness h [L] keeps invariant to neglect. Furthermore, we simply suppose that the injection and

extraction flowrate Q_i and Q_e [L^3 T^{-1}] is identical since the variation tendency is the same for testing the dimensionless groups and we choose Q_i^* on behalf of. As set forth, the influence of V_t [L^3] is established on the combined action of Q_i [L^3 T^{-1}] and T_i [T]. The contribution of V_t [L^3] for RE dimensionless tests can be more specifically represented by which of Q_i [L^3 T^{-1}] and T_i [T]. So we choose Q_i^* and T_i^* on behalf of. The dimensionless RE function for tests can be simplified as

$$RE = f(\alpha_L^*, \alpha_T^*, S_s^*, Q_i^*, T_i^*, T_s^*) \quad (5.7)$$

In which, the RE is the function controlled by 6 dimensionless parameters in terms of 2 independent dimensions (i.e. *B* [L] and *K* [L T^{-1}]). The different cases of parameter values are detailed in ***Table 5.3***.

There are total 13 cases for dimensionless group tests. Case 1 is the BC. We increase *B* [L] values and keep *K* [L T^{-1}] the same as Case 1 from Case 2 to 4. Then we keep *B* [L] invariant as Case 1 but increase *K* [L T^{-1}] from Case 6 to 9. For Case 10 and 13, the ratio of *B* [L] and *K* [L T^{-1}] is constant. For Case 11 and 12, we take the double-half rule. To be specific, we take half *B* [L] but double *K* [L T^{-1}] for Case 11 and double *B* [L] but half *K* [L T^{-1}] for Case 12 both by contrast with Case 1. We can observe the RE results of different groups. Also, the mean and standard deviation for the RE can be calculated to express the relatively small fluctuation by the fully-penetrating well. Namely, the dimensionless groups we defined are rational.

Table 5.3 Different parameters testing cases

Case	B (m)	K (m d^{-1})	α_L (m)	α_T (m)	S_s (m^{-1})	Q_i (m^3 d^{-1})	T_i (d)	T_s (d)	RE
1	50	5	1	0.1	0.005	4000	90	180	18.6%
2	25	5	0.5	0.05	0.01	1000	45	90	18.0%
3	40	5	0.8	0.08	0.00625	2560	72	144	18.5%
4	80	5	1.6	0.16	0.003125	10240	144	288	17.9%
5	100	5	2	0.2	0.0025	16000	180	360	17.6%
6	50	1.25	1	0.1	0.005	1000	360	720	18.7%
7	50	2.5	1	0.1	0.005	2000	180	360	18.6%
8	50	10	1	0.1	0.005	8000	45	90	18.4%
9	50	20	1	0.1	0.005	16000	22.5	45	18.2%
10	25	2.5	0.5	0.05	0.01	500	90	180	18.2%
11	25	10	0.5	0.05	0.01	2000	22.5	45	18.3%
12	100	2.5	2	0.2	0.0025	8000	360	720	17.6%
13	100	10	2	0.2	0.0025	32000	90	180	17.6%
Mean									18.2%
Std.									0.4%

5.2 Illustrative Example

Figure 5.2 (a), (b), (c) and ***(d)*** respectively show the standardized concentration distribution and contour lines at the phase of injection end (90 days), storage end (270 days), extraction at the breakthrough point (276.7 days, i.e. the moment when the salinity of recovered water reaches the criterion 0.35g/kg), and extraction end (360 days). The RE of BC can be calculated by Equation (5.5), which is 18.6%.

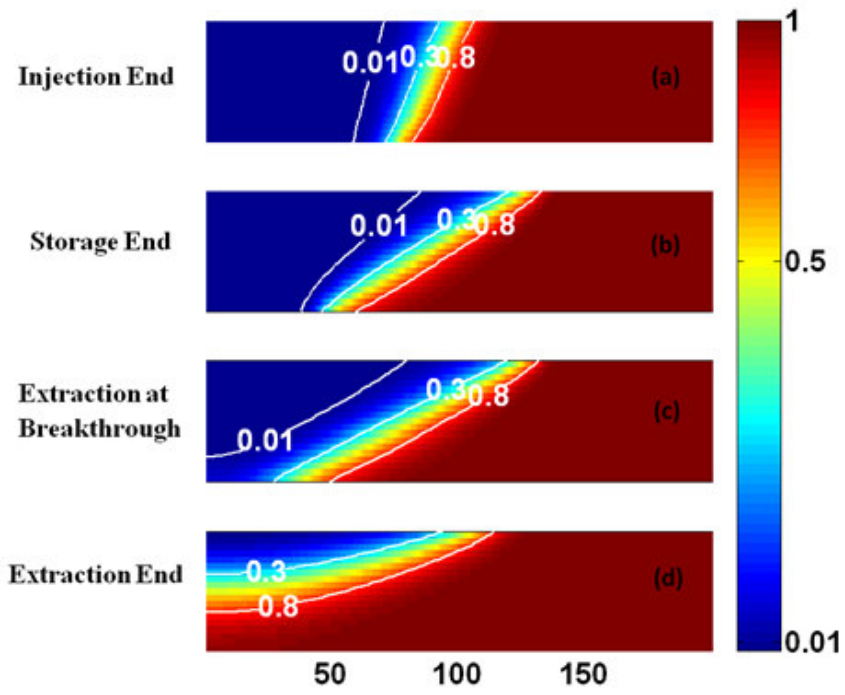

Figure 5.2 Standardized concentration distribution and contour line of BC for one cycle ASR system

During the injection phase, freshwater is injected into the aquifer and a concentration front moves away from the pumping well. The freshwater-saltwater interface may slightly tilt due to density gradient. During the storage phase, no flow occurs but the interface is further tilted by density gradient. It is clear that the mixing zone exaggerates at the end of storage. During the recovery phase, stored water is extracted via the same pumping well and the concentration front moves toward the pumping well. At the breakthrough point, the contour line "0.01" reaches the pumping well, reminding that we cannot recover more freshwater after this moment. At the end of extraction, the freshwater-saltwater interface is tilted most by extraction force and density gradient. The mixing zone expands and the pumping well is intruded by high concentrated saltwater.

5.3 Sensitivity Analysis

5.3.1 Hydrogeological Parameters Analysis

It is necessary and significant to well understand the influence of hydrogeological parameters on the RE for one cycle ASR system, although the hydrogeological parameters as the aquifer's own properties cannot be changed for one cycle ASR system in the actual field.

Seawater density ρ_s [M L^{-3}] / Seawater salinity [g kg^{-1}]:

The salt water salinity C_s [-] is corresponding to the seawater density ρ_s [M L^{-3}]. So we can vary different C_s [-] to investigate the RE. We assume the analysis based on the normal temperature as 20˚C. The conversion from C_s [-] to ρ_s [M L^{-3}] is corresponding in ***Table 5.4***. The threshold criterion of extraction water is also defined as 1% of the ambient salinity. In this study, C_s [-] varies from low to high accompanied by the initial ambient salinity C_i [-] and we keep all other parameters the same as BC. 5 representative cases are set and Case 3 is the BC. ('*': ppt is the abbreviation of part per thousand.)

Table 5.4 Seawater salinity and density conversion, salinity criterion

Case No.	C_s/C_i (ppt*)	ρ_s (kg m^{-3})	C_s Criterion (ppt)	RE
1	5	1002	0.05	52.2%
2	20	1013	0.20	34.3%
3	35	1025	0.35	18.6%
4	50	1036	0.50	8.9%
5	65	1048	0.65	3.1%

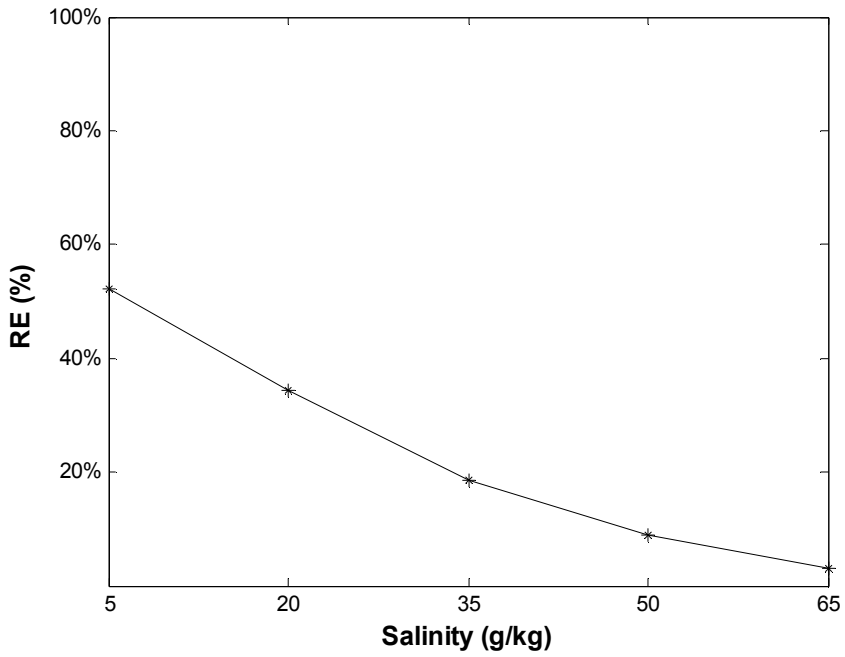

Figure 5.3 RE variation as salinity by FPW

Figure 5.3 also shows the numerical simulation RE results as the variation of salinity. We can clearly observe that the high salinity is harmful to the RE by applying the fully-penetrating well for one cycle ASR. This satisfies the conventional comprehension of the RE variation regulation of one cycle ASR system (e.g. Ward et al., 2007). The lower C_s implying the weaker density effects leads to the less tilting mixing zone. Undoubtedly, if the slope of mixing zone is not sharp enough, we can extract more freshwater from the well.

Specific storage S_s [L^{-1}]:

In this study, the numerical simulation is based on simulating axisymmetric groundwater flow and solute transport by adjusting several input parameters to account for the increase

in flow area with radial distance from the injection or extraction well (Langevin, 2008). S_s [L^{-1}] is one of main input parameters necessary to be modified. Moreover, S_s [L^{-1}] expresses the aquifer's own capability of releasing groundwater from storage due to the depressurization. It plays a significant role in 3D groundwater transport model analysis. In reality, there is a wide range of S_s [L^{-1}] values on the basis of different orders of magnitudes. We set S_s [L^{-1}] respectively as 0.0001, 0.001, 0.005 & 0.01 m^{-1} in accordance with possible cases. ***Figure 5.4*** exhibits the RE variation results as S_s [L^{-1}]. We can observe that, the big specific storage is helpful to the RE by applying fully-penetrating wells (FPW) in the homogeneous, isotropic aquifer for one cycle ASR.

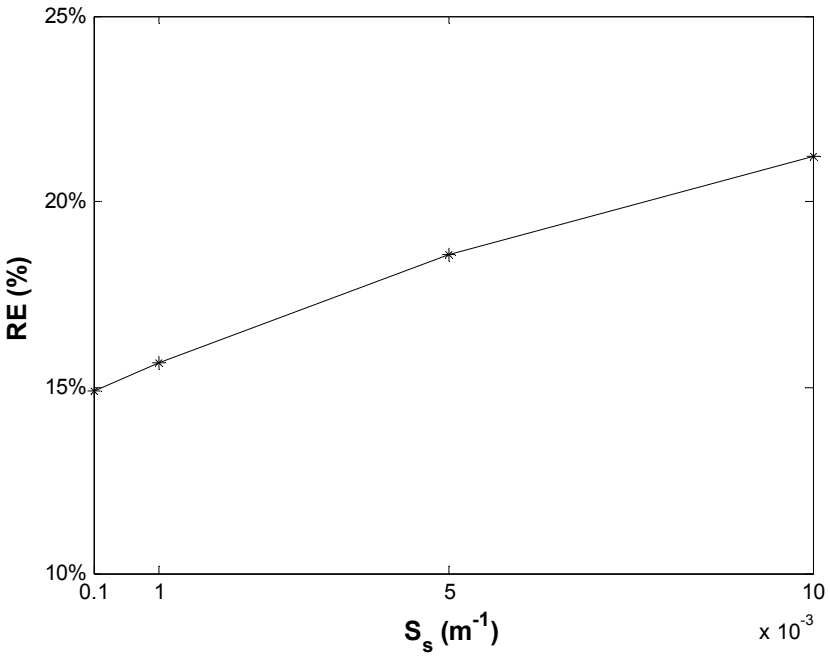

Figure 5.4 RE variation as specific storage by FPW

Aquifer thickness *B* [L]:

We define the aquifer thickness *B* [L] as one of the independent basic dimension variables in this study. In most previous studies, the aquifer thickness *B* [L] is usually set as an invariant variable, though it is without doubt that the RE for one cycle ASR system is varied when the aquifer thickness *B* [L] is distinct. We take 7 different *B* [L] respectively as 20, 30, 40, 50, 60, 80 and 100 m concerning common actual cases. The only variable here is the aquifer thickness *B* [L], and other parameters are invariant as the BC. ***Figure 5.5*** exhibits the RE variation results as *B* [L]. We can observe that, the deep thickness is harmful to the RE by applying fully-penetrating wells in the homogeneous, isotropic aquifer for one cycle ASR.

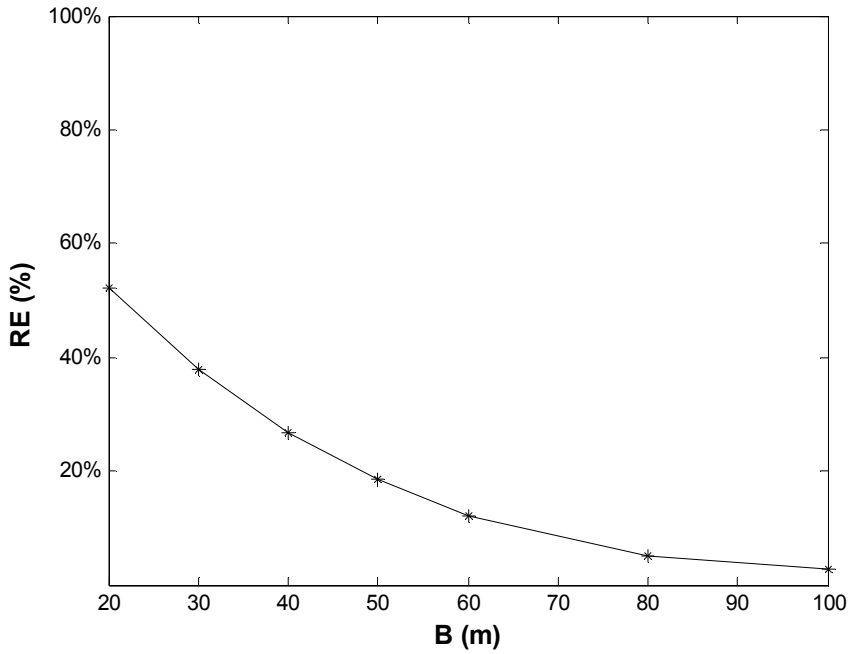

Figure 5.5 RE variation as thickness by FPW

Hydraulic conductivity *K* [L T^{-1}]:

Hydraulic conductivity *K* [L T^{-1}] is regarded as one of the most important aquifer parameters in the groundwater transport process. *K* [L T^{-1}] expresses the capability of transmitting groundwater in the subsurface transport. We define *K* [L T^{-1}] as an independent basic dimension variable in this study. We have some preliminary cognition of *K* [L T^{-1}] in terms of the previous study. Ward et al. (2007) concluded that high hydraulic conductivity would exacerbate the density effects. ***Figure 5.6*** shows the RE results as the variation of *K* [L T^{-1}]. We can find that, the high hydraulic conductivity is harmful to the RE by applying fully-penetrating wells in the homogeneous, isotropic aquifer for one cycle ASR.

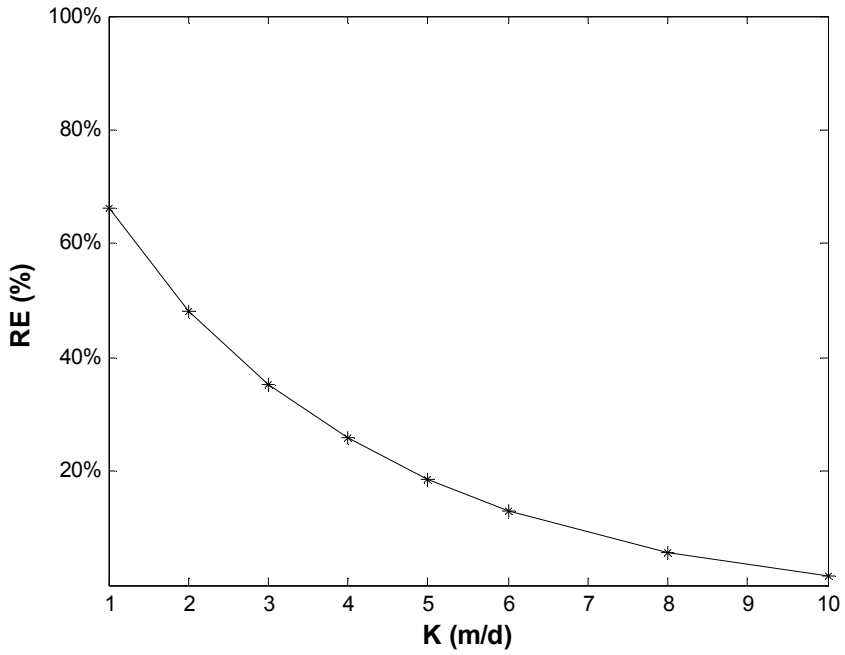

Figure 5.6 RE variation as hydraulic conductivity by FPW

Longitudinal dispersivity α_L [L]:

Dispersion plays a vital role in the groundwater transport, especially the longitudinal dispersion in the large field site. For the ASR system, the subsurface transport and mixing spread out mainly along the longitudinal direction. Ward et al. (2007) suggested that a high value for dispersivity can lead to a significant reduction in recoverable volume and hence reduce the RE. It provides us the basic cognition of longitudinal dispersivity α_L [L] on the RE variation through full-penetrating extraction wells. ***Figure 5.7*** shows the RE results as the variation of α_L [L]. We can observe that, the high longitudinal dispersivity is harmful to the RE by applying fully-penetrating wells in the homogeneous, isotropic aquifer for one cycle ASR.

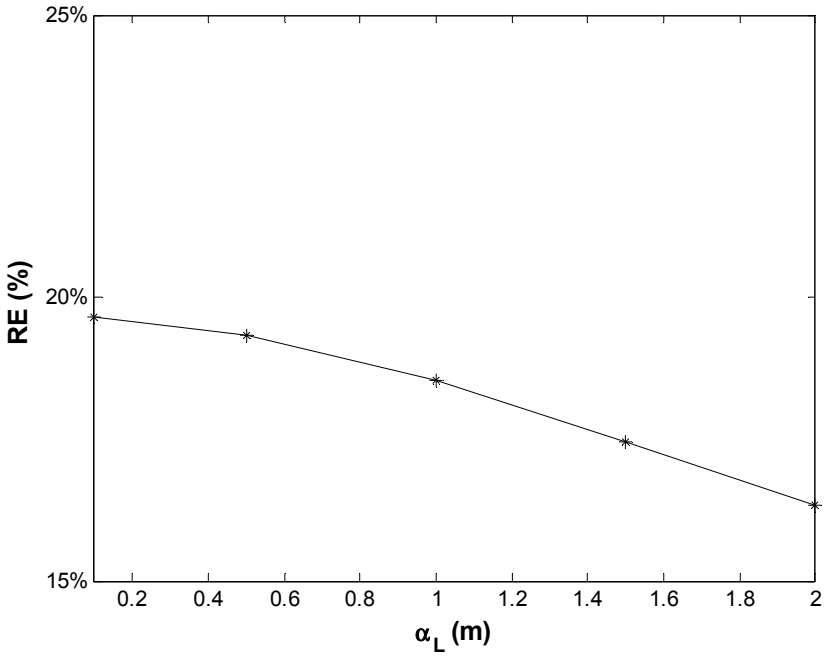

Figure 5.7 RE variation as longitudinal dispersivity by FPW

Transverse dispersivity α_T [L]:

The transverse dispersion controls the vertical direction mixing. It is the main mechanism creating mixing in the seawater-freshwater interface (Dagan, 2006).The mixing zone width is greatly affected by the transverse dispersion ignoring the mass transfer (Ataie-Ashtiani et al., 1999; Dagan, 2006). Moreover, the transverse dispersivity not only contributes to the width of the mixing zone but also controls further increase of this width in the midportion of the interface (Abarca et al., 2007). For ASR system, water is pumped out from the vertical well, implying the significance of vertical direction mixing in the subsurface transport process. ***Figure 5.8*** shows the RE results as the variation of α_T [L]. We can observe that, the high vertical dispersivity is helpful to the RE by applying fully-penetrating wells in the homogeneous, isotropic aquifer for one cycle ASR.

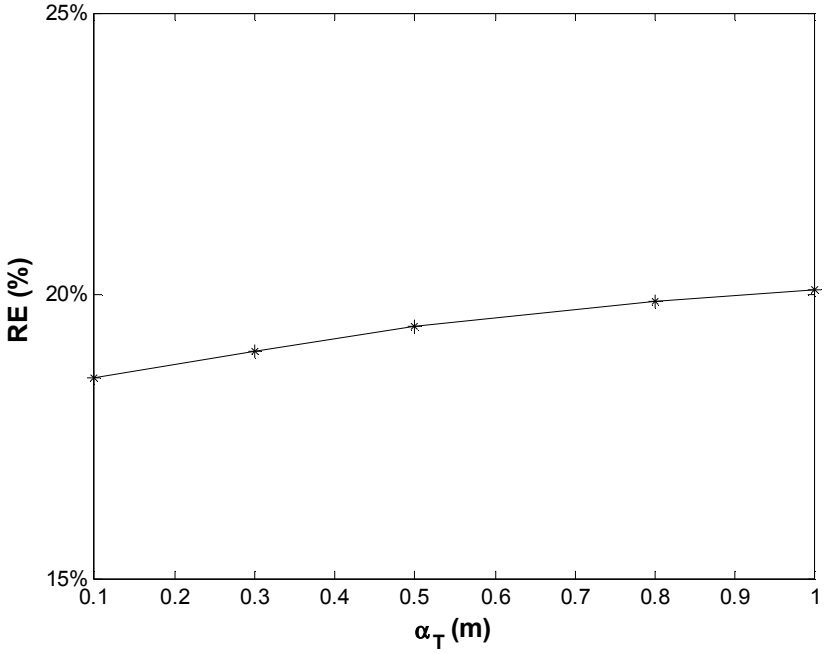

Figure 5.8 RE variation as vertical dispersivity by FPW

5.3.2 Operational Parameters Analysis

In comparison with hydrogeological parameters, we should pay more attention to the operational parameters since we can control these parameters in reality. Total 5 operational parameters (i.e. Q_i [L^3 T^{-1}], T_i [T], V_t [L^3], T_s [T] and Q_e [L^3 T^{-1}]) will be investigated.

Injection flowrate Q_i [L^3 T^{-1}]:

The injection flowrate Q_i [L^3 T^{-1}] is regarded as the key factor that most directly affecting the RE for one cycle ASR system (Peters, 1983; Pavelic et al., 2002; Ward et al., 2007; Lu et al., 2011). Since Q_i [L^3 T^{-1}] greatly affects the density effects (Ward et al., 2007). That implies that the RE will vary much at different Q_i [L^3 T^{-1}]. Total 7 cases are set that Q_i is changing from 4000 to 30000 m^3/d. One note is that we assume the injection flowrate Q_i [L^3 T^{-1}] and the extraction flowrate Q_e [L^3 T^{-1}] is the same for each case. Other parameters will keep the same as the BC. ***Figure 5.9*** shows the RE results as the variation of Q_i [L^3 T^{-1}]. We can obviously observe that, the high injection flowrate is helpful to the RE by applying fully-penetrating wells in the homogeneous, isotropic aquifer for one cycle ASR. And the influence of injection flowrate on the RE is dramatic.

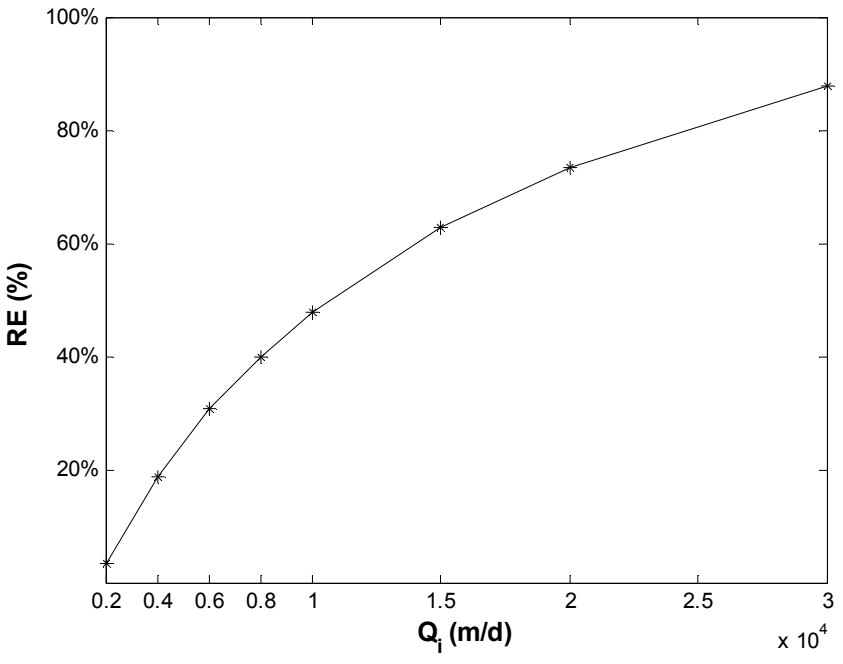

Figure 5.9 RE variation as injection flowrate by FPW

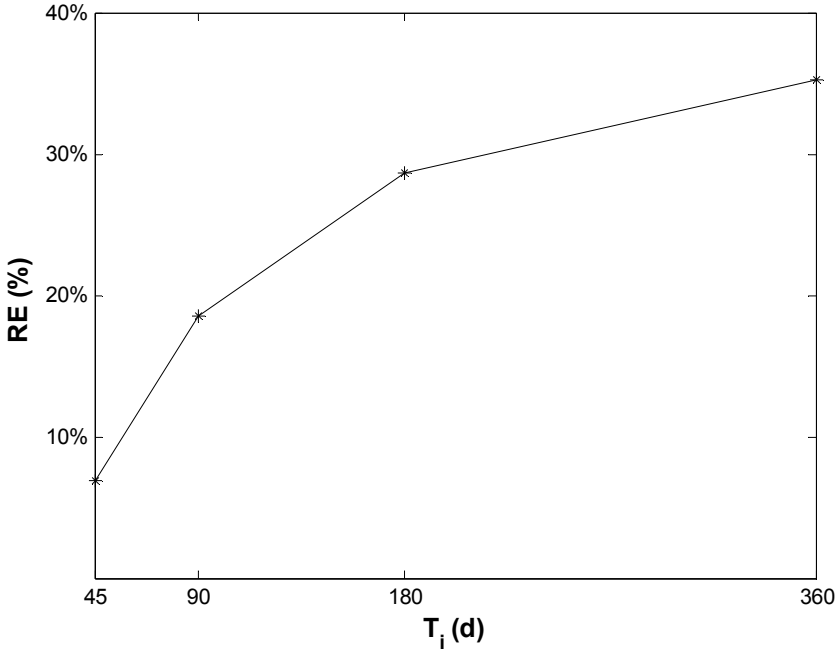

Figure 5.10 RE variation as injection duration by FPW

Injection duration T_i [T]:

As known, the injection duration T_i [T] is the other key parameter determining the RE in the ASR system. In fact, the injection duration T_i [T] decides the impulsion persistency of the ASR system. T_i [T] is the same as the Q_i [L^3 T^{-1}] that the magnitude of which directly affects the RE of one cycle ASR system. It is straightforward to imagine that T_i [T] supplies a time scale accumulation to the groundwater transport. And even we can predict that the longer T_i [T] will produce the bigger RE since the positive effects to the RE improvement is enhancing. But unfortunately, the discussion about the injection duration T_i [T] is not specific and informative in the previous study, and T_i [T] is often assumed as the constant (e.g., Ward et al., 2007). It is necessary to investigate how the injection duration T_i [T] affects the RE in the homogeneous, isotropic aquifer. Total 4 cases are set that T_i is respectively 45, 90, 180 and 360 days. ***Figure 5.10*** shows the RE results as the variation of T_i [T]. We can observe that, the long injection duration is helpful to the RE by applying fully-penetrating wells in the homogeneous, isotropic aquifer for one cycle ASR.

Total injection volume V_t [L^3]:

As discussed above, the sensitivity analysis cases for Q_i [L^3 T^{-1}] & T_i [T] can be regarded as the varied V_t [L^3] cases. We cannot consider the influence of injection excluding from the total injection volume V_t [L^3]. If we keep the total injection volume V_t [L^3] invariable, how do Q_i [L^3 T^{-1}], T_i [T] and V_t [L^3] affect the ASR performance in the homogeneous, isotropic aquifer? For the BC, we set V_t 360,000 m^3 (shown in ***Table 5.1***), so we keep the same V_t [L^3] here and respectively set total 5 cases listed in ***Table 5.5***.

Table 5.5 Total injection volume $\boldsymbol{V_t}$ [L^3] sensitivity analysis

Case No.	Q_i [m^3 d^{-1}]	T_i [d]
1	1000	360
2	2000	180
3	4000	90
4	8000	45
5	16000	22.5

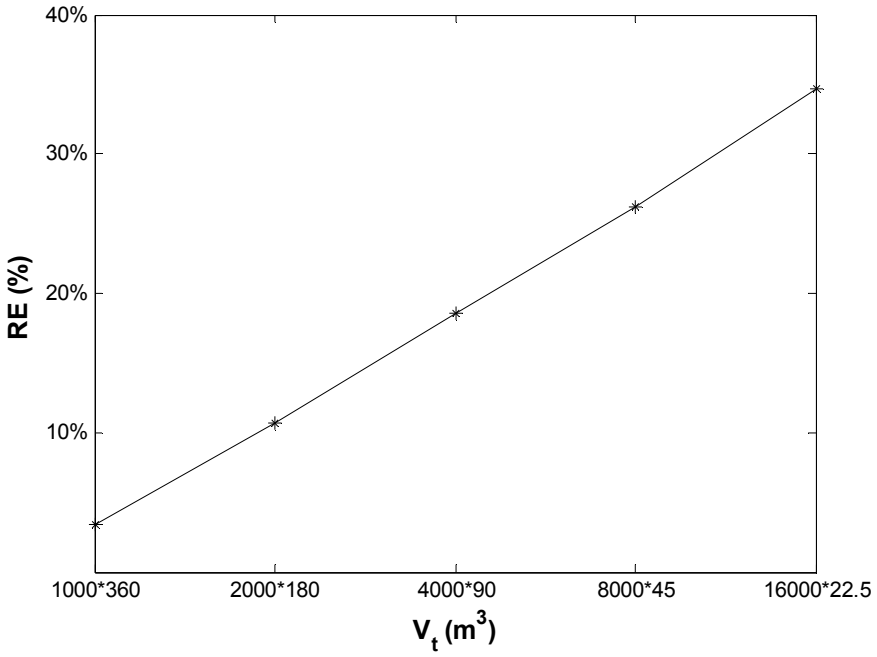

Figure 5.11 RE variation as total injection volume by FPW

Figure 5.11 shows the RE results as the variation of V_t [L^3]. We can find that, for the fixed V_t [L^3], the high Q_i [L^3 T^{-1}] and the short T_i [T] will produce the big RE, which should be our preference when we apply the fully-penetrating well in the homogeneous, isotropic aquifer for one cycle ASR.

Storage Duration T_s [T]:

The storage seems a simple phase for the whole ASR operational process since not complicated operation is required. However, it is vital to the ASR system and deemed as the key transition phase connecting the injection and extraction. Many previous studies emphasize the storage duration T_s [T] affects the surface tilting and density effects, also some real field storage cases of the ASR are discussed (e.g. Esmail and Kimbler, 1967; Kumar and Kimbler, 1970; Missimer et al., 2002; Misut and Voss, 2007; Ward et al., 2007, 2008, 2009). But, as the key transition phase of the ASR system, it is necessary to synthetically investigate the influence of T_s [T] on the RE for one cycle ASR system. Total 7 cases are set to make a comprehensive investigation. We set T_s as 0, 45, 90, 180, 270, 360 and 450 days. ***Figure 5.12*** exhibits the RE results as the variation of T_s [T]. We can observe that, the long storage duration is truly harmful to the RE by applying fully-penetrating wells in the homogeneous, isotropic aquifer for one cycle ASR. This implies that the longer storage duration would promote stronger density effects, which dramatically alleviate the RE.

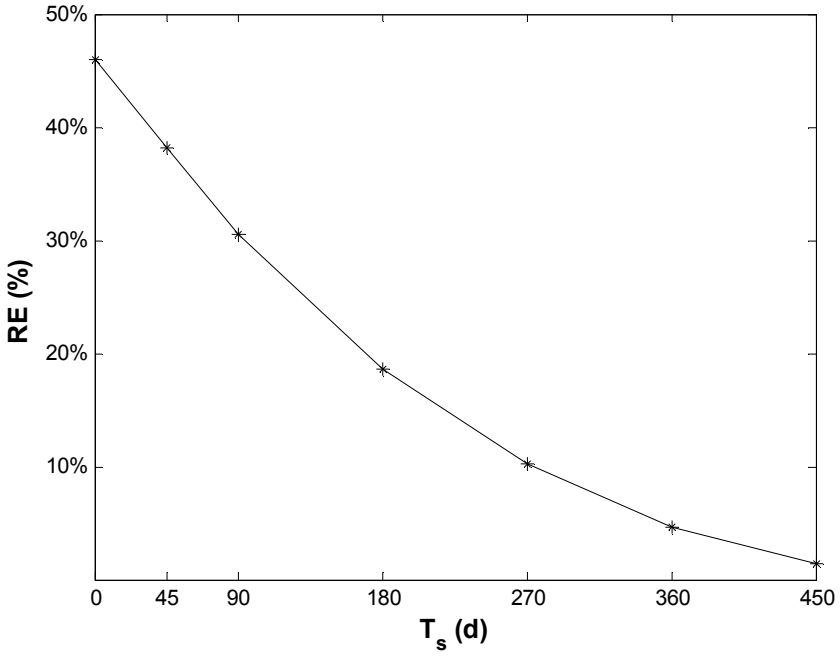

Figure 5.12 RE variation as storage duration by FPW

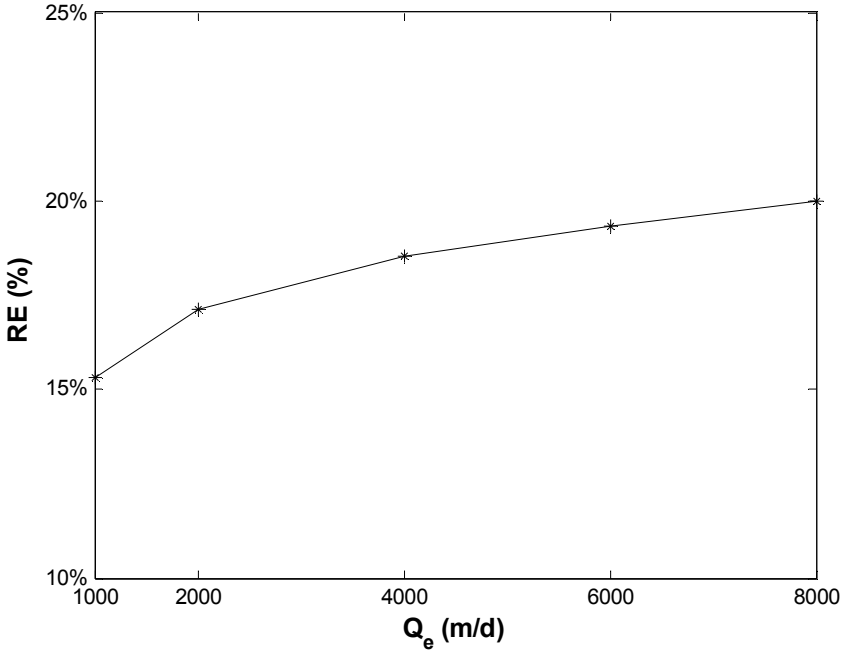

Figure 5.13 RE variation as extraction flowrate by FPW

5.4 Uncertainty Analysis

Hydraulic conductivity K [LT^{-1}] is one of the most significant parameters introducing uncertainty in groundwater transport. K [LT^{-1}] presents the capability of transmitting groundwater in the subsurface transport and may vary several orders of magnitude in different locations. Thus, uncertainty analysis for K [LT^{-1}] is necessary to provide a confidence interval for the RE investigation of ASR.

According to the sensitivity analysis of hydraulic conductivity above, we can make a *K-RE* plot to describe the relationship between K [LT^{-1}] and RE when other parameters keep invariant as the BC. By assuming that $ln\,K \sim N\ (\mu, \sigma^2)$, and the mean of $ln\,K$ varies from -12 to -9 while the standard deviation σ is fixed as 0.1, we sample 10,000 random numbers for each group. Then, we evaluate the RE for each group of parameters. Finally, we can calculate the sample mean and standard deviation of RE for each group, and the 95% confidence interval (shown in ***Figure 5.14***).

We can also plot the coefficient of variation (CV) for 16 groups of samples, shown in ***Figure 5.15***. We can observe that the CV enhances as the increase of K. That means, the relative variability grows as the increment of K.

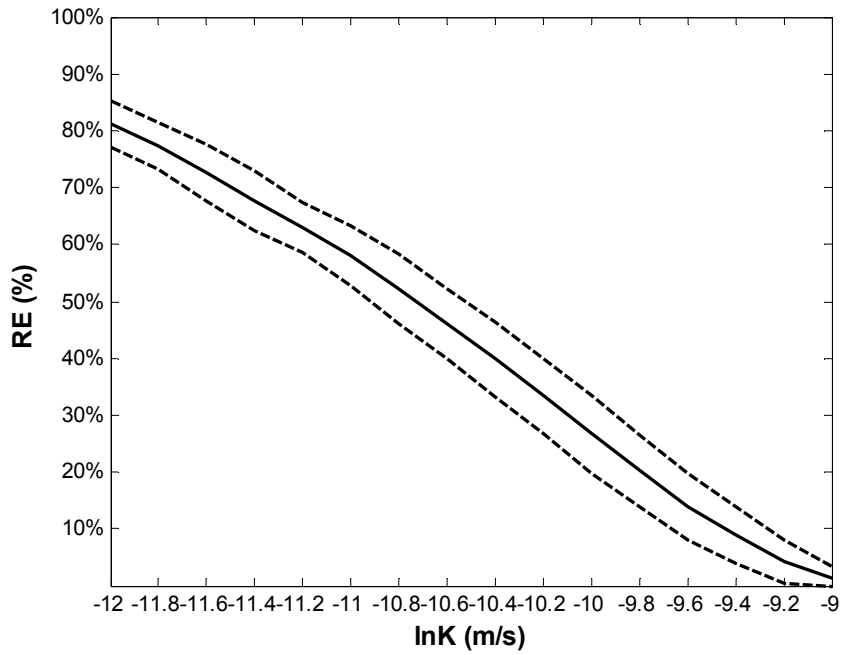

Figure 5.14 RE uncertainty analysis by FPW

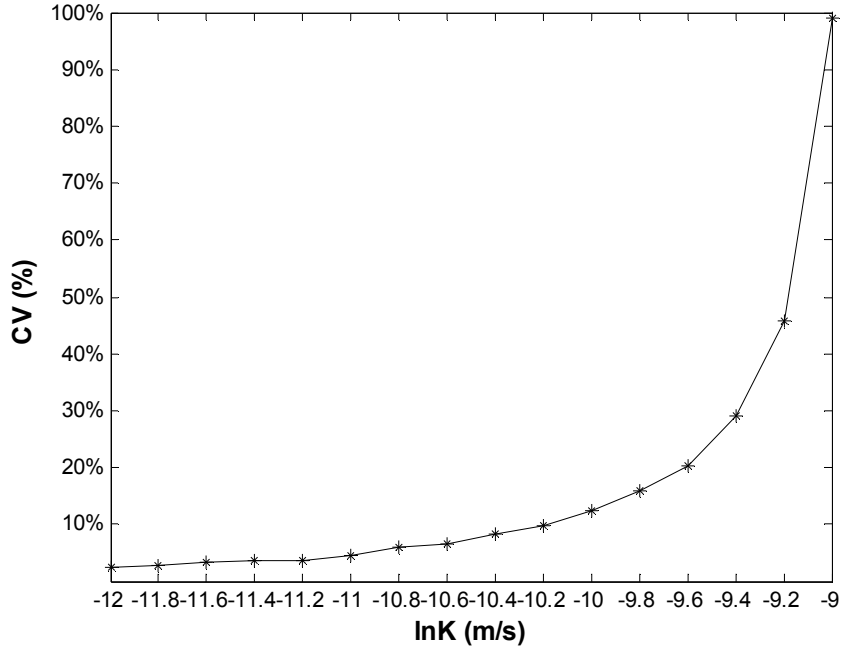

Figure 5.15 Coefficient of variation plot by FPW

5.5 Conclusion

After investigating the effects of hydrogeological and operational parameters on ASR performance by applying the fully-penetrating well in the homogeneous, isotropic aquifer, we have the following conclusions:

Hydrogeological Parameters

(1) RE in saline aquifers is controlled by the breakthrough of the interface toe at the aquifer bottom due to density effects.

(2) Higher RE can be achieved in aquifers with lower density, higher specific storage, shorter aquifer thickness, lower hydraulic conductivity, lower longitudinal dispersivity and higher transverse dispersivity. All these conditions can lead to reduced density effects by limiting or diluting the tilting interface at the toe.

Operational Parameters

(1) Injection Phase:

(a) We recommend to increase the total injection volume to generate a better RE in the homogeneous isotropic aquifer. (b) To achieve the goal of recovering more freshwater, we can either increase the injection flowrate or extend the injection duration. (c) If the total water volume is constant, we should enhance the injection flowrate while shorten the injection duration to gain a big RE.

(2) Storage Phase:

Short storage duration is recommended to promote a better RE. The best RE is gained at the case with no storage duration.

(3) Extraction Phase:

We recommend to increase the extraction flowrate to generate a better RE.

CHAPTER 6

ASR PERFORMANCE AND EFFECTS OF TRANSVERSE DISPERSION ON ASR EFFICIENCY IN STRATIFIED ANISOTROPIC AQUIFERS

In previous studies, we applied a modeling study to discuss the main factors affecting the RE of an ASR scheme in homogeneous isotropic aquifers. We evaluated the impacts of different hydrogeological and operational parameters, including hydraulic conductivity, density, dispersivity, pumping rates, pumping and storing durations, etc. However, subsurface formations are generally heterogeneous because geologic processes do not yield uniform porous media characteristics over appreciable areas and because of the layering of different sediment packages (Charbeneau, 2006). In other words, it is necessary to extend the evaluation to investigate ASR performance in more realistic heterogeneous and anisotropic aquifers. Hydrogeophysical methods and multiscale tracer testing were applied to analyze the ASR system in different types of heterogeneous aquifers (e.g., Pavelic et al., 2006; Minsley et al., 2011). But they did not address the RE. This study focuses on modeling the ASR processes in homogeneous anisotropic aquifers and structured heterogeneous layered aquifers (i.e. horizontally stratified aquifer). We will particularly investigate how the RE varies with the hydraulic conductivity ratios of structured layers in heterogeneous and anisotropic coastal aquifers.

Diersch and Kolditz (2002) reviewed the state in modeling of variable-density flow and transport in porous media, and showed examples of field applications to demonstrate the

importance of considering heterogeneities and large scales. It has been shown that aquifer heterogeneity can greatly affect ASR system performance by reducing the recoverable volume of low-salinity water (Pavelic et al., 2006 and Maliva et al., 2006). Maliva et al. (2006) presented the modeling results and field investigations to emphasize the pressing need for more sophisticated data collection and solute-transport modeling to predict how stored water migrates in heterogeneous aquifers. Ward et al. (2008) discussed the change of RE in different types of stratified heterogeneous aquifers. They concluded that the RE of a simulated ASR operation is sensitive to density gradients and anisotropic ratio, but relatively insensitive to the hydraulic conductivity distribution in stratified aquifers. They found that the RE in a stratified heterogeneous medium can be approximated well by the RE in an equivalent homogeneous (anisotropic) medium. However, their finding was based on only one type of layer placement and it is not clear that how the RE varies in different types of aquifer layer placement with different hydraulic conductivity ratios of horizontal structured layers. Moreover, it is doubtful whether stratified aquifers can be simplistically homogenized. Dispersion is another critical process for creating mixing. Ward et al. (2007) found that high dispersion can significantly reduce the RE of ASR schemes. In particular, transverse dispersion was regarded as the main mechanism creating mixing in the seawater-freshwater interface (Dagan, 2006). Transverse dispersion not only greatly affects the mixing zone width (Ataie-Ashtiani et al., 1999; Dagan, 2006), but also controls the growth and decay of the mixing zone (Abarca et al., 2007).

In the first part, to better understand the variation of RE in heterogeneous and anisotropic brackish aquifers, we aim to investigate the ASR performance in different types of

aquifers in terms of anisotropy and hydraulic conductivity contrast. The first part will focus on four main aspects: 1) to explore the main effects of various anisotropy ratios on the one cycle ASR system in the layered aquifer; 2) to explore the main effects of various hydraulic conductivity contrasts on the one cycle ASR system; 3) to investigate and analyze the RE variation of one cycle ASR system in the layered aquifer, and to identify the RE discrepancy created by the aquifer layer placement; 4) to examine the feasibility whether stratified aquifers can be homogenized, and to indicate the difference between stratified aquifers and equivalent homogenized aquifers.

In the second part, we will investigate the effects of transverse dispersion on the efficiency of ASR. To assess the effects of transverse dispersion on ASR performance in stratified coastal aquifers.

6.1 Problem Identification

6.1.1 Layered Heterogeneity

In engineering analysis of groundwater flow problems, it is often useful to replace the true heterogeneous medium with an equivalent homogeneous medium, which means a conceptually simple, homogeneous system yields the similar results as the actual complex, heterogeneous medium (Charbeneau, 2006). In previous studies of analyzing the effects of anisotropy and heterogeneity, the aquifer was conceptualized as a structured brick tower with the base unit consisting of two horizontally homogeneous layers with different hydraulic conductivities K_1 and K_2 (e.g. Johnson et al., 2002; Kim and Parizek, 2005; Ward et al., 2008). In this study, we assume a uniform structured set of aquifers consisting of a sequent layer combination with hydraulic conductivities K_1 and K_2 and a

uniform thickness b_i for each layer. The total thickness of the aquifer is B. ***Figure 6.1*** shows such a base unit system with two layers. The equivalent horizontal hydraulic conductivity of the aquifer, K_H, is given by the arithmetic average weighted by the thickness. Meanwhile, the equivalent vertical hydraulic conductivity of the aquifer K_V is calculated by the thickness-weighted harmonic mean (Charbeneau, 2006):

$$K_H = \frac{\sum K_{ix} b_i}{B} \quad (6.1a)$$

$$K_V = \frac{B}{\sum\left(\frac{b_i}{K_{iz}}\right)} \quad (6.1b)$$

where K_H [LT^{-1}] is the equivalent horizontal hydraulic conductivity; K_V [LT^{-1}] is the equivalent vertical hydraulic conductivity; K_{ix} *and* K_{iz} [LT^{-1}] are the horizontal and vertical hydraulic conductivity of layer i (i.e. K_1 or K_2). b_i [L] is the thickness of layer i; B [L] is the total aquifer thickness.

K_H is very significant in this study since we will select a particular value of K_H as the reference hydraulic conductivity to develop the investigation of heterogeneity and anisotropy. Namely, we will maintain the value of K_H invariant when varying the ratio between K_1 and K_2.The combination of K_H *and* K_V represents a simplistically equivalent homogeneous, anisotropic medium (e.g. Ward et al., 2008). We will apply this homogenized aquifer to examine the difference between stratified and equivalent aquifers.

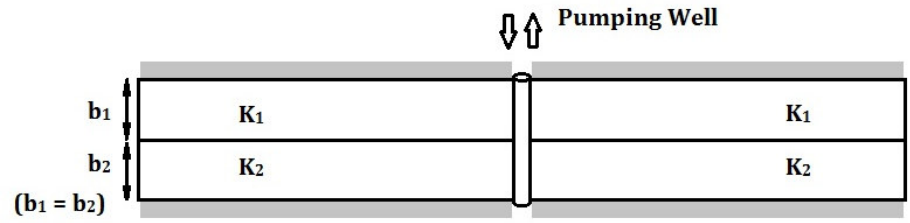

Figure 6.1 Base unit with two hydraulic conductivities K_1 and K_2

6.1.2 Anisotropy in Layered Aquifers

In previous studies, we investigated the ASR system by neglecting the directional variations of hydraulic conductivity (i.e. isotropic). However, anisotropy occurs commonly in porous media (Charbeneau, 2006). After defining two horizontally homogeneous layers with hydraulic conductivities K_1 and K_2, we consider three directional hydraulic conductivities along the principal directions, *x, y*, and *z*:

$$\mathbf{K}_i = \begin{bmatrix} K_{ix} & 0 & 0 \\ 0 & K_{iy} & 0 \\ 0 & 0 & K_{iz} \end{bmatrix} \quad (6.2)$$

where $\mathbf{K}_i$ [LT^{-1}] is the hydraulic conductivity tensor of layer *i*, and K_{ix}, K_{iy}, *and* K_{iz} [LT^{-1}] are *x, y, z* directional hydraulic conductivities of layer *i*.

6.2 Numerical Methods

6.2.1 Conceptual Model

In this study of anisotropy and heterogeneity, we apply the similar numerical models as in the homogeneous and isotropic aquifers by the graphic user interface software 'Groundwater Vista Version 5.20 (GWV). Each case considers only one complete ASR cycle (i.e. injection, storage, and recovery). And we define that the aquifer consists of 5 base units (***Figure 6.1***) with two hydraulic conductivities $\mathbf{K}_1$ and $\mathbf{K}_2$ (shown in ***Figure 6.2***). For each layer, we divide it into 5 parallel layers with the same thickness, i.e., there are totally 50 layers in the vertical direction. In one base unit, we assume that the thickness of either layer is equal (i.e. $b_1 = b_2$). Then, the average horizontal and vertical hydraulic conductivity become:

$$K_H = \frac{K_{1x}+K_{2x}}{2} \quad (6.3a)$$

$$K_V = \frac{2}{\frac{1}{K_{1z}}+\frac{1}{K_{2z}}} \quad (6.3b)$$

Similar to the previous chapter, the three-dimensional (3D) ASR domain is modeled by a two-dimensional (2D) axisymmetric cross-section with the vertical axis of rotation located at the pumping well. The 3D Cartesian coordinate (*x, y, z*) is simplified to the 2D axisymmetric geometry (*r, z*). The radius *r* represents the distance to the pumping well.

By making the transformation to 2D axisymmetric coordinate (*r, z*), the hydraulic conductivity tensor is simplified to:

$$\mathbf{K}_1 = (K_{1r}, K_{1z}) \quad (4a)$$

$$\mathbf{K}_2 = (K_{2r}, K_{2z}) \text{ (4b)}$$

We will fix the horizontal hydraulic conductivity values and vary the vertical hydraulic conductivities to examine the effects of anisotropy.

Figure 6.2 shows the conceptual model for the axisymmetric ASR simulation in layered aquifers. We set the pumping well (injection/extraction) as the z-axis at the left boundary of the domain and the constant seawater level at the right boundary. At the initial stage, we assume that the entire domain is full of seawater. As known, dispersion is essential in the transport process, particularly in anisotropic layered aquifers (Charbeneau, 2006). We can expect that both longitudinal (x-axis) and vertical (z-axis) dispersion would play an important role.

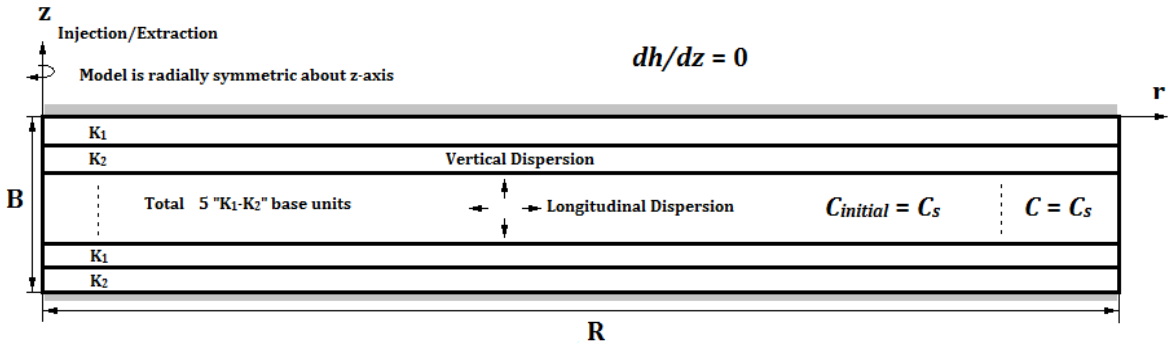

Figure 6.2 Conceptual model for axisymmetric ASR in layered aquifers

6.2.2 Governing Equations

The graphic user interface software 'Groundwater Vista Version 5.20 (GWV) is essentially a combination of USGS software such as MODFLOW-2000, MT3DMS, SEAWAT-2000. For better using MODFLOW and MT3DMS, the variable-density groundwater flow equation is usually expressed in terms of equivalent freshwater head and fluid density by:

$$\rho S_f \frac{\partial h_f}{\partial t} + \theta \frac{\partial \rho}{\partial t} = \nabla \cdot \left[\rho K \left(\nabla \cdot h_f + \frac{\rho - \rho_f}{\rho_f} \nabla z \right) \right] \quad (6.5)$$

where K [LT^{-1}] is the equivalent freshwater hydraulic conductivity; ρ [ML^{-3}] is the fluid density; ρ_f [ML^{-3}] is the freshwater density; h_f [L] is the equivalent freshwater head; S_f [L^{-1}] is the equivalent freshwater storage coefficient; θ [-] is the effective porosity; t [T] is the time; z [L] is the vertical coordinate directing upward.

The initial condition is actually the same as the case we presented in the homogeneous and isotropic confined aquifers, i.e., uniform hydraulic heads are distributed over the domain. Besides, the flow across the well screen into the well is equal to the pumping rate Q. So the boundary condition at the well is determined by:

$$Q = 2\pi r_w K b \left(\frac{\partial h_f}{\partial r} \right)_{r=r_w} \quad (6.6)$$

where r [L] is the radial coordinate direction; r_w [L] is the well radius; b [L] is the well screen length.

The governing equation for solute transport is given by:

$$\frac{\partial c}{\partial t} = \nabla \cdot (\mathbf{D} \nabla \mathrm{c} - \mathbf{v} \mathrm{c}) \quad (6.7)$$

where c [ML^{-3}] is the dissolved solute concentration; **v** [LT^{-1}] is the pore water velocity; **D** [L^2T^{-1}] is the hydrodynamic dispersion coefficient tensor.

As shown in ***Figure 6.2***, there is an initial salt concentration in stratified aquifers; and the concentration gradient at the well boundary is zero.

The movement of groundwater and the transport of solutes in the aquifer are coupled processes. To set up the relationship between Equations (6.5) and (6.7), we can apply the linear relationship between the fluid density and solute concentration shown as:

$$\rho = \rho_f + \varepsilon c \quad (6.8)$$

where ε [-] is a dimensionless constant with a value of 0.7143 (i.e. $\varepsilon = \frac{\rho_s - \rho_f}{C_s - C_f}$ = (1025-1000)/(35-0) = 0.7143) for solute concentrations ranging from zero to which of seawater.

The governing equations are expected to solve in 2D axisymmetric coordinates with the density-dependent groundwater flow codes, SEAWAT-2000. Langevin (2008) demonstrated that the axisymmetric model is much faster than an equivalent three-dimensional Cartesian model for some particular problems such as upconing problem. It confirmed that the axisymmetric model is suitable to solve the ASR problem analogous to the upconing problem. Several input parameters such as hydraulic conductivities, effective porosity, and storage coefficient need to be adjusted to account for the radial flow area change from the pumping well.

6.2.3 Evaluation of ASR Performance

The same as Chapter 5.

6.2.4 Model Parameters

Table 6.1 shows model inputs including geometrical, hydrogeological and transport parameters. The 2D axisymmetric domain is 50 m high and 350 m long. The pumping rate (i.e. injection/ extraction flowrate) is set as 5000 m^3d^{-1}, appropriate for a large scale ASR operation. For simplicity, injection and extraction durations are both set to 90 days (3 months), while the total storage period is employed for 180 days (6 months), representing a yearly-based ASR cycle. Our heterogeneous models are divided into 50 equal horizontal layers of 1m thickness (i.e. 5 base units). To explore the influence of anisotropy on the ASR performance in stratified aquifers, we keep the value of K_1/K_2 and K_H constant and modify the value of K_{ix}/K_{iz} = 1, 10, 100 and ∞ to investigate the variation of RE. To investigate the influence of heterogeneity on the ASR performance in different types of hypothetical layered aquifers, we fix the value of K_{ix}/K_{iz} and K_H and vary the hydraulic conductivities of each layer (K_1 and K_2) to achieve ratios of K_1/K_2 = 0.001, 0.01, 0.1, 1, 10, 100 and 1000. To examine the homogenized feasibility of stratified aquifers, we fix K_H invariant and vary the values of K_{ix}/K_{iz} and K_1/K_2 to indicate the difference between stratified aquifers and equivalent homogenized aquifers. To investigate the ASR performance in stratified aquifers, we will fix the transverse dispersivity as 0.1m. But to investigate the effects of transverse dispersion, we maintain all parameters the same except the transverse (vertical) dispersivity. We will vary α_v as 0, 0.01, 0.1 or 0.2m respectively. α_v= 0 theoretically represents an extreme condition without any vertical dispersion.

Table 6.1 Model input parameters in stratified aquifers

Model Parameters	Variable Symbol	Value
Aquifer Thickness (m)	B	50
Domain Radius (m)	R	350
Individual Layer Thickness (m)	b	1
Single K_1/K_2 Layer Thickness (m)	b_i	5
Seawater/Freshwater Level (m)	h_s / h_f	50
Seawater/Freshwater Density (kgm^{-3})	ρ_s / ρ_f	1025 / 1000
Initial Solute/Salt Water Salinity (gkg^{-1})	C_i / C_s	35
Injected Water Salinity (gkg^{-1})	C_f	0
Effective Porosity (-)	θ	0.3
Specific Storage (m^{-1})	S_s	0.005
Molecular Diffusivity (m^2s^{-1})	D_m	10^{-9}
Longitudinal Dispersivity (m)	α_L	1
Vertical Dispersivity (m)	α_v	0, 0.01, 0.1, 0.2
Equivalent Horizontal Hydraulic Conductivity (md^{-1})	K_H	5
Equivalent Vertical Hydraulic Conductivity (md^{-1})	K_V	Varied (see Table 6.3)
Ratio of Hydraulic Conductivity for each layer (-)	$\frac{K_1}{K_2}$	0.001, 0.01, 0.1, 1, 10, 100, 1000
Ratio of Directional Hydraulic Conductivity of each layer (-)	$\frac{K_{ix}}{K_{iz}}$ $(i = 1, 2)$	1, 10, 100, ∞ (i.e. $K_{iz} = 0$)
Injection/Extraction Flowrate (m^3d^{-1})	Q_i / Q_e	5000 / -5000
Injection/Extraction Duration (d)	T_i / T_e	90
Storage Duration (d)	T_s	180

6.3 Results and Discussions

6.3.1 Anisotropy Analysis

To analyze the influence of anisotropy on the ASR performance in stratified aquifers, the control variables method is anticipated to apply to eliminate potential biasing effects resulting from other variables. Namely, we control the hydraulic conductivity as the only variable. To isolate the impacts from the anisotropy, in the first case, we assume the whole layered aquifer is homogeneous (i.e. $K_1 = K_2$). Then, the heterogeneous cases are expected to discuss (i.e. $\frac{K_1}{K_2}$ = 10 and 0.1).

Homogeneous and Anisotropic Illustrative Case

In the cases of homogeneous aquifers (K_H = 5 m/d, $K_1 = K_2$), the ratio of longitudinal and vertical hydraulic conductivity $\frac{K_{ix}}{K_{iz}}$ varies in the range of 1, 10, 100 and ∞ (i.e. K_{iz} = 0). The case $\frac{K_{ix}}{K_{iz}}$ = 1 represents the isotropy of aquifer while other cases $\frac{K_{ix}}{K_{iz}}$ = 10, 100 and ∞ displays the anisotropy. Theoretically, $\frac{K_{ix}}{K_{iz}}$ = ∞ (i.e. K_{iz} = 0) represents an extreme condition that there is no vertical flow across the layers, which is valuable to quantify the scope of anisotropy's influence although it is rare in reality.

Figure 6.3 displays the concentration plots in the homogeneous aquifer for $\frac{K_{ix}}{K_{iz}}$ = 1, 10, 100 and ∞ at the end of the different periods (injection, storage and extraction) for one ASR cycle. We can see several noticeable flow phenomena from the concentration plots.

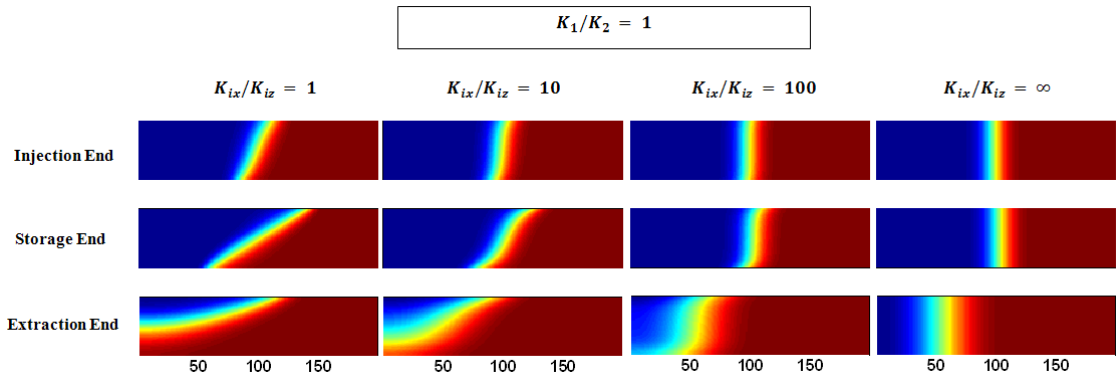

Figure 6.3 Concentration plots in the homogeneous aquifer with different anisotropy

Firstly, at the end of injection period, there is a clear tilting in the homogeneous, isotropic case, but the tilting fades away as the anisotropy increases, and becomes unnoticeable at the case of K_{iz} = 0, which represents a perfectly stratified aquifer without flow across layers. Secondly, after a storage period of 180 days, all cases, except the perfectly anisotropic case, show that the mixing zone tilts further because of the density effects. However, the extent of mixing is not the same for different anisotropic cases. In the isotropic case, the tilting is intensified significantly after a long time storage, but the tendency diminishes as the increase of anisotropy. The case with K_{iz} = 0 exhibits an almost invisible tilting, and only the intra-layer mixing extends along the longitudinal direction. Thirdly, at the end of recovery period, the shape of mixing zone changes significantly due to the variation of anisotropy. For the isotropic case, freshwater in the top layer is hard to pull back while saltwater in the bottom layer is effortless to pump out. By contrast, in the anisotropic cases, freshwater turns more accessible in not only the top but also the bottom layers. That is, the flow becomes more uniform in different layers as

the increase of anisotropy. In these homogeneous cases, the amount of recovered freshwater is evenly contributed by each layer. Thus, excessive salt supplied by several particular layers would promote the ASR system prematurely reaching the breakthrough. This implies that the RE is greatly affected by the anisotropy due to the variation of salt contributions from different layers.

In comparison with the homogeneous and isotropic case, we can conclude at least three main impacts on the ASR system from the homogeneous anisotropic cases. i) In the injection period, the difference between pushing distances in the top and bottom layer tends to decrease gradually as the anisotropy increases , reaching the minimum at the case of $\frac{K_{ix}}{K_{iz}} = \infty$ (i.e. $K_{iz} = 0$). ii) In the storage period, the degree of macroscopic tilting decreases as the enhancement of anisotropy. In other words, the high anisotropy would alleviate the density-induced tilting effects owing to the small vertical hydraulic conductivity and flow across layers. iii) RE increases with the anisotropic ratio. We can also confirm this tendency from ***Figure 6.4***. It shows the RE results in the conditions of the same homogeneity (i.e. K_H = 5 m/d) but different anisotropy (i.e. varying K_V). The RE monotonously decreases from 54.0% to 23.9% as K_V increases from 0 to 5 m/d. Thus, the RE increases with the anisotropy and achieve the maximum when ignoring K_V.

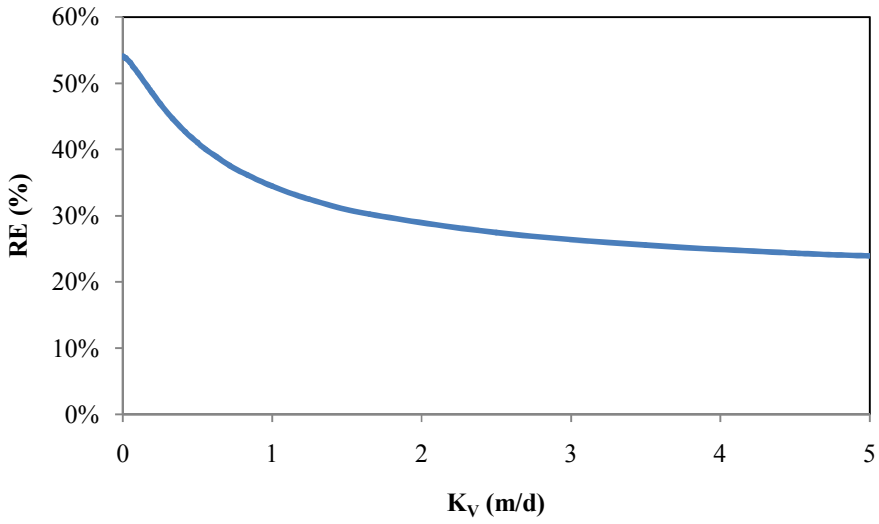

Figure 6.4 RE variation when varying K_V at K_H = 5 m/d

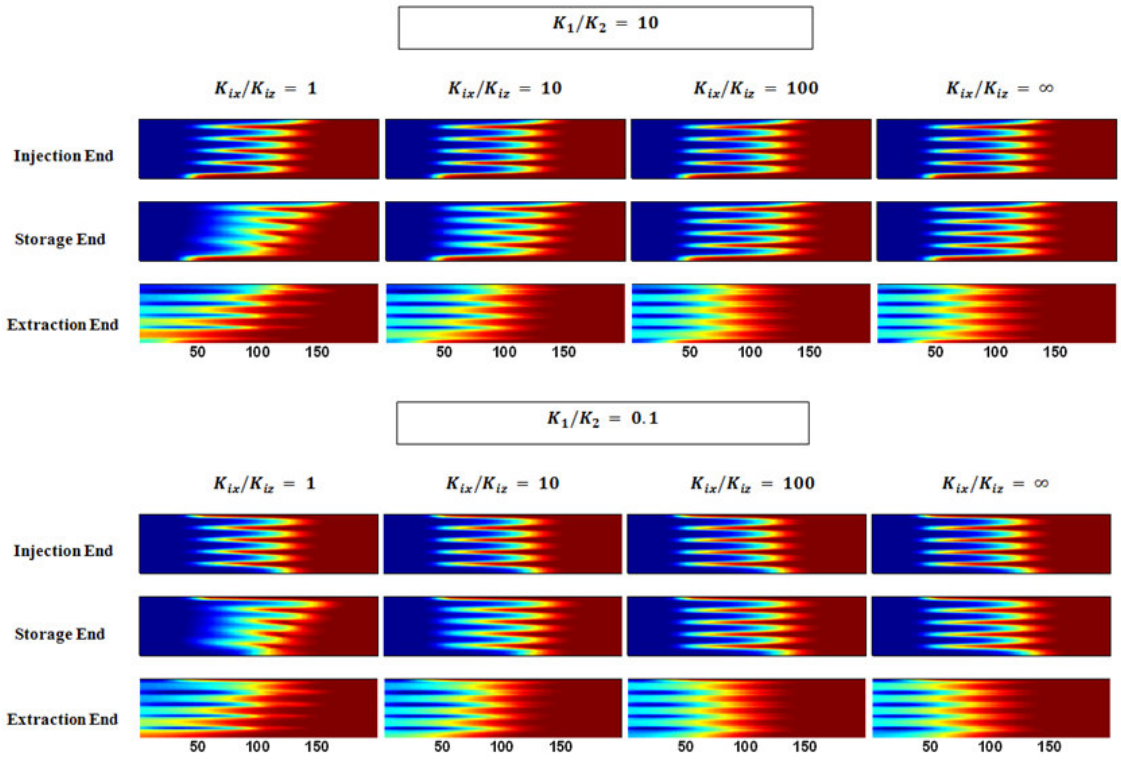

Figure 6.5 Concentration plots in anisotropic layered aquifer for cases $\frac{K_1}{K_2} =$ 10 and 0.1

Heterogeneous and Anisotropic Illustrative Cases

To investigate the anisotropy effects in heterogeneous and anisotropic layered aquifers, and $\frac{K_1}{K_2}$ varies as 10 and 0.1.

Figure 6.5 displays the concentration plots in the anisotropic layered aquifer for the cases $\frac{K_1}{K_2} =$ 10 and 0.1 when $\frac{K_{ix}}{K_{iz}}$ changes in the range of 1, 10, 100 and ∞ (i.e. K_{iz} = 0) at the end of the different periods for one cycle ASR system.

Injection end: For 4 cases at $\frac{K_1}{K_2}$ = 10, we can see that the maximum pushing distance occurs in the top high K layer while the minimum occurs in the bottom low K layer. By observing other medium layers of 4 different $\frac{K_{ix}}{K_{iz}}$ cases, the pushing distances of other high (or low) K layers tend to the same as the gradually increase of anisotropy. If we consider the forehead of pushing as the "toe", the toes of high K layers present a macroscopic tilting through the whole aquifer. The macroscopic tilting in the isotropic case (i.e. $\frac{K_1}{K_2} =$ 10, $\frac{K_{ix}}{K_{iz}}$ = 1) is more evident than which in the anisotropic cases (i.e. $\frac{K_1}{K_2}$ = 10, $\frac{K_{ix}}{K_{iz}}$ = 10, 100, or ∞). And the macroscopic tilting weakens as the enhancement of anisotropy. For 4 cases at $\frac{K_1}{K_2}$ = 0.1, the toe reaches the nearest in the top low K layer while the farthest in the bottom high K layer. Irrespective of the bottom high K layer, the macroscopic tilting appears as expected, and it follow the same rule as the cases at $\frac{K_1}{K_2}$ = 10, i.e. the tilting turns unobvious as the anisotropy grows. From another perspective by respectively comparing the cases of same $\frac{K_{ix}}{K_{iz}}$ but different $\frac{K_1}{K_2}$ (i.e. 10 or 0.1), the approximate mirror-image symmetry comes out. And more anisotropic is the case, more

impressive is the phenomenon. That implies, by neglecting the effects of vertical hydraulic conductivity, the cases at $\frac{K_1}{K_2}$ = 10 play almost the same role as those at $\frac{K_1}{K_2}$ = 0.1 on the one cycle ASR system. This drops a hint that the RE would approach a very similar value when $\frac{K_{ix}}{K_{iz}} = \infty$ for the cases at $\frac{K_1}{K_2}$ = 10 and 0.1.

Storage end: The expected density-induced mixing dominates the flow processes in all cases, but the strengths of mixing are various for cases with different anisotropy. For the cases at $\frac{K_1}{K_2}$ = 10, the macroscopic tilting progresses further, however, the trend wanes as the anisotropy expands. For the cases at $\frac{K_1}{K_2}$ = 0.1, although the macroscopic tilting grows as the augment of anisotropy, the extent of tilting weakens comparing with the cases at $\frac{K_1}{K_2}$ = 10 especially when $\frac{K_{ix}}{K_{iz}}$ = 1 or 10. This suggests, the mixing in the cases of $\frac{K_1}{K_2}$ = 10 is much stronger than that in the cases of $\frac{K_1}{K_2}$ = 0.1, particularly in the case with low anisotropy (e.g. $\frac{K_{ix}}{K_{iz}}$ = 1 or 10). The mixing is related to the RE to some degree. The phenomenon helps us comprehend the density-induced mixing effects, and implies that the RE would be not the same owing to the varying mixing effects in different layered aquifers.

Extraction end: As expected, water is promptly pumped out through the high K layers while water retards in the low K layers. For cases with various anisotropies, we see the concentration distributions are greatly different. The concentration distribution in the high anisotropy case (e.g. $\frac{K_{ix}}{K_{iz}} = \infty$) seems more uniform than which in the isotropic case, for both $\frac{K_1}{K_2}$ = 0.1 and 10. And it is clear that the total breakthrough concentration is

contributed by individual layers. Namely, the discrepancy of concentration distribution inevitably leads to a different RE.

6.3.2 Heterogeneity Analysis

We apply the similar control variables method to analyze the influence of heterogeneity on the ASR performance in stratified aquifers. To isolate the impacts from the heterogeneity, in the first case, we assume the whole layered aquifer is isotropic (i.e. $K_{ix} = K_{iz}$). Then, the anisotropic cases are expected to discuss (i.e. $\frac{K_{ix}}{K_{iz}} = 10$).

Isotropic Illustrative Layered Case

In the cases of isotropic layered aquifers (K_H = 5 m/d, $K_{ix} = K_{iz}$), the ratio of hydraulic conductivity for each layer K_1/K_2 varies in the range of 0.001, 0.01, 0.1, 1, 10, 100 and 1000. In fact, the conditions that $\frac{K_1}{K_2} = 0.001$ and 1000, 0.01 and 100, or 0.1 and 10 exhibit the consistency of layered aquifers in terms of the corresponding transposition of each layer. In other words, the two cases that $\frac{K_1}{K_2} = 0.001$ and 1000 (0.01 and 100, or 0.1 and 10) represent a similar heterogeneity. We look forward to the same RE results for the corresponding conditions (i.e. $\frac{K_1}{K_2} = 0.001$ and 1000, 0.01 and 100, or 0.1 and 10) under the ideal circumstances (i.e. neglecting the vertical impacts). However, the hydraulic conductivity impacts from the vertical directions cannot be ignored especially in the isotropic stratified aquifers in reality. It is logical to consider six conditions of K_1/K_2 together, so that we can better comprehend the influence from the different ratios of hydraulic conductivities on the ASR performance.

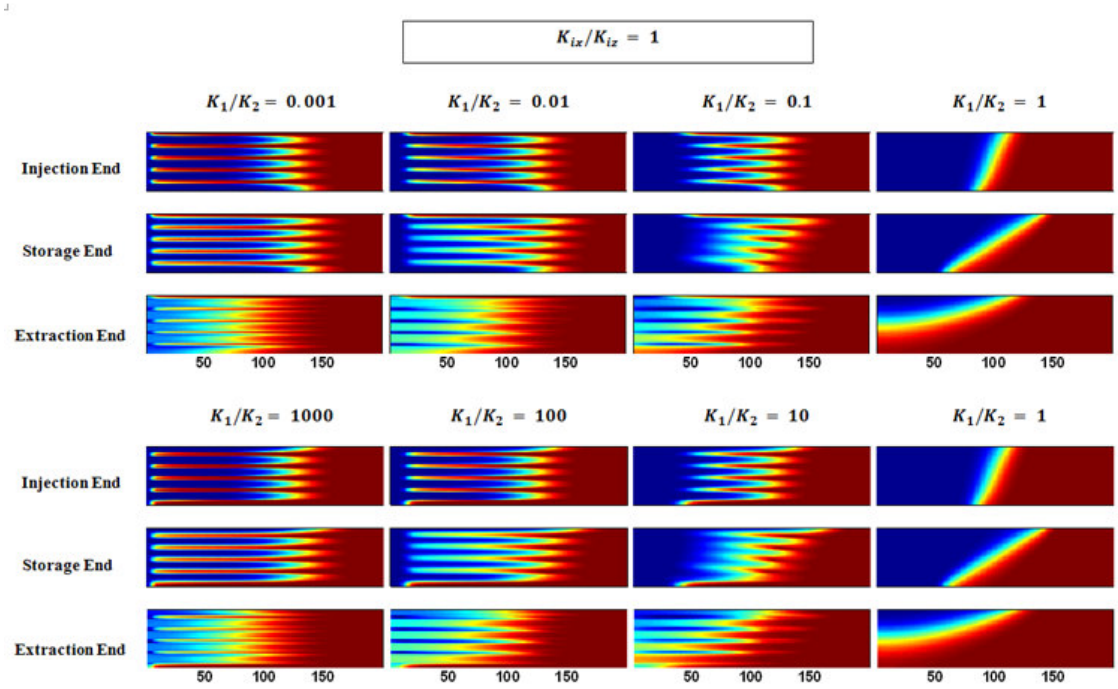

Figure 6.6 Concentration plots in isotropic layered aquifer with different heterogeneity

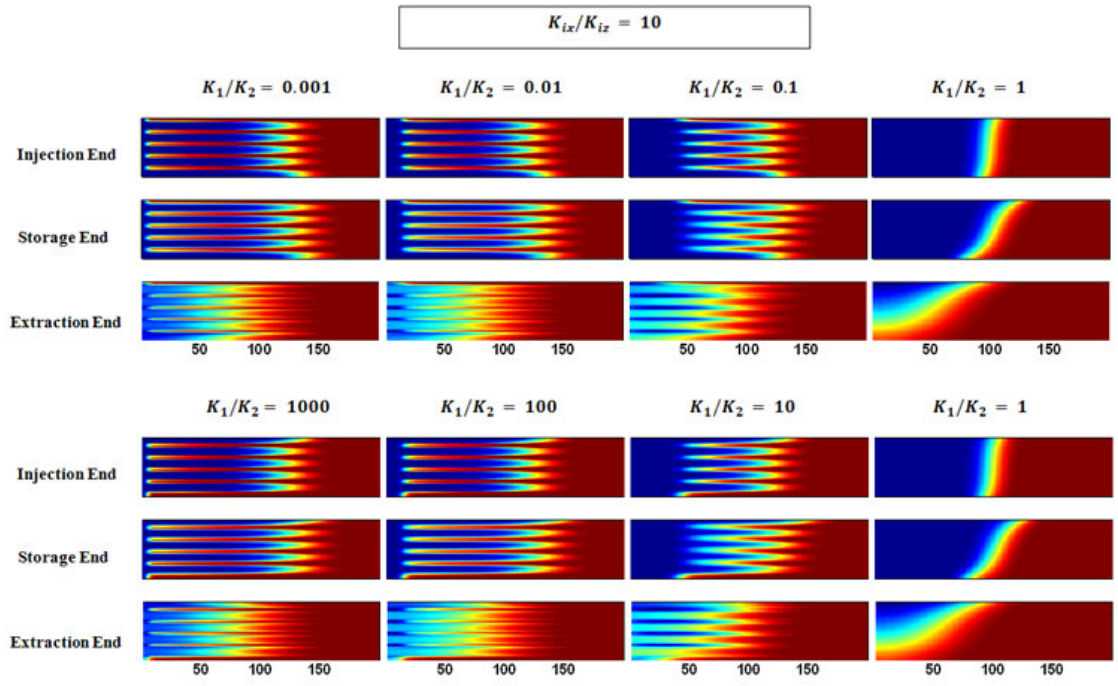

Figure 6.7 Concentration plots in anisotropic layered aquifer with different heterogeneity

Figure 6.6 separately displays the concentration plots in the isotropic layered aquifer for $\frac{K_1}{K_2}$ = 0.001, 0.01, 0.1, 1, 10, 100 and 1000 at the end of the different periods for one ASR cycle. We can qualitatively discover some impressive flow phenomena from the concentration plots. Firstly, let us focus on the injection process. During the period of injection, all cases illustrate that the solutes are promptly pushed aside in the high K layers, while comparatively immobilized in the low K layers. But at the end of injection, we see that the pushing distances of layers in different $\frac{K_1}{K_2}$ are quite different. For the cases that $\frac{K_1}{K_2}$ < 1, it is difficult to push away the top low K layer in comparison of other layers in the domain and the tendency turns more conspicuous as the increase of $\frac{K_1}{K_2}$; meanwhile, it is easy to push the bottom high K layer far away, particularly under the circumstance that $\frac{K_1}{K_2}$ = 0.001. For the cases that $\frac{K_1}{K_2}$ > 1, it becomes easy when pushing the top high k layer comparing with other layers of the aquifer; while, for any individual case, it turns much harder to push away the bottom low K layer. And both trends develop to the extent that we can even observe the macroscopic tilting of overall layers occurs at the case $\frac{K_1}{K_2}$ = 10. Secondly, during a storage period of 180 days, all cases clearly reveal two consequences: i) the mixing among layers becomes dominant in the density driven flow processes, including both the inter-layer and intra-layer concentration interchange; ii) the entire (50) solute interfaces demonstrate an integral noticeable slope over the whole aquifer depth. The density differences among layers obviously determine the macroscopic tilting effects, similarly as the homogeneous cases. Moreover, the moving velocities in different K layers are greatly distinct, to some extent, intensifying the tilting tendency. We can imagine that the inevitable mixing would definitely aggravate the

situation that freshwater is intruded by saltwater. By the nature of heterogeneous layered aquifers, freshwater is apt to be stuck in the low K layers while saltwater is easy to extract from the high k layers. This moderately exerts a negative influence on the recovery of freshwater. Thirdly, at the end of recovery period, the mixing develops further driven by the irresistible extracting force so as to accelerate the solute breakthrough. It is obvious that the amount of recovered freshwater is subject to some particular layers, namely the contributions from the layers with different hydraulic conductivities are actually different. To determine the amount of contributions from each layer is truly helpful to understand the meaning of RE value.

To compare with the homogeneous and isotropic case, we can conclude at least 3 main impacts on the ASR system from the heterogeneous isotropic layered aquifer. i) In the injection period, the maximum pushing distances in the heterogeneous cases are much farther than which in the homogeneous case. ii) In the storage period, the slopes of macroscopic tilting in the heterogeneous cases are distinct from which in the homogeneous case. When $\frac{K_1}{K_2}$ approaches 1 (i.e. smaller difference between K_1 and K_2), the slope of macroscopic tilting turns smaller. The smallest slope happens at the homogeneous ($K_1 = K_2$) and isotropic case. iii) The area of mixing zone in the heterogeneous layered aquifer is much bigger than which in the homogeneous aquifer. In other words, the mixing in the heterogeneous layered aquifer develops more drastically than which in the homogeneous aquifer. That implies a lot about the RE of one cycle ASR system. In fact, freshwater is expected to pump out from less mixed aquifers. So, the broader mixing zone would indeed suggest the less amount of recovered freshwater.

Anisotropic Illustrative Layered Cases

The isotropic layered cases present a fundamental view on how one cycle ASR system operates in the heterogeneous layered aquifer. Next, let us detect the influence of heterogeneity on one cycle ASR system in the cases of anisotropic layered aquifers. In this anisotropic case, we still assume K_H = 5 m/d, but $\frac{K_{ix}}{K_{iz}}$ = 10. And the ratio of hydraulic conductivity for each layer K_1/K_2 still varies in the range of 0.001, 0.01, 0.1, 1, 10, 100 and 1000.

Figure 6.7 displays the concentration plots in the anisotropic (i.e. $\frac{K_{ix}}{K_{iz}}$ = 10) layered aquifer for $\frac{K_1}{K_2} =$ 0.001, 0.01, 0.1, 1, 10, 100 and 1000 at the end of the different periods for one ASR cycle. First of all, we can qualitatively find that the flow processes at $\frac{K_{ix}}{K_{iz}} =$ 10 are similar to which at $\frac{K_{ix}}{K_{iz}}$ = 1 in the heterogeneous layered aquifers. We can still make 3 main conclusions similar as the isotropic cases ($\frac{K_{ix}}{K_{iz}}$ = 1) regarding the heterogeneity's influence on the ASR system, such as the phenomena about the maximum pushing distance, the slopes of macroscopic tilting, and the area of mixing zone. But from all cases shown in ***Figure 6.6***, we can clearly observe that the mixing between two adjoining layers weakens a lot comparing with isotropic cases. That really makes sense since the hydraulic conductivity impacts from vertical directions are reduced as ten percent of the original. The decrease of vertical mixing would be beneficial to the recovery of freshwater.

6.3.3 RE Analysis

RE Variation in Layered Aquifer

After qualitatively analyzing the anisotropy's and heterogeneity's influence on the one cycle ASR system, let us relatively quantitatively discover their effects by presenting the RE results. ***Table 6.2*** shows the RE results of one cycle ASR system for all kinds of cases with varying $\frac{K_1}{K_2}$ and $\frac{K_{ix}}{K_{iz}}$. We can clearly see that, for each of homogeneous ($\frac{K_1}{K_2}$ = 1) and heterogeneous cases ($\frac{K_1}{K_2}$ = 0.001, 0.01, 0.1, 1, 10, 100 and 1000), the RE gradually increases from the isotropic ($\frac{K_{ix}}{K_{iz}}$ = 1) to the extremely anisotropic ($\frac{K_{ix}}{K_{iz}} = \infty$) case, in well accordance with the mixing phenomenon we observed. In other words, the high anisotropy creates a helpful aquifer condition to achieve the goal of recovering more freshwater. In essence, the vertical mixing contributes a lot to the whole flow process. The isotropic aquifer generally provides a smooth condition for solute mixing, which promotes saltwater intruding into freshwater. Nevertheless, as the anisotropy increases, freshwater is more secure to pump out against being contaminated by saltwater since the vertical mixing weakens. Besides, for any of isotropic ($\frac{K_{ix}}{K_{iz}}$ = 1) and anisotropic ($\frac{K_{ix}}{K_{iz}}$ = 10, 100 and ∞) cases, the RE reaches the maximum at the homogeneous condition ($\frac{K_1}{K_2}$ = 1). That implies that the heterogeneity of layered aquifer would be harmful to the ASR performance. With the exception of the case at $\frac{K_{ix}}{K_{iz}} = \infty$ (i.e. $K_{iz} = 0$), the RE monotonously approaches the maximum as the decrease of difference between K_1 and K_2. In other words, under normally anisotropic circumstances, the RE would decrease as the enhancement of aquifer's heterogeneity. Whereas, we can observe an unusual RE jump

taking place at $\frac{K_1}{K_2}$ = 0.001 or 1000 and $\frac{K_{ix}}{K_{iz}} = \infty$ (i.e. K_{iz} = 0). This excites our curiosities about what determines the RE intrinsically in the layered aquifer. We will go through the concentration distribution profiles to discuss in the following. From the other perspective by respectively observing 3 parallel groups of the similar heterogeneity (i.e. $\frac{K_1}{K_2}$ = 0.001 and 1000, 0.01 and 100, or 0.1 and 10), we can find the values of RE are approximate for any group of the similar heterogeneity. And the trend is reinforced as the enhancement of anisotropy, particularly when K_{iz} = 0, the values of RE are even the same. Though, we can still clearly recognize the RE difference occurring in groups of the similar heterogeneity through the isotropic cases. More specifically, the RE of cases at $\frac{K_1}{K_2} > 1$ (i.e. $\frac{K_1}{K_2}$ = 10, 100, or 1000) is smaller than which at $\frac{K_1}{K_2} < 1$ (i.e. $\frac{K_1}{K_2}$ = 0.1, 0.01, or 0.001) respectively. This phenomenon is very remarkable because it reveals an interesting conclusion: although there is a similar heterogeneity in two layered aquifers, the sort order of layers plays an important role in determining the ASR performance. But this phenomenon decays as the enhancement of anisotropy, denoting again that the vertical mixing is very important to the ASR system.

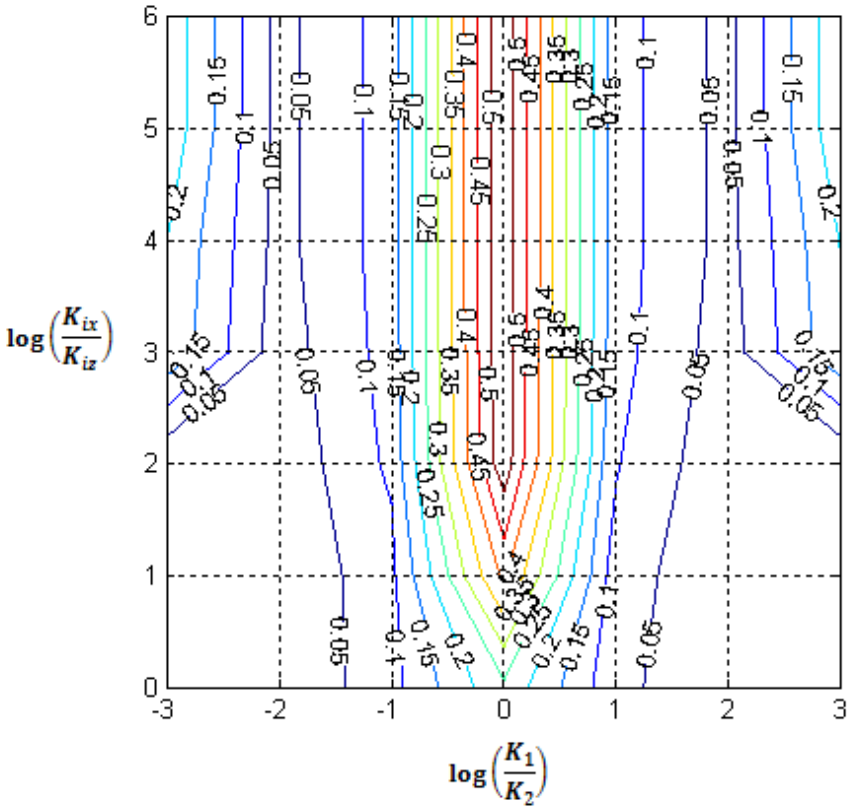

Figure 6.8 The log-log contour plot for RE variation in the layered aquifer

Table 6.2 RE results of one cycle ASR for all kinds of cases with varying $\frac{K_1}{K_2}$ and $\frac{K_{ix}}{K_{iz}}$

	$\log(K_1/K_2)$						
$\log(K_{ix}/K_{iz})$	-3	-2	-1	0	1	2	3
0	0.01%	0.30%	8.32%	23.89%	6.58%	0.21%	0.00%
1	0.06%	0.64%	8.40%	41.00%	7.61%	0.54%	0.06%
2	0.50%	1.11%	10.92%	53.11%	10.48%	1.09%	0.50%
3	19.22%	2.42%	11.96%	54.00%	11.86%	2.41%	19.17%
inf.	23.74%	3.39%	12.30%	54.00%	12.30%	3.39%	23.74%

We can check the RE for various cases with different anisotropy and heterogeneity in ***Table 6.2***. Also, we can draw a log-log contour plot to express RE variation in the layered aquifer, as shown in ***Figure 6.8***. It is intuitive to observe that the RE at the same horizontal line (i.e. same $\frac{K_{ix}}{K_{iz}}$) is axially symmetric about the vertical 0-axis, which proves again there would be an approximate axial (i.e. mirror-image) symmetry for both cases with the same anisotropy. Generally speaking, as the growth of the aquifer's homogeneity, the RE increases progressively and reaches the peak in the homogeneous aquifer. The only exception takes place at the region between $\left|\log\left(\frac{K_1}{K_2}\right)\right|$ = 2 and 3 when $\left|\log\left(\frac{K_{ix}}{K_{iz}}\right)\right|$ > 2. It seems a breakpoint to interrupt the RE decline trend as the heterogeneity develops further. We can consider an extreme case that K_1 or K_2 is zero. As holding K_H invariant, the K_1 ($/K_2$) is equal to 2 K_H while K_2 ($/K_1$) is zero. That means double discharges are applied to a half thickness aquifer. As discussed before, both the high flowrate and the narrow aquifer are beneficial to the RE. So we can imagine this extreme case with K_1 ($/K_2$) = 0 would achieve a higher RE than the homogeneous case while holding other parameters unchanged. Namely, the resilience of RE is strong enough to achieve a much higher RE than the homogeneous case. As a whole, when the average hydraulic conductivity is maintained in the layered aquifer, the common heterogeneity is harmful to the RE of one cycle ASR system, and we can achieve the optimal RE in the homogeneous aquifer; nevertheless, when facing the excessive layered heterogeneous aquifer, the RE would surpass the value in the homogeneous case and reach the maximum when there is no hydraulic conductivity through several layers at all. Next, let us consider the influence of anisotropy. At the same vertical line (i.e. same $\frac{K_1}{K_2}$), the RE monotonously increases as the augment of the aquifer's anisotropy. Other than that, as

the enhancement of $\frac{K_{ix}}{K_{iz}}$, the axial symmetry approaches a perfect match, implying that the high anisotropy tends to diminish the discrepancy created by the opposite layer ranking order between the both cases with the same anisotropy type (e.g. $\frac{K_1}{K_2}$ = 0.1 and 10, 0.01 and 100, or 0.001 and 1000). As a whole, the anisotropy is helpful to the RE of one cycle ASR system, and the high anisotropy would strengthen the ASR system operation consistency in the layered aquifer and remove the difference resulted from cases with the same anisotropy type but the opposite layer ranking order.

RE Determinants in Layered Aquifer

Next, let us go through the representative cases, and detect the concentration profiles at the breakthrough point to see what determines the RE in the layered aquifer. As shown in previous figures of layered aquifers, water runs fast through the high K layers while retards in the low K layers, regardless of injection or extraction period. This nature of layered aquifer determines that the concentration contributions from individual layers are different. This definitely affects the RE because the integral breakthrough is decided by each layer's contributions.

Figure 6.9 exhibits the concentration plot, salinity and mass flux distribution of each layer at the RE breakthrough moment for the isotropic (i.e. $\frac{K_{ix}}{K_{iz}}$ = 1) cases at $\frac{K_1}{K_2}$ = 1, 0.1, 0.01 or 0.001 respectively. We define that the mass flux of each layer is calculated by the product of each layer's discharge and salinity, shown as:

$$\boldsymbol{F} = q \cdot c \quad (6.10)$$

where $\boldsymbol{F}$ [$m^3d^{-1}\cdot10^{-3}$] is mass flux of each layer; q [m^3d^{-1}] is the discharge of each layer; c [gkg^{-1}] is the salinity of each layer. From the definition, it is obvious that mass flux expresses each layer's weighting component in the extraction process. In other words, mass flux we defined represents how much weight (influence) each layer contributes to the RE. The plot of salinity displays the real salinity of each layer but not the real each layer's contribution to the RE. The plot of mass flux distribution can intuitively provide a comprehensive view regarding which layers contribute much or little to the RE.

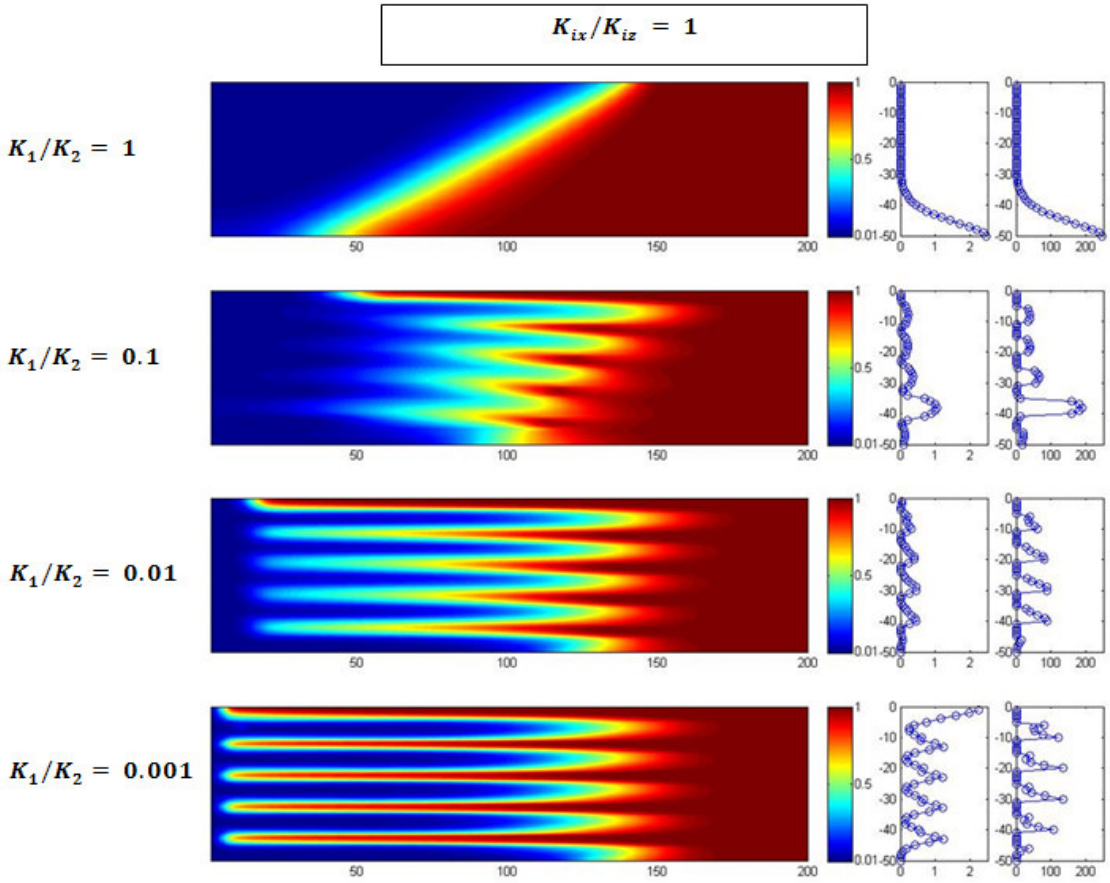

Figure 6.9 Concentration plot, salinity and mass flux distribution of each layer at the RE breakthrough moment for the isotropic (i.e. $\frac{K_{ix}}{K_{iz}} = 1$) cases at $\frac{K_1}{K_2} = 1$, 0.1, 0.01 or 0.001

We see that, the salinity is very consistent with mass flux distribution in the homogeneous case, however, the consistency declines as the increment of heterogeneity particularly across the intra-layer borders. Finally the case of $\frac{K_1}{K_2} = 0.001$ represents that the salinity distribution is almost completely inconsistent with the mass flux distribution. For instance, the top 10m layers exhibit the high salinity but the small mass flux, while the following downward 10m layers present an exactly opposite case that the low salinity corresponds to big mass flux. That means, the layers with high salinity do not play critical roles in the mass flux, by contrast, the layers with low salinity dominate the mass flux distribution and determine the RE at the breakthrough moment. This essentially explains the doubt why there is an unusual RE jump taking place at $\frac{K_1}{K_2} = 0.001$ and 1000. Although we pump the high salinity water out from the low K layers while the relatively low salinity water out from the high K layers, the weight of high salinity layers is much less than which of low salinity layers. From another perspective, this regulation denotes that, the salinity distribution can well indicate each layer's influence on the RE at the low heterogeneity case. But, as the layered heterogeneity increases, to some degree, the salinity distribution cannot express each layer's contribution to the RE any more. When the layered heterogeneity exceeds a certain value, the weight of each layer will play the critical role on the RE.

6.3.4 Stratified Aquifers and Equivalent Homogenized Aquifers

The stratified medium provides so many uncertainties and complexities that the scientists expect to simplify it by an equivalent homogenized medium (e.g. Missimer et al., 2002; Maliva et al., 2006; Ward et al., 2008). But, it is doubtful whether the stratified aquifers

can be simplistically homogenized, especially under various heterogeneous, anisotropic circumstances. Thus, it is necessary to examine the simplification feasibility and identify the influence difference between stratified and homogenized aquifers on the ASR performance.

Table 6.3 shows the RE results of stratified aquifers and equivalent homogenized aquifers in terms of different heterogeneities and anisotropies. First of all, we can clearly see that the RE results of stratified aquifers are different from which of equivalent homogenized aquifers. That means, the stratified aquifers cannot be simplistically replaced by the homogenized aquifers in the one cycle ASR system. Secondly, the RE results in the equivalent homogenized aquifers are much bigger than which in the stratified aquifers. Namely, the RE of one cycle ASR will be overestimated in the homogenized aquifers. Thirdly, as the increase of heterogeneity, the extent of RE overestimate turns much greater. That implies we cannot substitute the equivalent homogenized aquifers for the stratified aquifers in the analysis of ASR system, particularly when facing a high heterogeneous scheme. ***Figure 6.10*** shows the ideal values of RE_H are expected to be consistent with RE_S, as shown in the red line (i.e. $\frac{RE_H}{RE_S} = 1$). However in fact, all estimated values of RE_H are much bigger than RE_S. And the estimate bias turns much greater as the increase of heterogeneity. That demonstrates again that we cannot apply homogenized aquifers for the stratified cases in the investigation of ASR system.

Table 6.3 RE results of one cycle ASR in stratified aquifers and homogenized aquifers

Heterogeneity	Anisotropy	Stratified Aquifers					Homogenized Aquifers		
K_1/K_2	K_{ix}/K_{iz}	K_{1x}	K_{1z}	K_{2x}	K_{2z}	RE_S	K_H	K_V	RE_H
1	1	5.0000	5.0000	5.0000	5.0000	23.9%	5	5.0000	23.9%
1	10	5.0000	0.5000	5.0000	0.5000	41.0%	5	0.5000	41.0%
1	100	5.0000	0.0500	5.0000	0.0500	53.1%	5	0.0500	53.1%
10	1	9.0909	9.0909	0.9091	0.9091	6.6%	5	1.6529	30.2%
10	10	9.0909	0.9091	0.9091	0.0909	7.6%	5	0.1653	49.6%
10	100	9.0909	0.0909	0.9091	0.0091	10.5%	5	0.0165	53.8%
100	1	9.9010	9.9010	0.0990	0.0990	0.2%	5	0.1961	48.6%
100	10	9.9010	0.9901	0.0990	0.0099	0.5%	5	0.0196	53.8%
100	100	9.9010	0.0990	0.0990	0.0010	1.1%	5	0.0020	54.0%
1000	1	9.9900	9.9900	0.0100	0.0100	0.0%	5	0.0200	53.8%
1000	10	9.9900	0.9990	0.0100	0.0010	0.1%	5	0.0020	54.0%
1000	100	9.9900	0.0999	0.0100	0.0001	0.5%	5	0.0002	54.0%

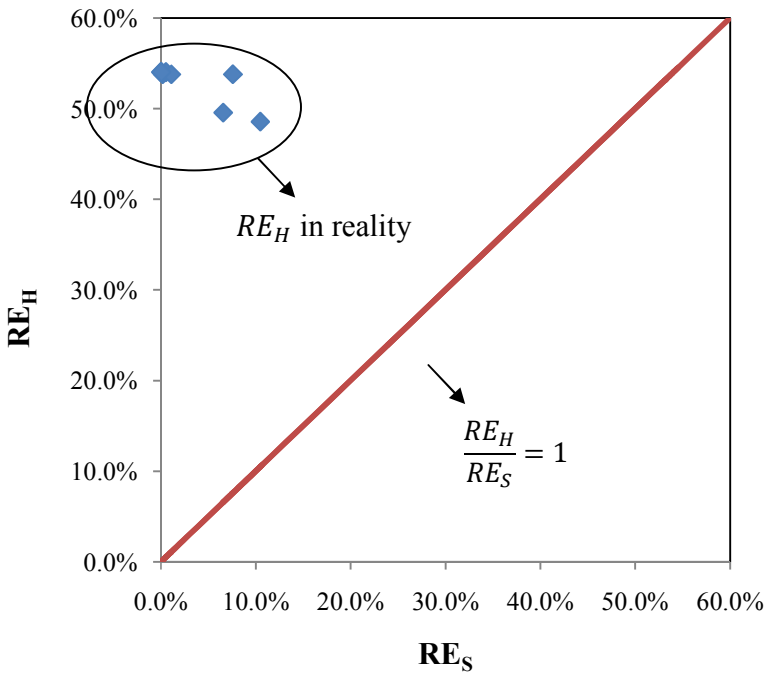

Figure 6.10 RE_H v.s. RE_S

6.4 Transverse Dispersion Effects on RE

6.4.1 Anisotropy Effects Analysis

In the first part, we recognized the effects of anisotropy on the ASR performance in stratified coastal aquifers when α_v is constant, 0.1m. Next, we will explore how the anisotropy affects the RE in stratified aquifers when varying α_v as 0, 0.01 or 0.2m, and investigate the differences in comparison with the case that α_v=0.1m.

Homogeneous and Anisotropic Cases

Figure 6.11 (a), (b), (c) and ***(d)*** display the concentration plots at the end of the different ASR periods (injection, storage and extraction) in the cases of α_v = 0, 0.01, 0.1 or 0.2m in homogeneous aquifers with anisotropy $\frac{K_{ix}}{K_{iz}}$ = 1, 10, 100 and ∞. We can obviously see that, in comparison with (c), (a), (b) and (d) do not vary much, indicating that the variation of transverse dispersivity does not affect much in the homogeneous cases.

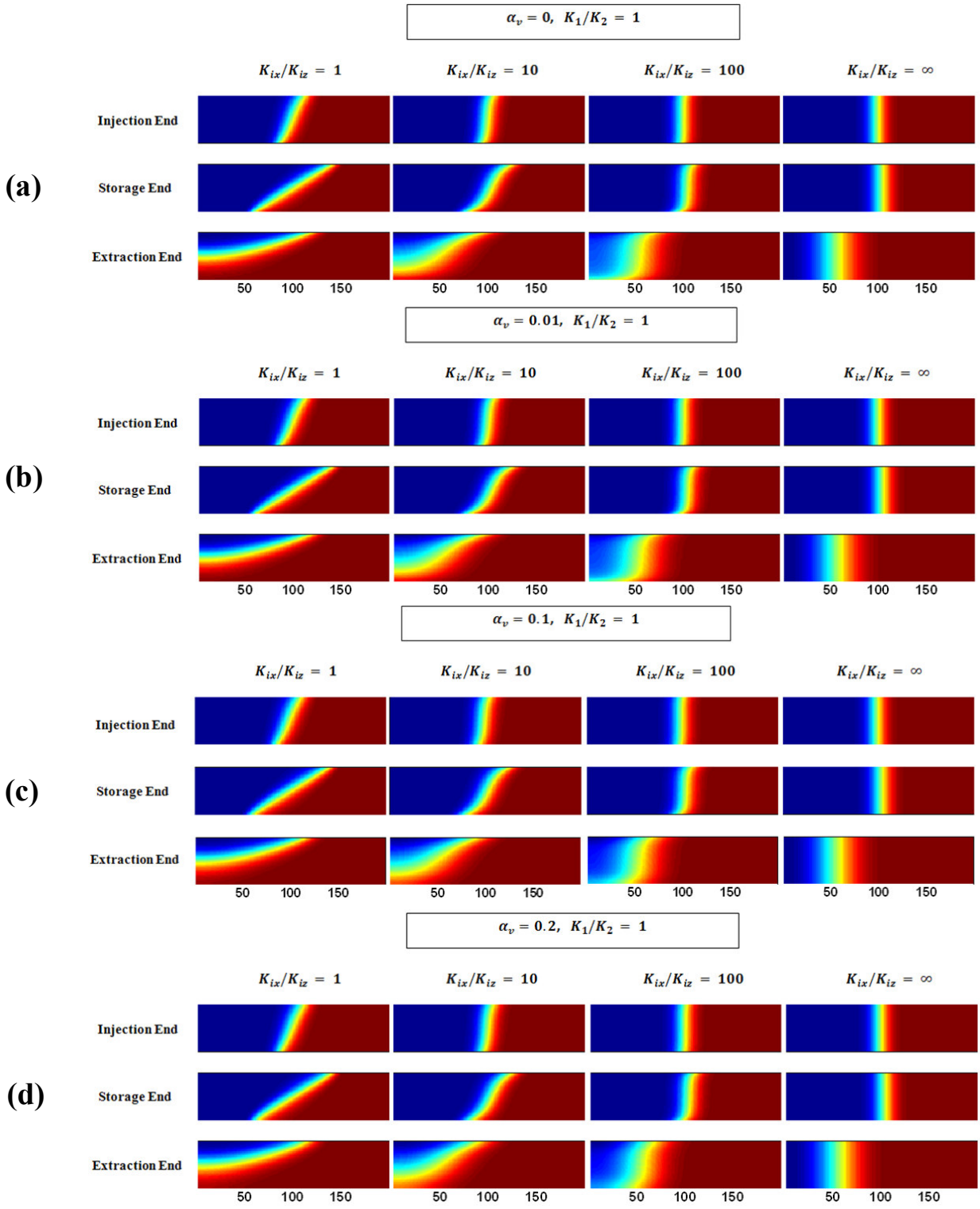

Figure 6.11 Concentration plots in the homogeneous aquifer (i.e. $\frac{K_1}{K_2} = 1$) with different anisotropy at α_v = 0, 0.01, 0.1 or 0.2m

Table 6.4 summarizes the RE results in the homogeneous aquifer cases with α_v = 0, 0.01, 0.1 or 0.2m, shown in ***Figure 6.11 (a), (b), (c)*** and ***(d)***. We can directly check that the RE almost remains constant will the increase of $\boldsymbol{\alpha_v}$. A slight increase can be found the isotropic cases, but lessens as the increase of anisotropy. This verifies the conclusion we made in Chapter 5, that the high transverse dispersivity is helpful to the RE by applying fully-penetrating wells in the homogeneous, isotropic aquifer. In addition, it denotes the influence of $\boldsymbol{\alpha_v}$ on the RE would diminish as K_{iz} decreases.

Table 6.4 RE results in the homogeneous aquifer at $\boldsymbol{\alpha_v}$ = 0, 0.01, 0.1 or 0.2m

K_1/K_2= 1	K_{ix}/K_{iz}			
α_v	1	10	100	∞
0	23.4%	40.7%	53.0%	54.0%
0.01	23.6%	40.8%	53.1%	54.0%
0.1	23.9%	41.0%	53.1%	54.0%
0.2	24.1%	41.1%	53.1%	54.0%

Heterogeneous and Anisotropic Cases

Figures 6.12 and ***6.13*** display the concentration plots for the cases $\frac{K_1}{K_2} =$ 10 and 0.1with the change of α_v = 0, 0.01, 0.1 or 0.2m.

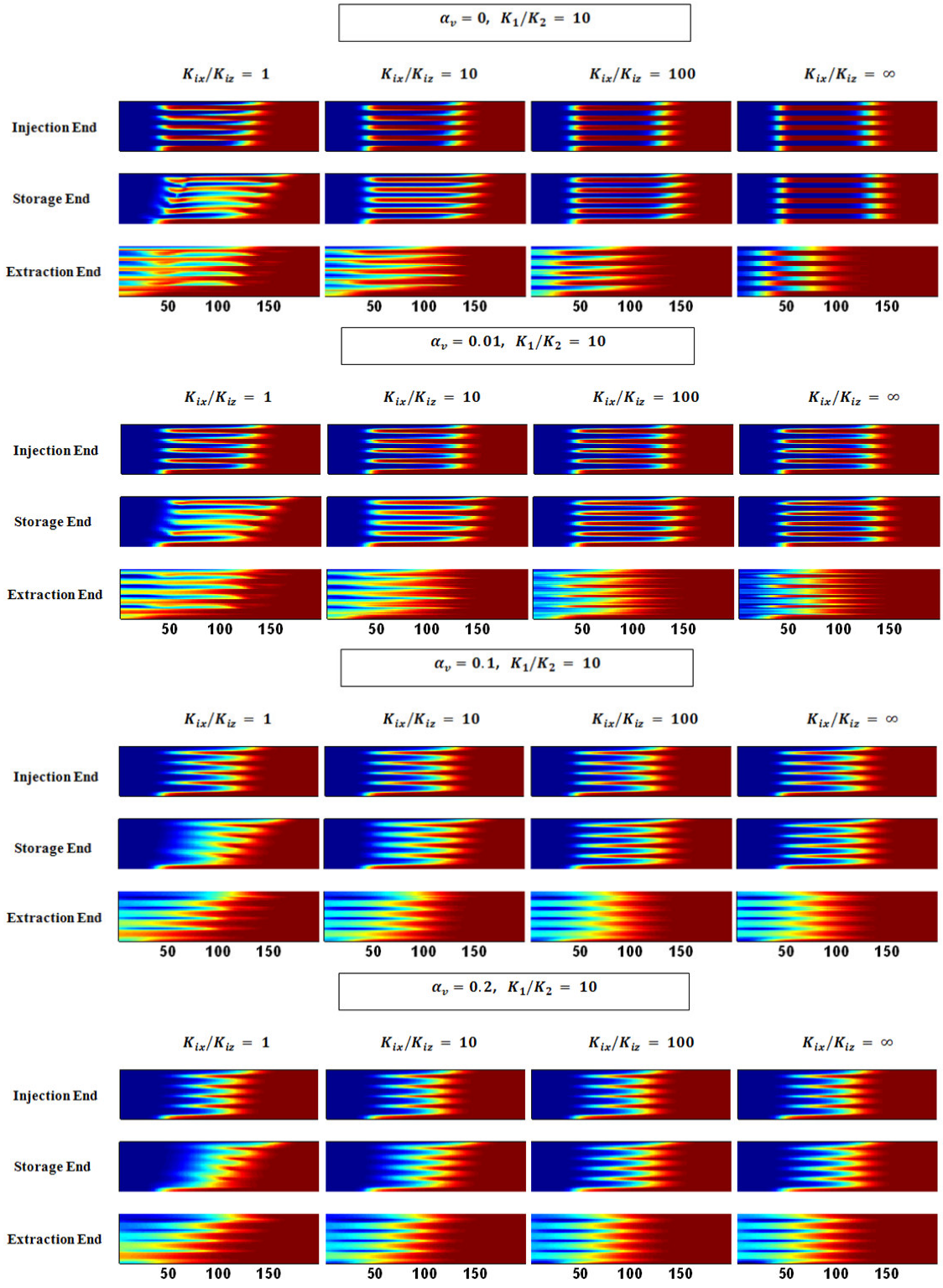

Figure 6.12 Concentration plots in the stratified aquifer (i.e. $\frac{K_1}{K_2} = 10$) with different anisotropy at α_v = 0, 0.01, 0.1 or 0.2m

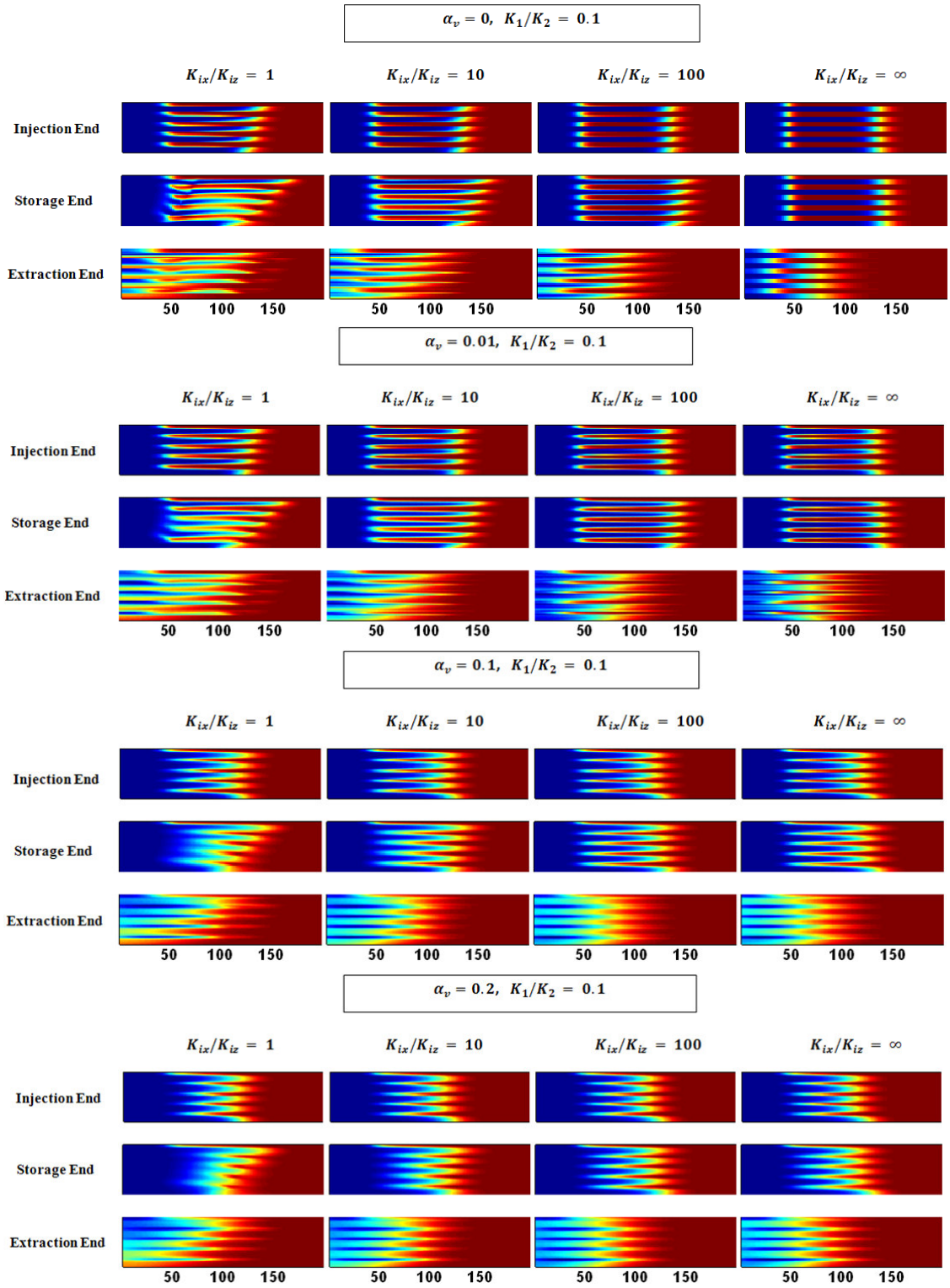

Figure 6.13 Concentration plots in the stratified aquifer (i.e. $\frac{K_1}{K_2} =$ 0.1) with different anisotropy at α_v = 0, 0.01, 0.1 or 0.2m

Unlike the homogeneous cases shown in ***Figure 6.11***, we can observe remarkable changes in the concentration plots as the change of transverse dispersivity. This is because the interface between the injected water body and the salt water becomes much longer than that in homogeneous cases. As a result, the transverse dispersion occurring at the interface is substantially enhanced, smearing the concentration differences among different layers.

Tables 6.5 and ***6.6*** summarize the RE results in the stratified aquifer shown in ***Figure 6.12*** and ***6.13***. Both cases exhibit that: 1) the RE increases as the anisotropy; 2) as α_v grows, the RE increases when $\frac{K_{ix}}{K_{iz}} = 1$, 10 or 100, but this tendency does not work when $\frac{K_{ix}}{K_{iz}} = \infty$; 3) for fixed α_v, the RE achieves the same value for both when $\frac{K_{ix}}{K_{iz}} = \infty$. On the other hand, Tables 7.3 and 7.4 also show that the RE at $\frac{K_1}{K_2} = 10$ is always smaller than that at $\frac{K_1}{K_2} = 0.1$ with a given transverse dispersivity and such difference decays as the anisotropy increases. Recalling the conclusion we found in Chapter 5, the high transverse dispersivity is helpful to the RE in homogeneous, isotropic aquifers. We can now generalize the conclusion to the anisotropic, stratified aquifer by excluding the stratified aquifer with extremely high anisotropy.

Table 6.5 RE results in stratified aquifers when $\frac{K_1}{K_2} = 10$ at α_v = 0, 0.01, 0.1 or 0.2m

K_1/K_2= 10	K_{ix}/K_{iz}			
α_v	1	10	100	∞
0	3.1%	4.3%	5.9%	43.3%
0.01	3.9%	4.9%	7.5%	13.4%
0.1	6.6%	7.6%	10.5%	12.3%
0.2	8.4%	10.1%	12.8%	13.4%

Table 6.6 RE results in stratified aquifers when $\frac{K_1}{K_2} = 0.1$ at α_v = 0, 0.01, 0.1 or 0.2m

K_1/K_2= 0.1	K_{ix}/K_{iz}			
α_v	1	10	100	∞
0	4.5%	4.6%	6.2%	43.3%
0.01	5.0%	5.2%	7.9%	13.4%
0.1	8.3%	8.4%	10.9%	12.3%
0.2	11.4%	11.4%	13.3%	13.4%

6.4.2 Heterogeneity Effects Analysis

We will explore how the heterogeneity affects the ASR performance in stratified aquifers when varying α_v as 0, 0.01, 0.1 or 0.2m.

Isotropic Layered Case

Figure 6.14 (a), (b), (c) and ***(d)*** displays the concentration plots in the conditions of α_v = 0, 0.01, 0.1 or 0.2m in the isotropic stratified aquifer when $\frac{K_1}{K_2}$ = 0.001, 0.01, 0.1, 1, 10, 100 and 1000 at the end of the different ASR periods.

We can observe some impressive phenomena when α_v varies: 1) no matter what the value of α_v is, we verify that the case $\frac{K_1}{K_2} = 0.001$ (or 0.01, or 0.1) and the case $\frac{K_1}{K_2} = 1000$ (or 100, or 10) demonstrates a similar transport pattern, implying in aquifers with high hydraulic conductivity contrasts, transport patterns are similar and independent of the layer placement; 2) if we focus on the aquifers with same heterogeneity (e.g. $\frac{K_1}{K_2} = 0.001$ and 1000, or $\frac{K_1}{K_2} = 0.01$ and 100, or $\frac{K_1}{K_2} = 0.1$ and 10), as α_v increases, the inter-layer vertical mixing increases; 3) the influences of α_v on the vertical mixing will diminish as the heterogeneity grows (i.e., $\frac{K_1}{K_2}$ increases from 10 to 1000, or 0.1 to 0.001).

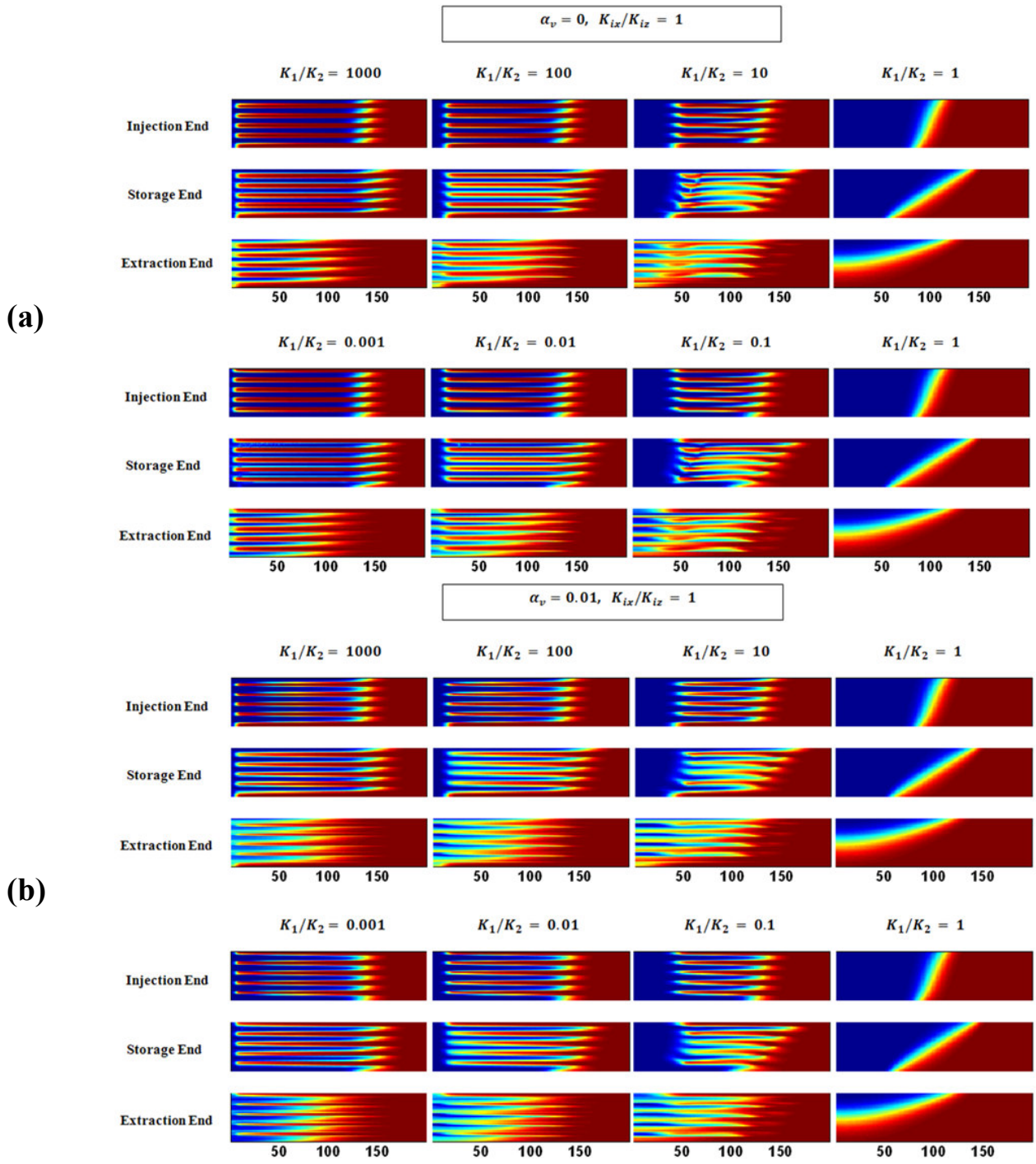
(a)
$\alpha_v = 0,\ K_{ix}/K_{iz} = 1$
$K_1/K_2 = 1000$
$K_1/K_2 = 100$
$K_1/K_2 = 10$
$K_1/K_2 = 1$
Injection End
Storage End
Extraction End
50 100 150
$K_1/K_2 = 0.001$
$K_1/K_2 = 0.01$
$K_1/K_2 = 0.1$
$K_1/K_2 = 1$
(b)
$\alpha_v = 0.01,\ K_{ix}/K_{iz} = 1$

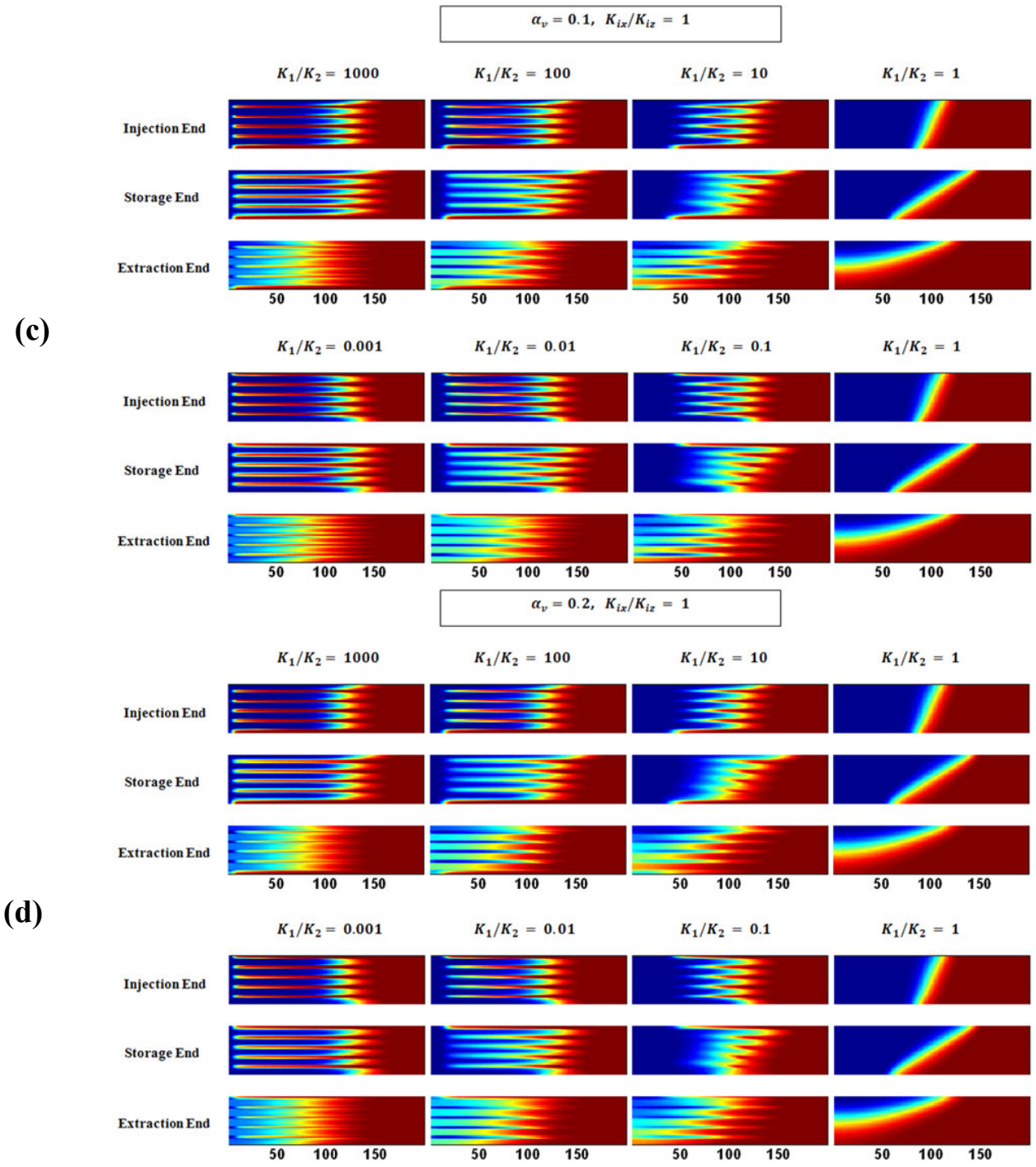

Figure 6.14 Concentration plots in the isotropic aquifer for the cases with different heterogeneity at $\boldsymbol{\alpha_v}$ = 0, 0.01, 0.1 or 0.2m

Table 6.7 lists the RE results in the isotropic stratified aquifer at α_v = 0, 0.01, 0.1 or 0.2m, in correspondence with cases shown in ***Figure 6.14***. The results exhibit: 1) no matter what the value of α_v is, the RE increases as the conductivity contrast decreases, and the maximum RE occurs in the homogeneous case; 2) as α_v grows, the RE increases for constant conductivity contrast (i.e., $\frac{K_1}{K_2} = 1000$ and 0.001, or 100 and 0.01, or 10 and 0.1); 3) for fixed α_v, the REs are all almost zero in the isotropic, highly stratified aquifer (i.e. $\frac{K_1}{K_2} = 1000$ and 0.001). On the other hand, for fixed α_v, the RE at $\frac{K_1}{K_2} = 1000$ (or 100, or 10) is always smaller than which at $\frac{K_1}{K_2} = 0.001$ (or 0.01, or 0.1) in this isotropic stratified aquifer. The results demonstrate that the high vertical dispersivity is helpful to the RE in the isotropic, stratified aquifer.

Table 6.7 RE results in the isotropic stratified aquifer at $\boldsymbol{\alpha_v}$ = 0, 0.01, 0.1 or 0.2m

K_{ix}/K_{iz}= 1	K_1/K_2						
α_v	1000	0.001	100	0.01	10	0.1	1
0	0.00%	0.00%	0.04%	0.07%	3.06%	4.48%	23.44%
0.01	0.00%	0.00%	0.10%	0.14%	3.89%	5.00%	23.56%
0.1	0.00%	0.01%	0.21%	0.30%	6.58%	8.32%	23.89%
0.2	0.00%	0.02%	0.33%	0.46%	8.44%	11.44%	24.11%

Anisotropic Illustrative Layered Cases

Figure 6.15 (a), (b), (c) and ***(d)*** displays the concentration plots in the conditions of α_v = 0, 0.01, 0.1 or 0.2m in the anisotropic (i.e. $\frac{K_{ix}}{K_{iz}} = 10$) stratified aquifer when $\frac{K_1}{K_2}$ = 0.001, 0.01, 0.1, 1, 10, 100 and 1000 at the end of the different ASR periods. The following behavior can be observed: 1) no matter what the value of α_v is, the case with $\frac{K_1}{K_2} = 0.001$ (or 0.01, or 0.1) and the case with $\frac{K_1}{K_2} = 1000$ (or 100, or 10) demonstrate similar transport patterns. 2) In aquifers with the same hydraulic conductivity contrast, as α_v increases, the inter-layer vertical mixing increases, but the extent of vertical mixing lessens comparing with the isotropic cases due to the increase of anisotropy; 3) for fixed α_v, the influences of α_v on the vertical mixing strengthen as the aquifer becomes more homogeneous (i.e., $\frac{K_1}{K_2}$ decreases from 1000 to 1, or 0.001 to 1).

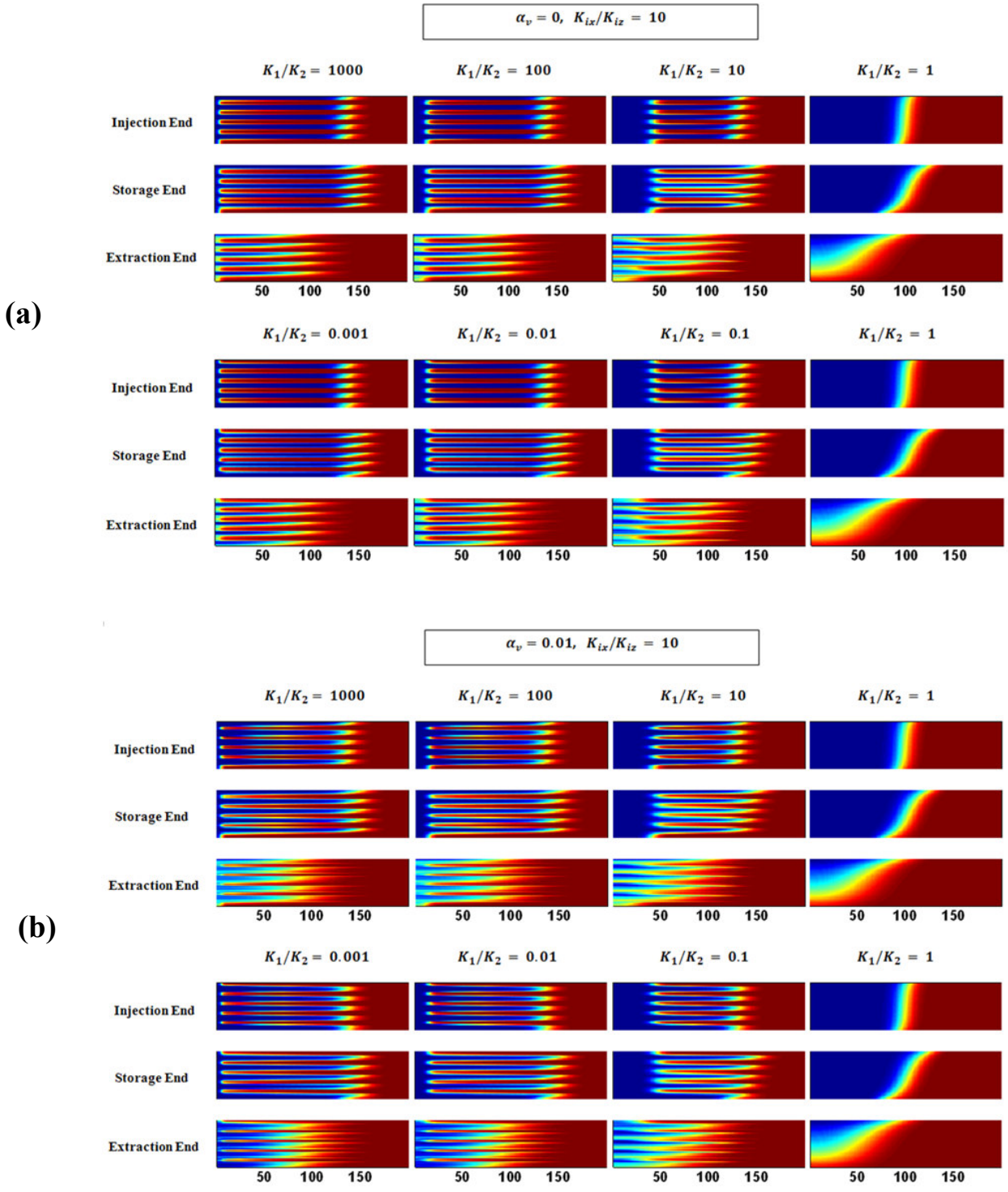
(a)
$\alpha_v = 0,\ K_{ix}/K_{iz} = 10$
$K_1/K_2 = 1000$
$K_1/K_2 = 100$
$K_1/K_2 = 10$
$K_1/K_2 = 1$
Injection End
Storage End
Extraction End
50 100 150
$K_1/K_2 = 0.001$
$K_1/K_2 = 0.01$
$K_1/K_2 = 0.1$
$K_1/K_2 = 1$
(b)
$\alpha_v = 0.01,\ K_{ix}/K_{iz} = 10$

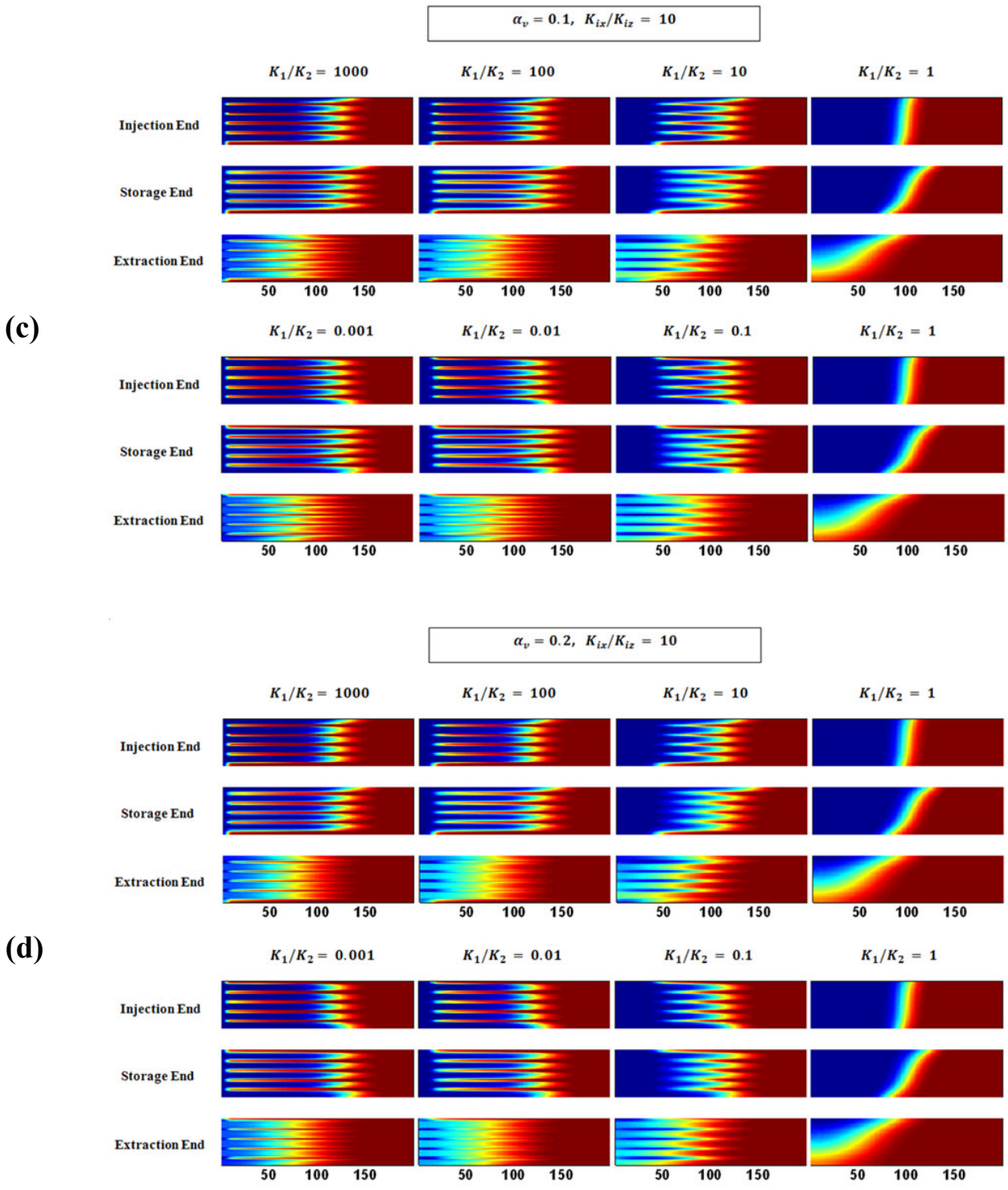

Figure 6.15 Concentration plots in the anisotropic stratified aquifer when $\frac{K_{ix}}{K_{iz}} = 10$ for the cases with different heterogeneity at α_v = 0, 0.01, 0.1 or 0.2m

Table 6.8 lists the RE results in the anisotropic stratified aquifer for $\frac{K_{ix}}{K_{iz}} = 10$ at α_v = 0, 0.01, 0.1 or 0.2m, in correspondence with cases shown in ***Figure 6.15***. The cases with the same type of heterogeneous show: 1) no matter what the value of α_v is, the RE increases as the conductivity contrast decreases, and the maximum occurs at the homogeneous cases; 2) as α_v grows, the RE increases with constant contrasts, including the homogeneous anisotropic cases. In addition, for fixed α_v, the RE at $\frac{K_1}{K_2} = 1000$ (or 100, or 10) is always smaller than which at $\frac{K_1}{K_2} = 0.001$ (or 0.01, or 0.1), demonstrating that the high vertical dispersivity is helpful to the RE in the anisotropic stratified aquifer.

Table 6.8 RE results in the anisotropic aquifer when $\frac{K_{ix}}{K_{iz}} = 10$ at α_v = 0, 0.01, 0.1 or 0.2m

K_{ix}/K_{iz}= 10	K_1/K_2						
α_v	1000	0.001	100	0.01	10	0.1	1
0	0.00%	0.00%	0.13%	0.17%	4.29%	4.64%	40.67%
0.01	0.04%	0.04%	0.33%	0.42%	4.89%	5.22%	40.78%
0.1	0.06%	0.06%	0.54%	0.64%	7.61%	8.40%	41.00%
0.2	0.06%	0.06%	0.71%	0.81%	10.11%	11.44%	41.11%

6.5 Conclusion

This study investigated the influence of anisotropy and heterogeneity and the transverse dispersion's effects on the RE of on the one cycle ASR system in the layered aquifer. We intuitively displayed the density effects on the different types of layered aquifers, and analyzed the effects of the anisotropy and heterogeneity on the ASR performances qualitatively and quantitatively.

In summary, the common heterogeneity is harmful to the RE of one cycle ASR system, and the RE increases progressively and reaches the peak in the homogeneous aquifer as the growth of the aquifer's homogeneity. Nevertheless, when facing the excessive layered heterogeneous aquifer, the RE would surpass the value in the homogeneous case and achieve an optimal value in the case that there is no hydraulic conductivity through several layers at all. In fact, the nature of layered aquifers determines that each layer's contributions to the entire RE are different.

In general, the anisotropy is helpful to the RE of one cycle ASR system, and the high anisotropy would strengthen the ASR system operation consistency in the layered aquifer and remove the difference resulted from cases with the same anisotropy type but the opposite layer ranking order.

Moreover, we found that the stratified aquifers cannot be simplistically replaced by the equivalent homogenized aquifer in the ASR system. The homogenized aquifers would overestimate the RE of one cycle ASR system, especially in the highly stratified aquifers.

Through transverse dispersion, it plays an important role in stratified aquifers because of significantly stretched interface. In the layered cases with communication between layers

with one moving faster than the neighboring layers, transverse dispersion serves to diminish the progress of the fast front and enhance the progress of the slow front. Such a self-limiting feature would reduce the overall rate of salt spreading and is beneficial for improving the ASR efficiency for hydraulic conductivity contrasts up to 100. However, in highly stratified aquifers with high conductivity contrasts, higher transverse dispersion may effectively enhance the mixing zone in the layers with high hydraulic conductivities, leading to lower ASR efficiency.

CHAPTER 7

IMPROVING ASR EFFICIENCY BY PARTIALLY-PENETRATING WELLS IN SALINE AQUIFERS

This chapter aims to study a particular ASR scheme with fully-penetrating wells (FPWs) for injection and partially-penetrating wells (PPWs) for recovery to improve the RE for ASR schemes implemented in brackish aquifers (***Figure 7.1 d*** and ***e***). This design appreciates the tilting shape of the interface with underlying heavier salt water. For fully-penetrating wells, recovery has to be terminated as soon as the interface toe reaches the well, while the toe can be pulled up to the partially-penetrating well for recovery termination, resulting in later breakthrough of salt water into the pumping well, more recoverable water extracted from the shallow layers, and a higher RE. The technique of pumping water from one part of a fully-penetrating well is mature in practice (e.g., Fienen et al., 2006). One may also simply install two adjacent wells, one fully-penetrating for injection and the other partially-penetrating for recovery. In this research, we develop numerical models to provide scientific understanding to support the design and implementation. Specific questions that will be addressed include: how significant can the RE be improved by using this particular ASR scheme? And what are the effects of hydrogeological conditions and ASR operational processes on the RE?

7.1 Numerical Methods

7.1.1 Conceptual Model

Figure 7.1 shows the conceptual model of typical ASR systems with a fully-penetrating pumping well (***Figure 7.1 c***) and a partially-penetrating pumping well (***Figure 7.1 d*** and ***e***) installed in a confined, homogeneous, isotropic aquifer with a uniform thickness B. By neglecting regional flow, the three-dimensional domain is modeled by a two-dimensional axisymmetric cross-section with the vertical axis of rotation located at the pumping well. For both ASR systems, the injection well is fully penetrated, i.e., ***Figure 7.1 a*** and ***b*** work for both systems. During the injection phase, fresh water is injected into the aquifer and a concentration front moves away from the pumping well. The freshwater-saltwater interface may slightly tilt due to density gradient. During the storage phase, no flow occurs but the interface is further tilted by density gradient. During the recovery phase, stored water is extracted via the same pumping well and the concentration front moves toward the pumping well. For simplicity, we assume the same total injection flow rate, Q [L^3T^{-1}], and the recovery rate, which implies larger specific pumping rate for the partially-penetrating extraction well. The RE is evaluated by setting a criterion of the average concentration of extracted water at the pumping well, such as the U.S. EPA potable-water standard. In this research, we choose 1% of the original groundwater concentration as the threshold concentration.

7.1.2 Governing Equations

The same as Chapter 5.

7.1.3 Evaluation of ASR Performance

The same as Chapter 5.

7.1.4 Model Parameters

Table 7.1 summarizes the hydrogeological, transport and operational parameters in a base numerical model, abbreviating as BC for the subsequent sensitivity analysis to investigate the effects of various hydrogeological conditions, transport and operational parameters. In fact, the BC here is very similar to base model we applied in Chapter 5. The only difference is the extraction thickness h [m]. By applying partially-penetrating wells, we vary extraction thickness h [m] to observe how it affects the ASR performance. We apply the same duration assumption as in Chapter 5, which is to represent a yearly-based ASR cycle in terms of 90 days injection, 180 days storage and 90 days extraction.

7.1.5 Dimensional Analysis

The same as Chapter 5.

Table 7. 1 Parameters used for BC model by partially-penetrating wells

BC Model Parameter	Variable	Value
Aquifer Thickness (m)	B	50
Domain Radius (m)	L	370
Seawater/Freshwater Level (m)	h_s/ h_f	50
Initial Ambient/Salt Water Salinity (g kg-1)	C_i/ C_s	35
Injected Water Salinity (g kg-1)	C_w	0
Effective Porosity (-)	θ	0.3
Molecular Diffusivity (m2 d-1)	D_m	0
Specific Storage (m-1)	S_s	0.005
Hydraulic Conductivity (m d-1)	K	5
Longitudinal Dispersivity (m)	α_L	1
Transverse Dispersivity (m)	α_T	0.1
Freshwater Density (kg m-3)	ρ_f	1000
Seawater Density (kg m-3)	ρ_s	1025
Injection/Extraction Flowrate (m3 d-1)	Q_i / Q_e	4000 / -4000
Injection Duration (day)	T_i	90
Storage Duration (day)	T_s	180
Total Injection Volume (m3)	V_t	360000
Extraction Depth (m)	h	$50 \cdot \varepsilon$

7.2 Illustrative Example

Figure 7.1 (a) and ***(b)*** show the normalized concentration distribution and contour lines at the end of injection phase ($T = 90$ days) and storage phase ($T = T_i + T_s = 270$ days), respectively. ***Figure 7.1 (c), (d)*** and ***(e)*** show the normalized concentration distribution

and contour lines of $\varepsilon = 1.0, 0.5$ & 0.2 at the moment when the salinity of extracted water reaches the criterion we set (i.e. 0.35g/kg).

We keep the same extraction flow rate but choose the different extraction position to achieve the goal pumping out more water. It is apparent that concentration contour lines are highly different at the pumping well position (i.e. x = 0). We can clearly observe the concentration distribution discrepancy among ***Figure 7.1 (c), (d)*** and ***(e)***. For the fully-penetrating case, the recovery phase has to be terminated when the toe of the contour lines reaches the well, while the contour lines are pulled up for the partially-penetrating cases so that more water can be extracted.

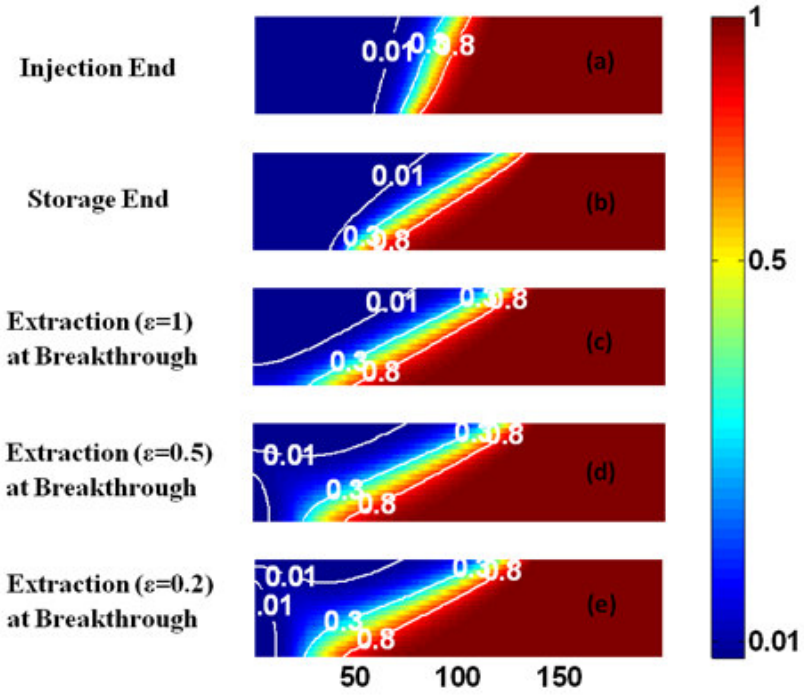

Figure 7.1 Standardized concentration distribution and contour line at different time for BC by PPW

Figure 7.2 shows the salinity (C) distribution at the position of pumping well (i.e. x = 0) for $\varepsilon = 1.0, 0.5$ & 0.2 respectively at the breakthrough moment with the salinity reaching the criterion (i.e. the end of recovery). For the fully-penetrating well, the concentration profile is a monotonically increasing function of the aquifer depth, indicating that the salinity at the interface toe controls the ASR efficiency. For partially-penetrating wells, the concentration profiles become non-monotonic with maximum concentration occurring in the middle layers, implying that the more water can be extracted from bottom layers.

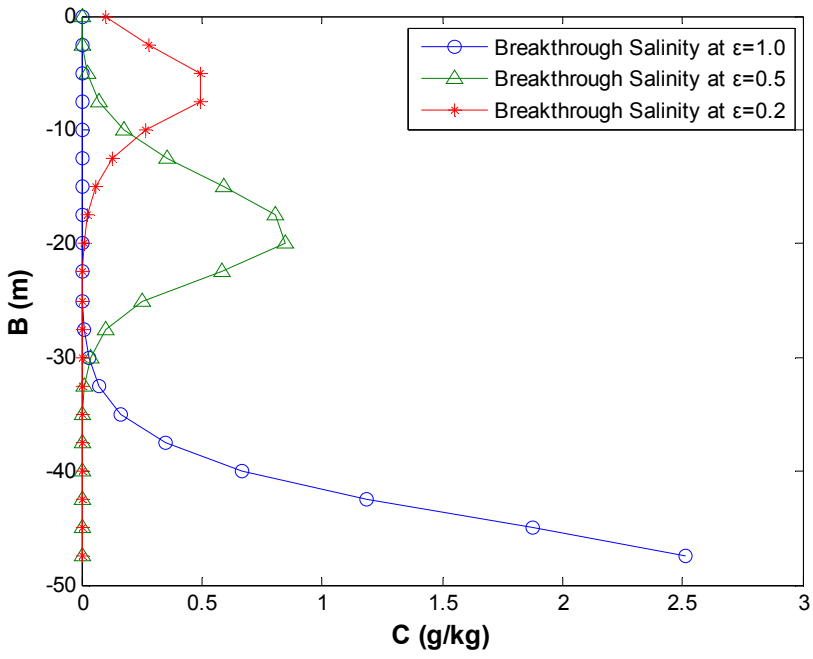

Figure 7.2 Breakthrough salinity distribution in the position of pumping well for different extracting position

Table 7.2 shows the actual extraction duration time T_e (i.e. the operation days from the end of storage duration to the moment when the salinity of extracted water reaches the criterion, 0.35g/kg), RE and increased RE results for BC when $\varepsilon = 1.0, 0.5$ & 0.2 respectively. Increased RE (IRE) is defined as the increment ratio compared with the fully-penetrating case:

$$IRE = \frac{T_e(\varepsilon<1) - T_e(\varepsilon=1)}{T_e(\varepsilon=1)} \quad (7.1)$$

where IRE can be positive or negative and its absolute value can be greater or smaller than 1. It is sure that the bigger IRE reveals the better improvement of RE.

The significant improvement of RE shown in ***Table 7.2*** demonstrate the feasibility of using the partially-penetrating wells to improve ASR efficiency.

Table 7.2 RE Results for BC by applying PPW

ε (-)	h (m)	T_e (day)	RE (%)	IRE (%)
1.0	50	16.7	18.6%	/
0.5	25	25.3	28.1%	51.5%
0.2	10	27.5	30.6%	64.7%

7.3 Analysis in Homogeneous and Isotropic Aquifers

In this section, we will investigate the performance of the proposed ASR scheme using partially-penetrating wells in aquifers with various hydrogeological and operational parameters so that we can examine if the improvement shown by the BC can be generalized and transferred to other sites with different conditions.

7.3.1 Hydrogeological Parameters Analysis

Saltwater density ρ_s [M L^{-3}] / Seawater salinity [g kg^{-1}]:

Figure 7.3 a compares the RE of FPWs and PPWs by varying the saltwater concentration from 20 to 65 g/L. As ε decreases from 1 to 0.2, the RE increases for most saltwater concentration C_s. The only exception is the case when C_s is equal to 5 g/L , in which the density effect is small. The idea of the PPW is actually based on strong density effects. If the density effects of the aquifer are weak, the PPW does not help improving the RE. In addition, for a given ε, the RE increases as the decrease of C_s because of the reduced density effects. The lower C_s implying the weaker density effect leads to the less tilting mixing zone. If the slope of the mixing zone is not sharp enough, we can extract more freshwater from the well. ***Figure 7.3 b*** shows the variation of IRE for density effects at different ε with the PPW method. As ε decreases from 0.75 to 0.2, the relative improvement of RE becomes bigger for large C_s. However, the gradient variation is very distinct. It is obvious, for Case 5 (i.e. C_s = 65 g/L), the absolute value of IRE gradient is much bigger than the others. Namely, the PPW method works better for higher C_s. Thus, if density effects are strong, we can gain good improvement of RE by applying the PPW

method. In addition, for saltwater concentrations less than typical seawater concentration, C_s = 35 g/L, the relative improvement of RE is not sensitive to the well penetrating depth.

(a)

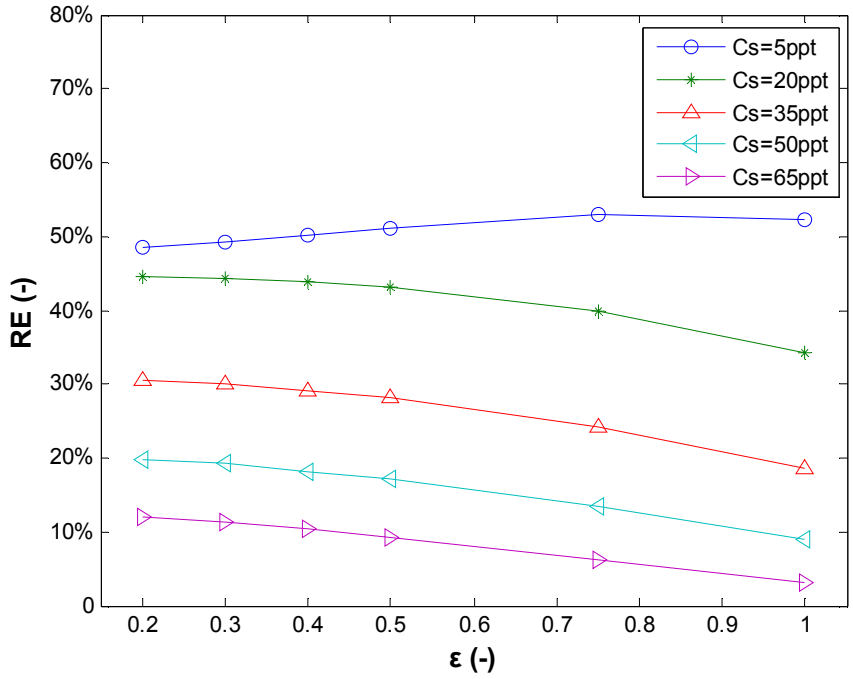

(b)

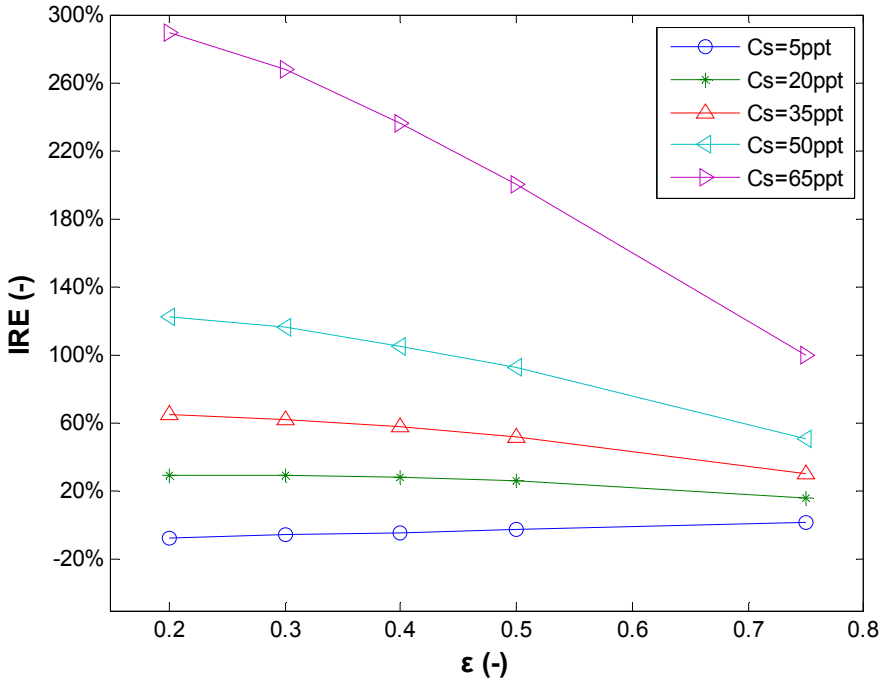

Figure 7.3 Sensitivity analysis for salinity by PPW method

Aquifer thickness *B* [L]:

Figures 7.4 a and ***b*** show that the RE improvement is dramatic with the increase of the aquifer thickness. Only slight improvement can be observed in aquifers with small thickness. In addition, the well penetrating depth takes effects only in thick aquifers. This is because the tilting interface intrudes further toward the well with the increase of the aquifer thickness, reducing the available freshwater for recovery for FPWs. In other words, density effects become more important in thick aquifers, rendering the PPW method more effective for improving the RE.

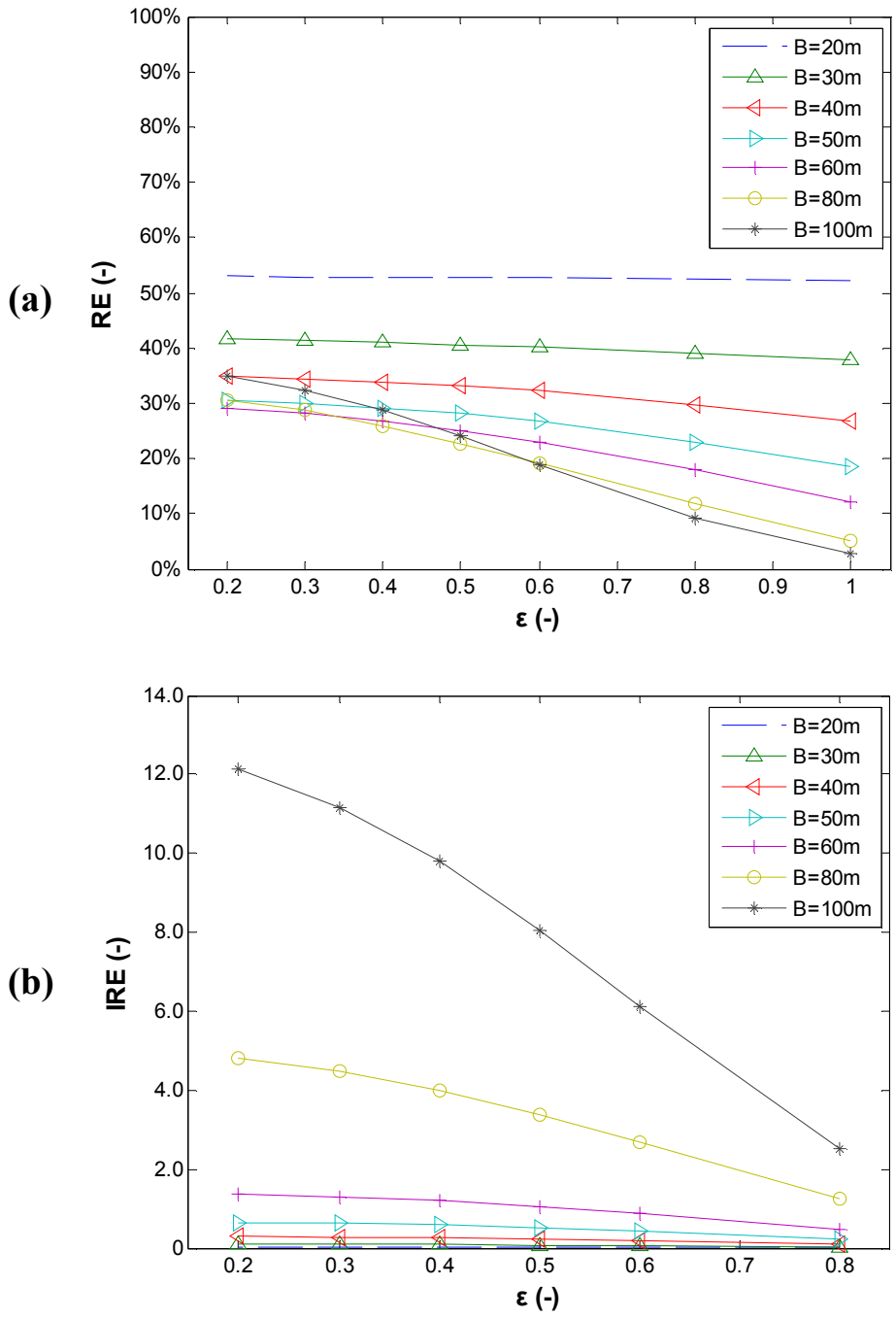

Figure 7.4 Sensitivity analysis for aquifer thickness by PPW method

Hydraulic conductivity *K* [L T^{-1}]:

Figure 7.5 a shows the RE variation when *K* varies from 1 to 10 m/d. We can find that the RE increases as ε decreases from 1 to 0.2 for almost all given *K* [L T^{-1}], except that *K* = 1m/d, in which, the RE fluctuates around 67.0% owing to the weak density effects when the hydraulic conductivity is small (Ward et al., 2007). By neglecting the extreme case, in consequence, we demonstrate that the PPW method works very well to improve the ASR performance in the homogeneous and isotropic aquifer with regular hydraulic conductivity. For a given *K* [L T^{-1}], the RE increases as ε decreases from 1 to 0.2. Thirdly, we find that the RE variation as *K* [L T^{-1}] by the PPW follows the same regulation as the fully-penetrating well cases, which is the low hydraulic conductivity aquifer would provide a good RE. Thus, theoretically, it recommends to apply the ASR in brackish aquifers with relatively low hydraulic conductivities because of constrained interface tilting. On the hand, low hydraulic conductivity is not suitable for pumping. Thus, there is a tradeoff for selecting sites based on hydraulic conductivity for ASR in brackish aquifers.

Figure 7.5 b shows the IRE results as *K* [L T^{-1}] through partially-penetrating extraction wells. The IRE enhances as ε decreases from 0.75 to 0.2 for given *K* [L T^{-1}], and the increment tendency is more significant for high *K* [L T^{-1}]. Namely, the higher *K* [L T^{-1}] is, the bigger RE increments are. If we focus on the RE improvement performance, we expect to apply the PPW in the aquifer with relatively high hydraulic conductivity, although the high hydraulic conductivity yields low RE.

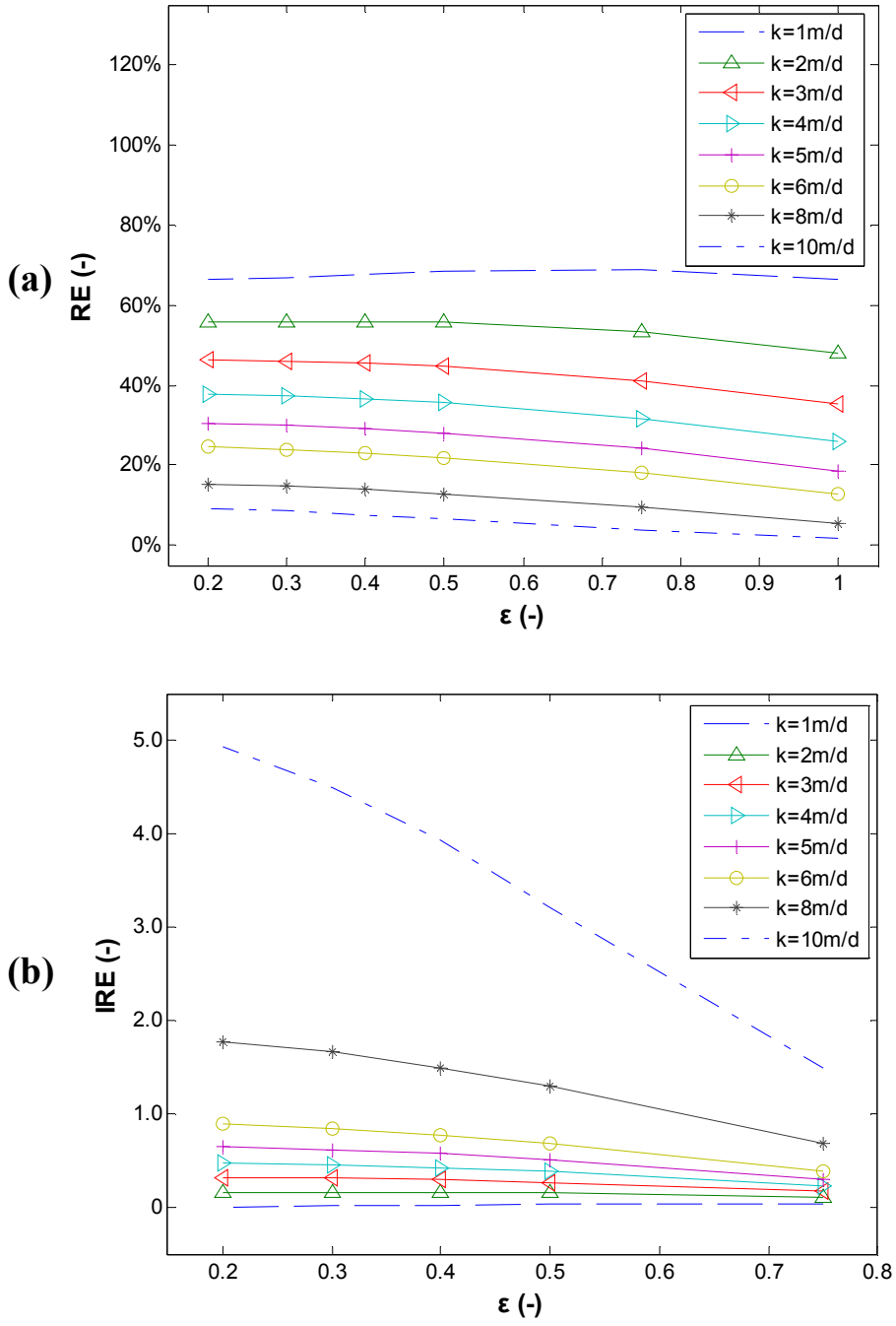

Figure 7.5 Sensitivity analysis for hydraulic conductivity by PPW method

Longitudinal dispersivity α_L [L]:

Figure 7.6 a shows that the RE grows as ε decreases from 1 to 0.2 for a given α_L [L]. It verifies again that the PPW method works very well to improve the ASR performance in the homogeneous and isotropic aquifer. Secondly, we can also confirm the monotonous RE improvement tendency as the gradual decrease of extraction depth for a given longitudinal dispersivity. Thirdly, for specific ε, the RE grows as α_L [L] decreases. Abarca et al. (2007) and Pool and Carrera (2011) demonstrated that increasing the longitudinal dispersivity can broaden the mixing zone. Ward et al. (2007) claimed that a high value for dispersivity can lead to the significant reduction of RE by applying the fully-penetrating wells. For the PPW, our results show that the high longitudinal dispersivity can also result in a small RE. It recommends to apply the ASR in the relatively low longitudinal dispersivity aquifer due to the big absolute RE value.

Figure 7.6 b shows the IRE results as α_L [L] through partially-penetrating extraction wells. As ε decreases from 0.75 to 0.2, the IRE increases for specific α_L [L], and the increment tendency is obvious for low α_L [L]. Namely, the lower α_L [L] is, the bigger RE increments are. This advises us to apply the PPW in the aquifer with relatively low longitudinal dispersivity because it provides remarkable RE improvement. This characteristic is very interesting since it is exactly opposite to the IRE variation results as K [L T^{-1}] shown in ***Figure 7.5 b***. Different from hydraulic conductivity K [L T^{-1}], the low longitudinal dispersivity is the preference for applying the PPW because it not only promotes a big absolute RE value but also big relative RE increments.

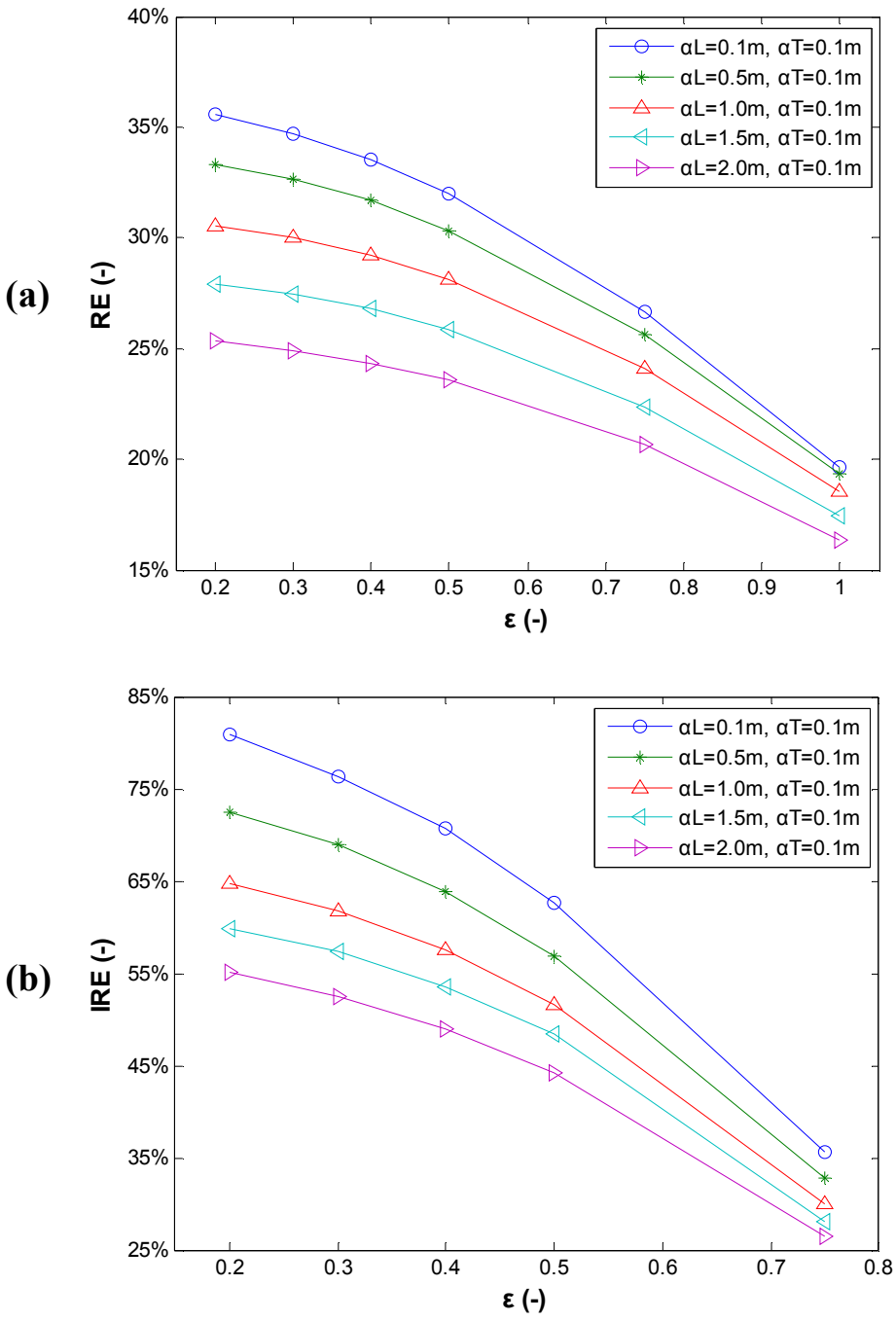

Figure 7.6 Sensitivity analysis for longitudinal dispersivity by PPW method

Transverse dispersivity α_T [L]:

In Chapter 5, we observed that the high transverse (vertical) dispersivity is helpful to the RE by applying fully-penetrating wells in the homogeneous, isotropic aquifer for one cycle ASR. That means the influence of transverse dispersivity is distinct from which of longitudinal dispersivity for the fully-penetrating wells.

Figure 7.7 a illustrates the PPW method works well for a given α_T [L] in the homogeneous, isotropic aquifer. The RE increases as ε decreases for specific α_T [L], implying that the RE can be monotonously improved as gradual decrease of extraction depth for a given transverse dispersivity. On the other hand, for a specific ε, the RE varies slightly as α_T, indicating that the RE is insensitive to transverse dispersion when PPW is applied. As discussed in Chapter 5 for fully-penetrating wells, the transverse dispersivity not only greatly affects the width of the mixing zone but also controls further increase of this width in the midportion of the interface (Abarca et al., 2007). When $\varepsilon <$ 0.5, it is common that the RE improvement for α_T [L] is the same as for α_L [L] due to the broadened mixing zone. The transverse (vertical) dispersion dominates the vertical mixing , and the high α_T [L] would spread out water particles from bottom to top. However, in the PPW, the extraction depth h [L] decreases as ε, leading that the role of α_T [L] weakens and gradually replaced by α_L [L]. Eventually, α_L [L] will dominate the whole extraction process. By considering the absolute RE value, generally speaking, if the fully-penetrating well is applied, then we would like to operate the ASR in a relatively high transverse dispersivity aquifer; if the PPW is applied, the value of transverse dispersivity becomes unimportant for a specific penetrating depth.

Figure 7.7 b shows the IRE variation results as α_T [L] by the PPW, similar to ***Figure 7.6 b***, As ε decreases from 0.75 to 0.2, the IRE enhances for specific α_T [L], and the increment tendency is obvious for low α_T [L]. Namely, the lower α_T [L] is, the bigger RE increments are. This suggests us to apply the PPW in the aquifer with relatively low transverse dispersivity In other words, when the transverse dispersivity is much smaller than the longitudinal dispersivity, the RE can be well improved by the PPW in the homogeneous, isotropic aquifer.

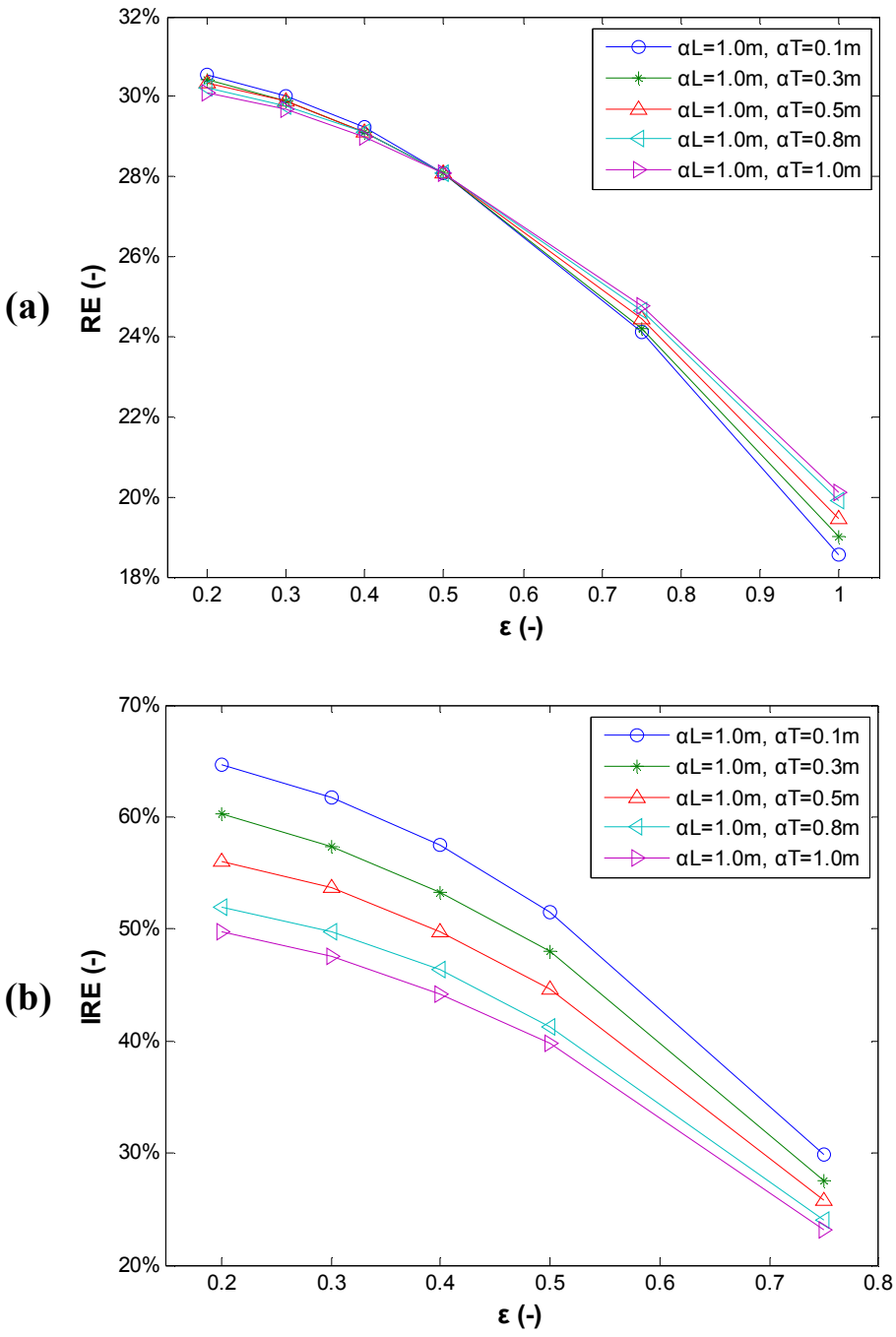

Figure 7.7 Sensitivity analysis for transverse dispersivity by PPW method

7.3.2 Operational Parameters Analysis

In Chapter 5, we investigated 5 operational parameters which would greatly affect ASR performance in the homogeneous, isotropic aquifer by applying fully-penetrating wells. The proposed PPW method involves one more parameter, the well penetrating depth.

Injection flowrate Q_i [L^3 T^{-1}]:

In Chapter 5, we recognized that higher injection flowrate Q_i [L^3 T^{-1}] yields higher RE for fully-penetrating wells. For PPW, we set that ε = 0.2, 0.3, 0.4, 0.5, 0.75 or 1.0 and Q_i [L^3 T^{-1}] varies from 4000 to 30000 m^3/d. We keep other parameters the same as the BC, except the assumption that injection flowrate Q_i [L^3 T^{-1}] is the same as extraction flowrate Q_e [L^3 T^{-1}] for each case.

Figure 7.8 a shows a consistent RE increase as ε decreases for a given Q_i [L^3 T^{-1}], demonstrating that the PPW method works well for a given Q_i [L^3 T^{-1}] in the homogeneous, isotropic aquifer. For a specific ε, the RE increases as Q_i [L^3 T^{-1}], the same pattern as the fully-penetrating well. Thus, large injection flow rates should be applied no matter what penetrating depth is. In addition, at large injection flow rates, the RE improvement becomes insensitive to the penetrating depth, implying that the penetrating depth is not the key parameter when large injection flow rates are applied.

Figure 7.8 b shows the IRE variation as Q_i [L^3 T^{-1}] by the PPW. As ε decreases from 0.75 to 0.2, the IRE enhances for a specific Q_i [L^3 T^{-1}], and the increment tendency is more noticeable for smaller Q_i [L^3 T^{-1}]. In other words, the smaller Q_i [L^3 T^{-1}] is, the better RE improvements are. This is consistent to the conclusion that the low pumping

rate would exacerbate the density effects (Ward et al., 2007). The successful PPW method depends on the tilting interface resulting from the density effects. This suggests that, if a relatively low injection flow rate is preferred, then we can obtain a remarkable RE improvement by the PPW. Namely, the PPW method is more applicable for small injection flow rate cases.

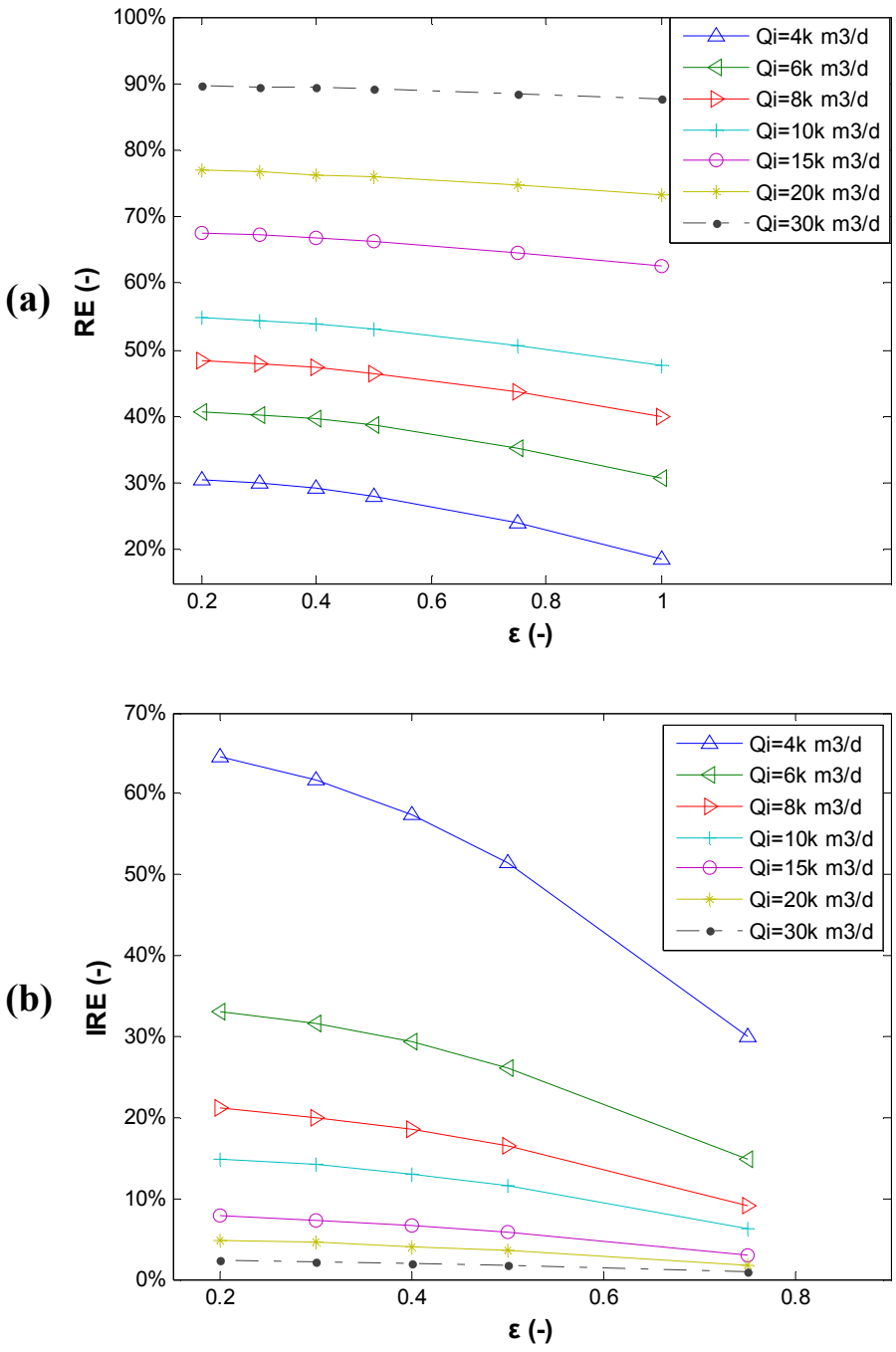

Figure 7.8 Sensitivity analysis for injection flowrate by PPW method

Injection duration T_i [T]:

In Chapter 5, we noticed that, long injection duration is helpful to the RE by applying fully-penetrating wells in the homogeneous and isotropic aquifer. But how the injection duration affects the RE by the PPW has not been studied yet. We set ε varying from 0.2 to 1.0 for a given T_i [T] and fix other parameters as the BC. T_i [T] is set to be 45, 90, 180 or 360 days respectively.

Figure 7.9 a shows a consistent RE increase as ε decreases for a given T_i [T]. It demonstrates that the PPW method works well for a given T_i [T] in the homogeneous, isotropic aquifer. For a specific ε, the RE increases as T_i [T]. The behavior is similar to that of injection flow rate. It is because that big injection flow rate and long injection duration reach the same consequence: pushing the interface further away from the injection well by increasing the total injection volume. This denotes the significant influence of injection volume on the RE, which will be discussed in the following.

Figure 7.9 b shows the IRE variation as T_i [T] by the PPW. As ε decreases from 0.75 to 0.2, the IRE enhances for a specific T_i [T], and the increment tendency is noticeable for short T_i [T]. In other words, the shorter T_i [T] is, the better RE improvements are, similar to IRE results of injection flow rate. Thus, if the injection time is considered to be relatively short, we should apply the PPW to achieve a noticeable RE improvement.

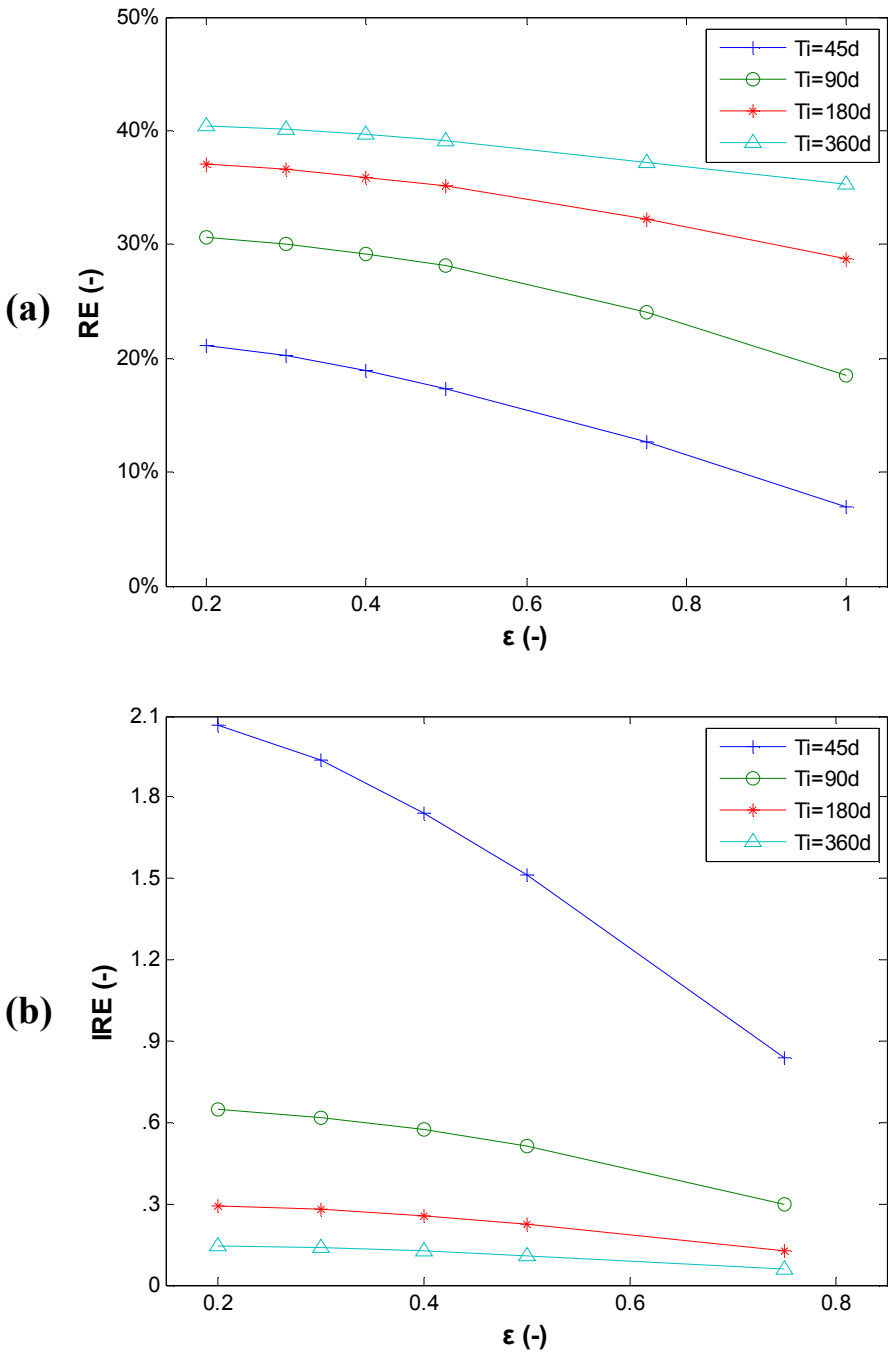

Figure 7.9 Sensitivity analysis for injection duration by PPW method

Total injection volume V_t [L^3]:

The total injection volume V_t [L^3] combines both Q_i [L^3 T^{-1}] and T_i [T]. In Chapter 5, we found that for the fixed V_t [L^3], the case with high Q_i [L^3 T^{-1}] and short T_i [T] will produce high RE, by applying the fully-penetrating well in the homogeneous and isotropic aquifer. We maintain V_t as 360,000 m^3 and other parameters the same as Chapter 5, and follow 5 cases listed in ***Table 3.5***.

Figure 7.10 a shows a consistent RE increase as ε for any group of Q_i [L^3 T^{-1}] and T_i [T]. Firstly, it demonstrates that the PPW method works well for any case with a fixed V_t [L^3] in the homogeneous, isotropic aquifer. Secondly, for any group of Q_i [L^3 T^{-1}] and T_i [T], the RE maintains a monotonous increment as ε gradually decreases. Thirdly, for a specific ε, the bigger RE is produced by the case with bigger Q_i [L^3 T^{-1}] and shorter T_i [T] for fixed V_t [L^3], which is due to the minimization of density effects. This reveals the injection strategy how to gain high RE with fixed water volume: we should increase the injection flow rate while shorten the injection time.

Figure 7.10 b shows the IRE variation analysis for V_t [L^3] by the PPW. As ε decreases from 0.75 to 0.2, the IRE enhances for any group of Q_i [L^3 T^{-1}] and T_i [T], and the increment tendency is noticeable at the case with small Q_i [L^3 T^{-1}] and long T_i [T]. In other words, when V_t [L^3] is fixed, the better RE improvement is achieved for the case with smaller Q_i [L^3 T^{-1}] and longer T_i [T]. This suggests that, when facing the case with small injection flow rate and long injection time, the PPW is able to gain a remarkable RE improvement.

Based on the absolute RE value, we conclude: 1) the higher injection volume generates the better RE, no matter what types of penetrating wells (i.e. fully or partially) in the homogeneous isotropic aquifer for one cycle ASR system; 2) to achieve the goal of recovering more freshwater, we can either increase the injection flowrate or extend the injection duration; 3) if the total water volume is constant, we should enhance the injection flowrate while shorten the injection duration to gain high RE.

Based on the RE improvement performance (i.e. relative RE increment), in terms of injection phase, we highly recommend to apply the PPW method in the homogeneous isotropic aquifer for the case with relatively small injection flowrate and long injection time.

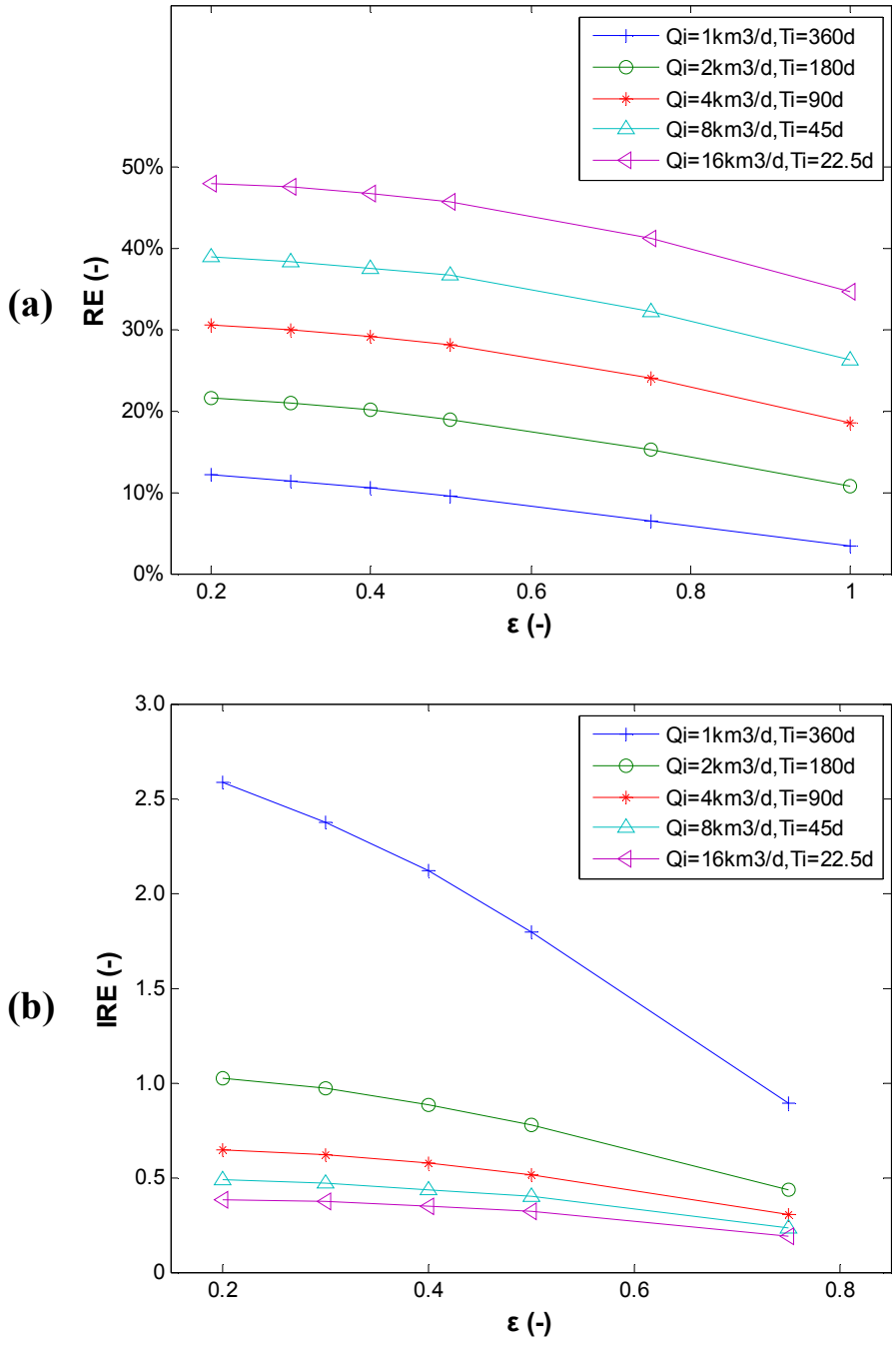

Figure 7.10 Sensitivity analysis for total injection volume by PPW method

Storage Duration T_s [T]:

In Chapter 5, we found that the longer storage duration would promote stronger density effects, leading to the dramatic reduction of RE by applying the fully-penetrating wells. The density effects are the key to the PPW method. T_s [T] is quite flexible in reality, even being zero. In this study, we assume T_s [T] as 0, 45, 90, 180, 270, 360 or 450 days. We vary ε from 0.2 to 1.0 and keep other parameters constant as the BC.

Figure 7.11 a shows a consistent RE increase as ε for a given T_s [T]. It demonstrates that the PPW method works well at given a T_s [T] in the homogeneous, isotropic aquifer, even for the no storage case. The RE maintains a monotonous increment as ε gradually decreases. For a specific ε, the RE enhances as T_s [T] decreases, namely the bigger RE is generated by shorter T_s [T] due to the minimized density effects. This reveals a clear storage strategy: the shorter storage duration is, the bigger RE is. Therefore, we should shorten the storage duration as much as possible to obtain a big RE.

Figure 7.11 b shows the IRE variation analysis as T_s [T]. As ε decreases from 0.75 to 0.2, the IRE enhances for specific T_s [T], and the increment tendency is noticeable at the case with long T_s [T]. In other words, the longer T_s [T] is, the better RE improvement performance is, which satisfies the conclusion in Chapter 5 that the long storage would promote stronger density effects. Therefore, if the ASR scheme schedules a long storage duration, then we should apply the PPW to achieve a remarkable RE improvement.

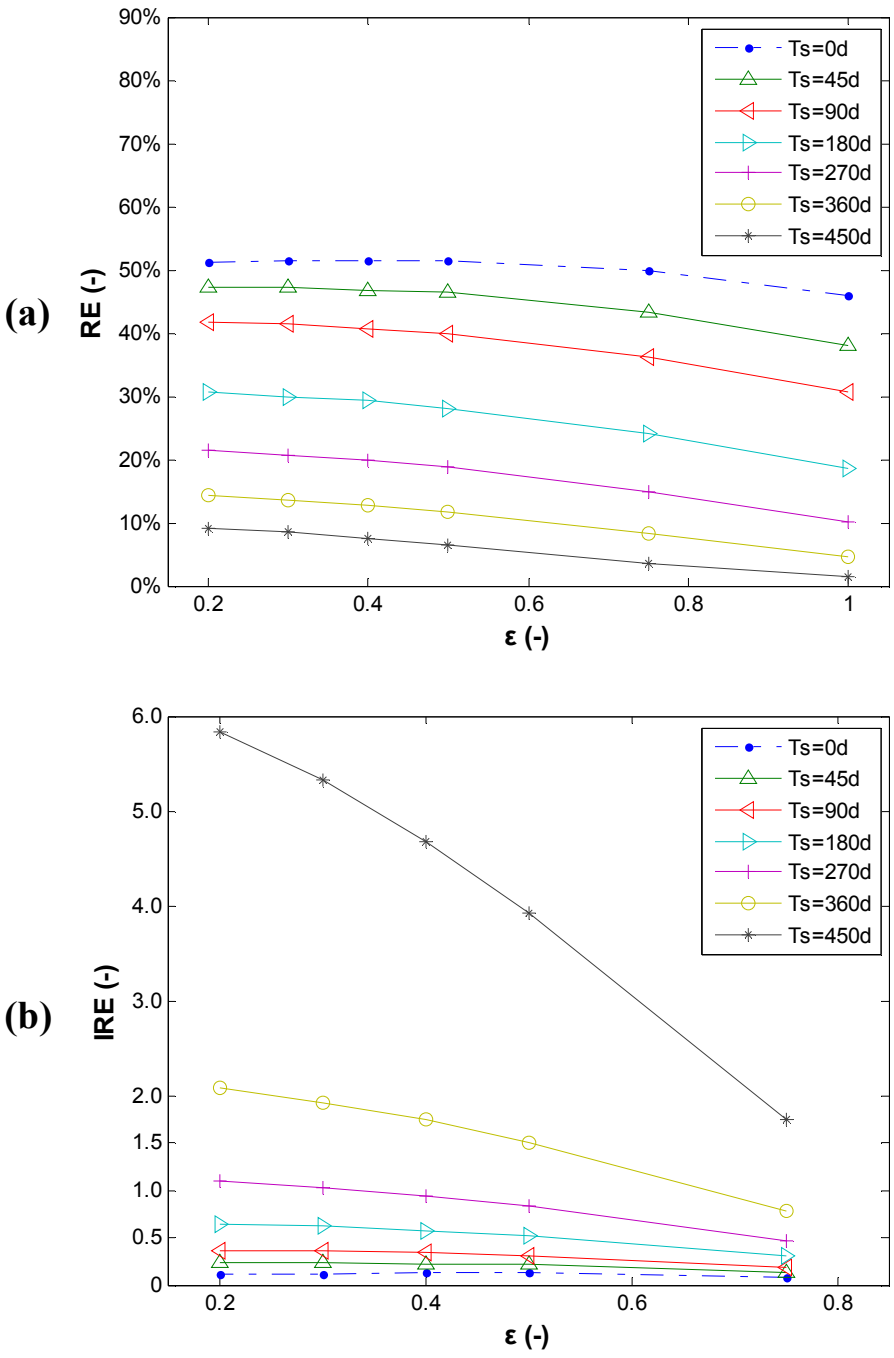

Figure 7.11 Sensitivity analysis for storage duration by PPW method

Extraction Flowrate Q_e [L^3 T^{-1}]:

In Chapter 5, we found that high extraction flow rate is helpful to the RE for fully-penetrating wells in the homogeneous, isotropic aquifer. We keep injection flowrate Q_i as 4000 m^3/d, but vary Q_e as 1000, 2000, 4000, 6000 and 8000 m^3/d respectively. And we assume ε varing from 1.0, 0.75, 0.5, 0.4, 0.3 & 0.2 for each case and keep other parameters constant as the BC.

Figure 7.12 a shows a consistent RE variation as ε for given Q_e [L^3 T^{-1}]. Firstly, it demonstrates that the PPW method works well for a given Q_e [L^3 T^{-1}] in the homogeneous, isotropic aquifer. Secondly, for any specific Q_e [L^3 T^{-1}], the RE maintains a monotonous increment as ε gradually decreases. Thirdly, for specific ε, the RE increases as Q_e [L^3 T^{-1}]. That implies, when the total water volume is constant, the higher Q_e [L^3 T^{-1}] yields the better RE.

Figure 7.12 b shows the IRE variation as Q_e [L^3 T^{-1}] by the PPW. As ε decreases from 0.75 to 0.2, the IRE enhances for a specific Q_e [L^3 T^{-1}]. However, for a given penetrating depth, the relative RE improvement is insensitive to the pumping rate.

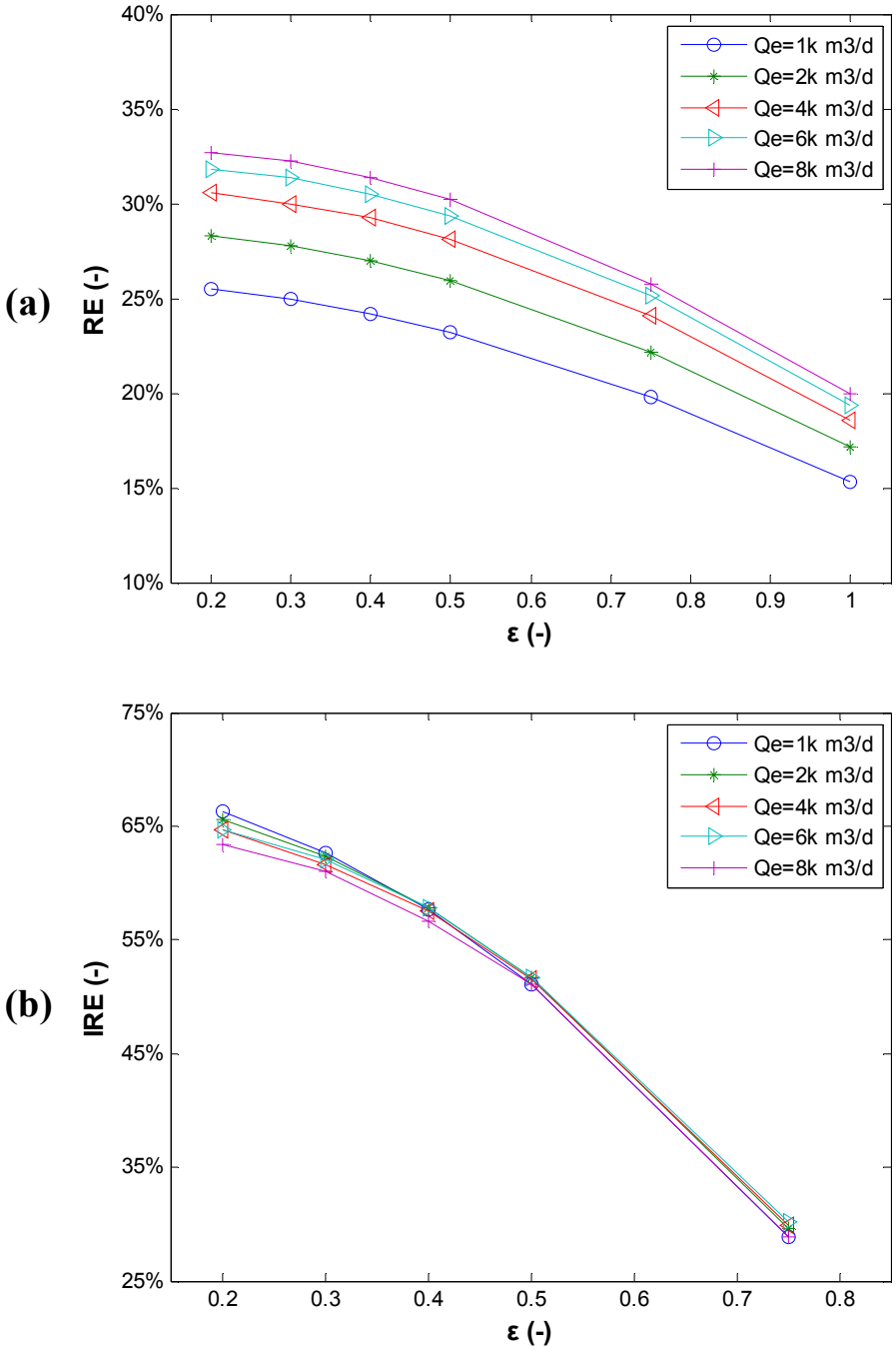

Figure 7.12 Sensitivity analysis for extraction flowrate by PPW method

7.4 Uncertainty Analysis

We consider the uncertainty of hydraulic conductivity by assuming that $ln\,K \sim N\,(\mu, \sigma^2)$. The mean of $ln\,K$ varies from -12 to -9 and the standard deviation σ is fixed as 0.1, representing weak variation. Namely, we totally have 16 groups with different $\mu_{ln\,K}$ and same $\sigma_{ln\,K}$ for a specific ε. For each ε, we sample hydraulic conductivities according to a mean $\mu_{ln\,K}$ and the standard deviation $\sigma_{ln\,K}$ for each group. The mean RE and its variance are evaluated based on the simulated results with the sampled hydraulic conductivities. For the PPW, we can illustrate ε = 0.5 to assess the uncertainty of hydraulic conductivity. ***Figure 7.13*** shows the mean RE and its confidence intervals when ε = 0.5 (semi-penetrating depth case). We can see that when σ^2 = 0.01, the confidence intervals keep consistency and show the reliability of the PPW results. But, when we transform that σ^2 = 1, the confidence intervals represent a wide range of uncertainty, which means when the variation of hydraulic conductivity is large, the success of PPW method is uncertain.

Figure 7.14 shows the coefficient of variation (CV) for specific ε, CV increases as mean conductivity, indicating that the relative variability grows as the increment of *K*.

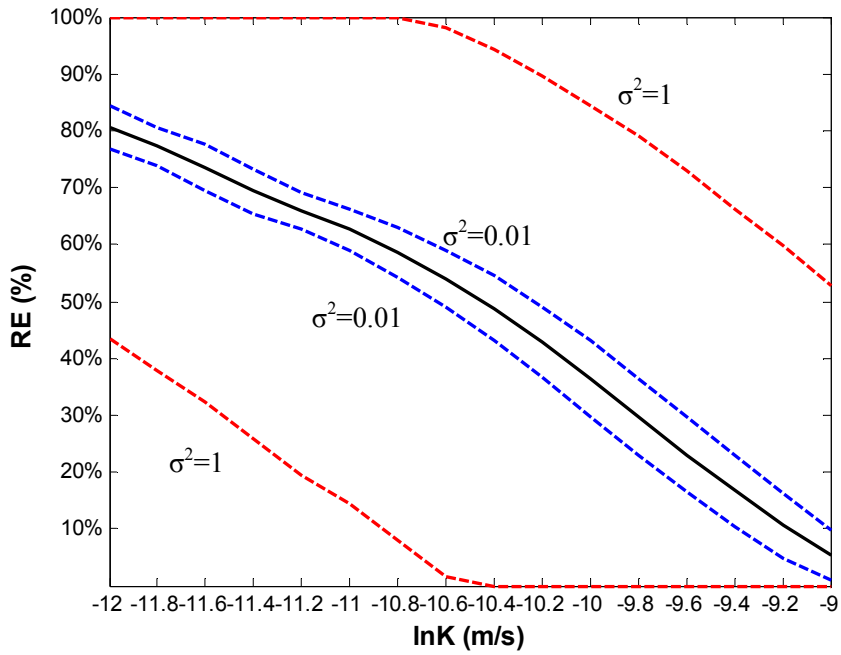

Figure 7.13 ***ln K*** uncertainty analysis by PPW for $\boldsymbol{\varepsilon}$=0.5

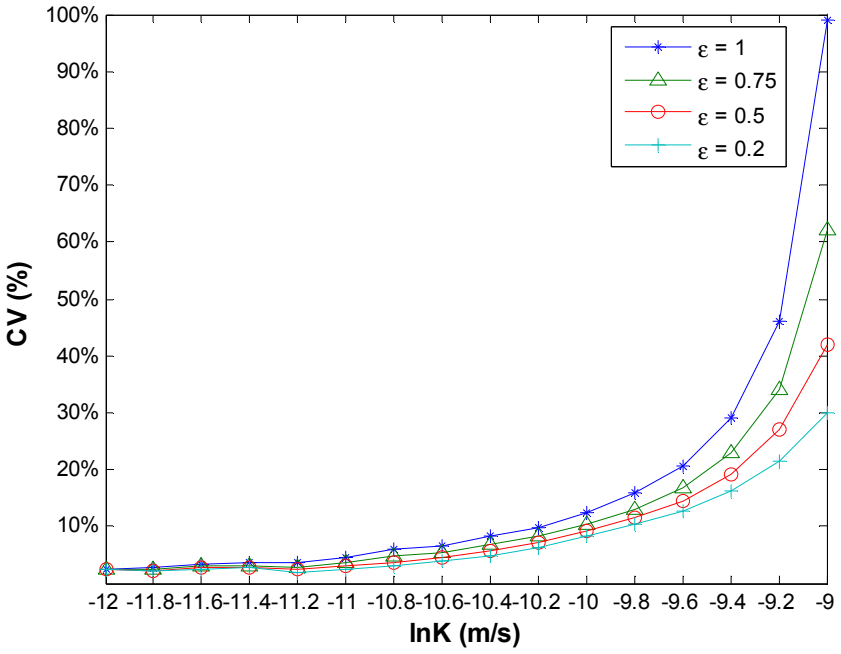

Figure 7.14 Coefficient of variation plot by PPW for various $\boldsymbol{\varepsilon}$

7.5 Partially-Penetrating Wells Application in Stratified Aquifers

In Chapter 6, we investigated the main effects of anisotropy and heterogeneity on ASR performance in stratified coastal aquifers. Also, we evaluated the effectiveness of the PPW in the homogeneous, isotropic aquifer above. In the following, we examine whether the RE can be well improved by the PPW in stratified coastal aquifers.

7.5.1 Model Parameters

We maintain all parameters the same as Chapter 6, except the extraction depth. In this study, we follow the similar method above to assume a fully-penetrating injection and a semi-penetrating well. In other words, we set the extraction depth as 25 m (i.e. ε = 0.5).

7.5.2 Results and Discussions

In terms of heterogeneity, we consider 3 different groups of hydraulic conductivity ratios, which are $\frac{K_1}{K_2}$ = 0.001 and 1000, 0.01 and 100, 0.1 and 10. In terms of anisotropy, we vary $\frac{K_{ix}}{K_{iz}}$ from the isotropic (i.e. 1) to extremely anisotropic (i.e. ∞) case. 24 cases are solved. ***Table 7.3*** exhibits the RE results by applying the semi-PPW in stratified coastal aquifers, in comparison with corresponding cases by applying the fully-penetrating wells in stratified coastal aquifers. ε = 1 or 0.5 stands for the fully-penetrating wells or semi-PPW.

From ***Table 7.3***, we can clearly see that, only the case when $\frac{K_1}{K_2}$ = 10 and $\frac{K_{ix}}{K_{iz}}$ = 1 (isotropic) can be improved by the half-extracted PPW, while other cases fails to improve RE. That implies, the PPW may improve the RE in stratified aquifers with intermediate conductivity contrasts (such as the case when $\frac{K_1}{K_2}$ = 10 and $\frac{K_{ix}}{K_{iz}}$ = 1), but may not be

effective in. highly stratified or anisotropic aquifers. As we discussed above, we have demonstrated that the PPW method truly depends on the density effects in reality. The homogeneous, isotropic aquifer usually offers a wide homogenized space to advance the extension of density effects. But stratification and anisotropy may inhibit the density effects, causing inefficiency of PPW. due to limited mass exchange across layers.

Table 7.3 RE results by PPW and FPW in stratified coastal aquifers

		K_{ix}/K_{iz}			
K_1/K_2	ε	1	10	100	∞
0.001	1	0.01%	0.06%	0.50%	23.74%
	0.5	0.00%	0.03%	0.21%	9.89%
1000	1	0.00%	0.06%	0.50%	23.74%
	0.5	0.00%	0.04%	0.36%	15.39%
0.01	1	0.30%	0.64%	1.11%	3.39%
	0.5	0.12%	0.23%	0.41%	1.34%
100	1	0.21%	0.54%	1.09%	3.39%
	0.5	0.13%	0.37%	0.76%	2.30%
0.1	1	8.32%	8.40%	10.92%	12.30%
	0.5	6.96%	4.17%	4.79%	5.33%
10	1	6.58%	7.61%	10.48%	12.30%
	0.5	7.87%	5.18%	6.69%	7.67%

Secondly, we can observe that, the cases with $\frac{K_1}{K_2}$ = 0.001 (or 0.01, or 0.1) are more inhibited to the RE than those with $\frac{K_1}{K_2}$ = 1000 (or 100, or 10). This denotes the difference between the aquifers with the same hydraulic conductivity contrast but with different layer placement. This is also firmly related to the density effects. The tiling can be regarded as an indicator of the density effects. Much stronger the density effects are, more serious the tilting is. In Chapter 6, we observe that the cases with $\frac{K_1}{K_2}$ = 0.001 (or 0.01, or 0.1) inhibit the tilting of entire aquifer, but the cases with $\frac{K_1}{K_2}$ = 1000 (or 100, or 10) enhances the tilting.

7.6 Conclusion

To sum up, we demonstrate that 1) the PPW can well improve the RE in the homogeneous, isotropic coastal aquifers for one cycle ASR system; 2) the PPW can conditionally improve the RE in stratified coastal aquifers.

7.6.1 PPW in Homogeneous and Isotropic Coastal Aquifer

In terms of influences of hydrogeological and operational parameters on the ASR by applying the PPW in the homogeneous, isotropic coastal aquifer, we conclude:

Hydrogeological Parameters

Salinity: 1) we verify the salinity affects the ASR performance by PPW; 2) through the absolute RE value, the lower salinity promotes the better RE; 3) through the RE improvement performance (i.e. relative RE increment), we highly recommend to apply the PPW in the homogeneous isotropic aquifer with high salinity.

Specific Storage: 1) we verify the specific storage affects the ASR performance by PPW; 2) through the absolute RE value, the higher specific storage promotes the better RE; 3) through the RE improvement performance (i.e. relative RE increment), we highly recommend to apply the PPW in the homogeneous isotropic aquifer with low specific storage.

Aquifer Thickness: 1) we verify the aquifer thickness affects the ASR performance by PPW; 2) through the absolute RE value, the shorter aquifer thickness promotes the better RE; 3) through the RE improvement performance (i.e. relative RE increment), we highly recommend to apply the PPW in the homogeneous isotropic aquifer with deep aquifer thickness.

Hydraulic Conductivity: 1) we verify the hydraulic conductivity affects the ASR performance by PPW; 2) through the absolute RE value, the lower hydraulic conductivity promotes the better RE; 3) through the RE improvement performance (i.e. relative RE increment), we highly recommend to apply the PPW in the homogeneous isotropic aquifer with high hydraulic conductivity.

Longitudinal Dispersivity, 1) we verify the longitudinal dispersivity affects the ASR performance by PPW; 2) through the absolute RE value, the lower longitudinal dispersivity promotes the better RE; 3) through the RE improvement performance (i.e. relative RE increment), we highly recommend to apply the PPW in the homogeneous isotropic aquifer with low longitudinal dispersivity.

Transverse Dispersivity: 1) we verify the transverse dispersivity affects the ASR performance by PPW; 2) through the absolute RE value, generally speaking, if the fully-

penetrating well is anticipated to apply, then we would like to operate the ASR in a relatively high transverse dispersivity aquifer due to a big absolute RE value; if the PPW with a relatively short extraction depth is anticipated to apply, then we would like to operate the ASR in a relatively low transverse dispersivity aquifer due to a big absolute RE value; 3) through the RE improvement performance (i.e. relative RE increment), we highly recommend to apply the PPW in the homogeneous isotropic aquifer with low transverse dispersivity.

Operational Parameters

Injection Phase:

We demonstrate: 1) the injection phase greatly affects ASR performance; 2) 3 injection parameters are extremely important to adjust to gain the perfect RE, and we need primarily to recognize and analyze the operational facts interactively, then to choose the operating strategy, lastly to operate the ASR system; 3) the proposed PPW method works very well in the homogeneous, isotropic aquifer under different injection circumstances; 4) the shorter extraction depth is, the better RE improvement performance is.

Through the absolute RE value, we mainly conclude: 1) the higher injection volume generates the better RE, no matter what types of penetrating wells (i.e. fully or partially) we choose in the homogeneous isotropic aquifer for one cycle ASR system; 2) to achieve the goal of recovering more freshwater, we can either increase the injection flowrate or extend the injection duration; 3) if the total water volume is constant, we should enhance the injection flowrate while shorten the injection duration to gain a big RE.

Through the RE improvement performance (i.e. relative RE increment), in terms of injection phase, we highly recommend to apply the PPW method in the homogeneous isotropic aquifer 1) when injection flowrate is relatively small but other parameters are similar; 2) or when injection duration is relatively short but other parameters are similar; 3) or when facing the case with relatively small injection flowrate and long injection time but maintaining the same total injection volume.

Storage Phase:

We demonstrate: 1) the storage phase significantly affects the one cycle ASR performance; 2) the one cycle ASR system is irreversible; 3) the proposed one cycle PPW method works very well in the homogeneous, isotropic aquifer for various storage duration cases; 4) the shorter extraction depth is, the better RE improvement performance is.

Through the absolute RE value, we mainly conclude: 1) the shorter storage duration promotes the better RE, no matter what types of extraction wells (i.e. fully-penetrating or partially-penetrating) we choose in the homogeneous isotropic aquifer for one cycle ASR system; 2) the best RE is gained at the case with no storage duration.

Through the RE improvement performance (i.e. relative RE increment), in terms of storage phase, we highly recommend to apply the PPW method in the homogeneous isotropic aquifer when storage duration is fairly long.

Extraction Phase:

We demonstrate: 1) the extraction phase significantly affects the one cycle ASR performance; 2) the proposed one cycle PPW method works very well in the homogeneous, isotropic aquifer under different extraction circumstances; 3) the shorter extraction depth is, the better RE improvement performance is.

Through the absolute RE value, we mainly conclude: 1) the bigger extraction flowrate generates the better RE, no matter what types of extraction wells (i.e. fully-penetrating or partially-penetrating) we choose in the homogeneous isotropic aquifer for one cycle ASR system; 2) we can increase the extraction flowrate to achieve the goal of recovering more freshwater.

Through the RE improvement performance (i.e. relative RE increment), in terms of extraction phase, we highly recommend to apply the PPW method in the homogeneous isotropic aquifer for all types of extraction flowrate cases.

7.6.2 PPW in Stratified Coastal Aquifer

In terms of influences of hydrogeological and operational parameters on the ASR by applying the PPW in the stratified coastal aquifer, we conclude that: 1) we may improve the RE by the PPW in stratified coastal aquifers in the condition of strong density effects; 2) the highly stratified, anisotropic coastal aquifers inhibit the application of PPW method, so that we need avoid applying the PPW in high stratified, anisotropic coastal aquifers; 3) we prefer applying the PPW in stratified coastal aquifers with high-K overlying low-K layers.

CHAPTER 8

CONCLUSIONS

8.1 Summary and Contribution

The successful design of an ASR scheme requires an integrated knowledge base of sound interdisciplinary science and understanding of the subsurface mixing processes under various ASR operational processes in aquifers with various hydrogeological conditions. Development of such an integrated knowledge base with associated operational guidance for successful ASR schemes is the main theme of this thesis research. The principal contributions of this work can answer two primary fundamental questions:

(a) How to select the aquifer appropriate for an ASR scheme?

(b) How to design ASR operations given a selected site?

We presented 5 chapters to answer these two questions, and the main contributions of this thesis can be summarized as following:

(1) Developed an efficient approach to analytically evaluate solute transport in a horizontal radial flow field with a multistep pumping and examine the ASR performance in homogeneous, isotropic aquifer with advective and dispersive transport processes.

(2) Numerically and analytically investigated the efficiency of an ASR system in dual-domain aquifers with mass transfer limitations under various hydrogeological and operational conditions. Simple and effective relationships between transport parameters

and ASR operational parameters are derived to quantify the effectiveness and ascertain the potential of ASR systems with mass transfer limitations.

(3) Assessed the effects of hydrogeological and operational parameters on recovery efficiency of ASR systems in homogeneous, isotropic coastal aquifers.

(4) Quantitatively investigated ASR performance in stratified, coastal aquifers under various heterogeneous and anisotropic conditions.

(5) Evaluated the effectiveness of partially-penetrating wells for ASR systems in coastal aquifers, and discussed the RE improvement by partially-penetrating wells in comparison with fully-penetrating wells.

8.2 Conclusions

The main conclusions of this thesis can be summarized as following:

(1) For advective-dispersive transport in radial flow systems in homogeneous, isotropic aquifers, by assuming a piecewise steady-state flow and transforming the time domain to the cumulative injected flow domain, the concentration distribution is found to be completely determined by the total volume of injected flow and independent of specific flow rates. Thus, ASR efficiency in such aquifers is completely controlled by the total injected flow volume at a given site. Furthermore, we theoretically examine the conditions for the assumption of piecewise steady-state flow to be valid. Based on the critical timescale of the "peudo-steady state condition", defined when velocity changes accomplish 99% of their steady-state differences, and the relative error in the mean travel time of plume front, we obtain conditions for neglecting the transitional period between

two pumping steps. Such conditions include (a) the duration of a pumping step, t_p, must be longer than the critical timescale, t_c, i.e., $t_p \geq t_c = 25r^2S/T$, where r is the radial distance, S is the storage coefficient, and T is the transmissivity; or similarly, a maximum problem domain needs to be defined for a given pumping strategy; and (b) the maximum well pumping rate, $q_{\max}$, should satisfy $q_{\max} \leq \pi\theta T/25S$, where θ is the effective porosity. When both conditions are satisfied, transitional periods may be neglected. These conditions can be used to simplify the ASR simulations by assuming piecewise steady-state flow.

(2) ASR performance in aquifers with mass transfer limitations is analyzed by combining the convergent and divergent dispersion models with a first-order mass transfer model. By analyzing the concentration history at the pumping well, we obtain simple and effective relationships for investigating ASR RE under various mass transfer parameters, including capacity ratio and mass transfer timescale, and operational parameters, including injection durations and well pumping rates:

$$\frac{\beta}{1+\beta}\exp(-T_i)\{1-\exp[-(1+\beta)T_s]\} < c^*_{crit}$$

$$n > 1+\left\{-T_i+\ln\left[\frac{1}{1+\beta}\{\beta+\exp[-2(1+\beta)T_i]\}\right]\right\}^{-1}\ln\left\{\frac{1+\beta}{\beta}\frac{\exp(T_i)}{1-\exp[-(1+\beta)T_i]}c^*_{crit}\right\}$$

Based on such relationships, one can conveniently determine whether a site with mass transfer limitations is appropriate or not for ASR and how many ASR cycles are required for achieving a positive RE. Results indicate that the immobile domain may function as a contaminant source or sink or both during the recovery phase and RE usually improves

with well flow rate, the decrease of capacity ratio, and the ASR cycles. However, RE is a non-monotonic function of the mass transfer timescale and the injection duration. A critical timescale is given for quantifying this non-monotonic behavior. When the injection period is greater than such a critical value, increasing injection period results in a higher RE. Contrarily, when the injection period is less than the critical value, increasing the injection period may even yield a lower RE.

(3) For ASR in homogeneous, isotropic saline aquifers, density effects play a significant role in determining ASR efficiency. Density effects are influenced by both hydrogeological conditions (such as seawater density, specific storage, aquifer thickness, hydraulic conductivity, longitudinal dispersivity and transverse dispersivity) and operational parameters (such as injection flowrate, injection duration, total injection volume, storage duration, extraction flowrate). When selecting the aquifer to appropriately operate the ASR, we highly recommend to apply the fully-penetrating ASR system in the homogeneous, isotropic aquifer with low density, high specific storage, short aquifer thickness, low hydraulic conductivity, low longitudinal dispersivity and high transverse dispersivity. All these conditions can mitigate the negative impact of tilting interface caused by density effects. We shall notice that high hydraulic conductivity is often preferred for water recharge. Our results indicate that aquifers with high conductivity may yield low recovery rate due to density effects.

When designing ASR operations given a selected site, through the absolute RE value, we recommend to increase the total injection volume, shorten the storage duration, or increase the extraction flowrate to generate a better RE in the homogeneous isotropic aquifer. If the total water volume is constant, we should enhance the injection flowrate

while shorten the injection duration to gain a high RE when applying the fully-penetrating wells in the homogeneous, isotropic aquifer.

(4) In stratified saline aquifers, hydraulic conductivity contrast, anisotropy and transverse dispersion are important for ASR performance.

The nature of layered aquifers determines that each layer's contributions to the RE are different. RE is not a monotonic function of the hydraulic conductivity contrast, i.e., a peak RE is achieved at the case with intermediate conductivity contrasts. In general, the anisotropy is helpful to the RE because high anisotropy essentially divides the domain into uncorrelated, individual layers without flow exchange across layers, minimizing the tilting behavior of interface and yielding high RE.

(5) Another important finding in stratified saline aquifers is that the stratified aquifer cannot be simply homogenized by the arithmetic (horizontal direction) and harmonic (vertical direction) means of the hydraulic conductivities in different layers. Such homogenization would significantly overestimate the RE, especially in the highly stratified aquifers. In fact, ASR in saline aquifers couples both flow and transport by the density effects. Thus, homogenization must include both flow and transport, i.e., both hydraulic conductivity and dispersion coefficients must be upscaled.

(6) Transverse dispersion plays an important role in stratified aquifers because of significantly stretched interface. In the layered cases with communication between layers with one moving faster than the neighboring layers, transverse dispersion serves to diminish the progress of the fast front and enhance the progress of the slow front. Such a self-limiting feature would reduce the overall rate of salt spreading and is beneficial for

improving the ASR efficiency for hydraulic conductivity contrasts up to 100. However, in highly stratified aquifers with high conductivity contrasts, higher transverse dispersion may effectively enhance the mixing zone in the layers with high hydraulic conductivities, leading to lower ASR efficiency.

(7) We demonstrate that the partially-penetrating wells can well improve the RE in the homogeneous, isotropic coastal aquifers for ASR systems, while can conditionally improve the RE in stratified saline aquifers with strong density effects.

When selecting the aquifer to appropriately operate the ASR, we highly recommend to apply the PPW in the homogeneous, isotropic aquifer with low salinity, high specific storage, short aquifer thickness, low hydraulic conductivity, low longitudinal dispersivity and uncertain transverse dispersivity regardless of extraction depth. These conditions are consistent to the fully-penetrating well cases. On the other hand, in terms of the RE improvement , the PPW is particularly efficient in the homogeneous, isotropic aquifer with high salinity, low specific storage, deep aquifer thickness, high hydraulic conductivity, low longitudinal dispersivity and low transverse dispersivity.

When designing ASR operations at a given site, we can enhance the injection volume, shorten the storage duration or increase extraction flowrate to achieve the goal of recovering more freshwater, no matter what types of penetrating wells (i.e. fully or partially); if the total water volume is constant, we should enhance the injection flowrate while shorten the injection duration to gain a high RE. The PPW method is recommended when injection flowrate is relatively small but other parameters are similar, or when injection duration is relatively short but other parameters are similar, or when facing the

case with relatively small injection flowrate and long injection time with the same total injection volume, or when storage duration is fairly long. In stratified saline aquifers, strong stratification typically prevents the application of PPW method because of insignificant density effects.

8.3 Recommendations for Future Work

Based on the models, solutions, analyses and results developed in the thesis, the following topics are suggested for future work:

(1) Laboratory and field study of ASR

This thesis mostly focused on the theoretical study on the ASR system. We developed numerical and analytical models to simulate various subsurface transport processes in radial flow systems. Most of the results are not validated by experimental data. It is highly recommended to conduct laboratory experiments and to collect field data to validate the modeling results. Besides, the field data of ASR scheme will provide chances to calibrate the theoretical research and inspire innovative ideas to improve the recovery efficiency of ASR scheme. In particularly, the PPW method needs to be tested in lab or field.

(2) Homogenization of stratified coastal aquifers

In this thesis, we defined the layered coastal aquifers in terms of two different hydraulic conductivities. This type of layered aquifer is a simple representative of complex stratified aquifers, but we do need to conduct further study on the aquifers with random hydraulic conductivities, which are typically used in stochastic hydrogeology for

studying the effects of heterogeneities. Monte-Carlo simulations can be applied on 2-D or 3-D variable-density flow and transport in heterogeneous hydraulic conductivity fields. However, the computation is expensive. In addition, we found that homogeneous of ASR in stratified saline aquifers is not as simple as what has been reported in literatures. We concluded that both hydraulic conductivity and dispersivity must be upscaled, i.e., both flow and transport behavior must be homogenized. Theoretical analysis following classical stochastic hydrogeology may not work for this case because the problem is nonlinear and the flow is radial. Monte-Carlo simulations may need to be applied.

(3) Study on stratified coastal aquifers with mass transfer

In this thesis, we investigated the efficiency of an ASR system in homogeneous, isotropic confined aquifers with mass transfer limitations under various hydrogeological and operational conditions. We assessed the ASR performance in stratified, coastal aquifers under various heterogeneous and anisotropic circumstances. What is the combined effect of rate-limited mass transfer and density gradients? How can we improve the ASR efficiency in a dual-porosity, brackish aquifer?

(4) Partially-penetrating wells in multi-cycle ASR schemes

Our study on the partially-penetrating extraction wells focused on the one-cycle ASR scheme. We pursue an effective ASR with a long operating term in reality. It is worthy to evaluate the effectiveness of the partially-penetrating wells during a long multi-cycle ASR system. More than that, it is significant to study how to enhance the recovery efficiency by partially-penetrating wells in the multi-cycle ASR system.

REFERENCES

[1] Abarca E., Vazquez-Sune E., Carrera J., Capino B., Gamez D., and Batlle F., 2006. Optimal design of measures to correct seawater intrusion. Water Resour. Res., 42(9), W09415.

[2] Ackerer P., Younes A., and Mose R., 1999. Modeling variable density flow and solute transport in porous medium: 1. Numerical model and verification. Transport Porous Med., 35(3), 345–373.

[3] Almulla A., Hamad A., and Gadalla M., 2005. Aquifer storage and recovery (ASR): A strategic cost-effective facility to balance water production and demand for Sharjah. Desalination, 174(2), 193–204.

[4] Ataie-Ashtiani B., and Ketabchi H., 2011. Elitist continuous ant colony optimization algorithm for optimal management of coastal aquifers. Water Resour. Manage, 25(1), 165–190.

[5] Ataie-Ashtiani B., Shafei B., Rashidian-Dezfouli H., and Mohamadzadeh M., 2012. Capture zone of a partially penetrating well with skin effects in confined aquifers. Transp. Porous Med., 91(2), 437–457.

[6] Bair E. S., and Lahm T. D., 1996. Variations in capture-zone geometry of a partially penetrating pumping well in an unconfined aquifer. Ground Water 34(5), 842–852.

[7] Bakker M., 2000. The size of the freshwater zone below an elongated island with infiltration. Water Resour. Res., 36(1), 109–117.

[8] Bakker M., 2001. An analytic, approximate method for modeling steady, three-dimensional flow to partially penetrating wells. Water Resour. Res., 37(5), 1301–1308.

[9] Bakker M., 2006. Analytical solution for interface flow in combined confined and semi- confined coastal aquifers. Adv. Water Resour., 29(3), 417–425.

[10] Bakker M., 2010. Radial Dupuit interface flow to assess the aquifer storage and recovery potential of saltwater aquifers. Hydrogeol. J., 18(1), 107–115.

[11] Barua G., and Bora S. N., 2010. Hydraulics of a partially penetrating well with skin zone in a confined aquifer. Adv. Water Resour., 33(12), 1575–1587.

[12] Bear, J., 1979. Hydraulics of Groundwater. New York: McGraw-Hill.

[13] Bear J., Cheng A. H. D., Sorek S., Ouzar D., and Herrera I., 1999. Seawater intrusion in coastal aquifers: concepts, methods and practices. Springer, New York.

[14] Bear, J., and Dagan G., 1964. Some exact solutions of interface problems by means of hodograph method. J. Geophys. Res., 69(8), 1563–1572.

[15] Becker, M.W., and R.J. Charbeneau, 2000. First-passage-time transfer functions for groundwater tracer tests conducted in radially convergent flow, J. Contam. Hydrol., 40, 299–310.

[16] Behrooz-Koohenjani S., Samani, N., and Kompani-Zare M., 2011. Steady flow rate to a partially penetrating well with seepage face in an unconfined aquifer. Hydrogeol. J., 19(4), 811–821.

[17] Bhattacharjya R. K., and Datta B., 2005. Optimal management of coastal aquifer using linked simulation optimization approach. Water Resour. Manage., 19(3), 295–320.

[18] Bray B., and Yeh W., 2008. Improving seawater barrier operation with simulation optimization in southern California. J. Water Resour. Plann. Manage., 134(2), 171–180.

[19] Brown C. J., Hatfield K., and Newman M., 2006. Lessons learned from a review of 50 ASR projects from the United States, England, Australia, India, and Africa. UCOWR Conference, Session 12.

[20] Brown C. J., and Misut P. E., 2010. Aquifer geochemistry at potential aquifer storage and recovery sites in coastal plain aquifers in the New York city area USA. Appl. Geochem., 25(9), 1431–1452.

[21] Butler, J., Jr., and C. McElwee, 1990. Variable-rate pumping tests for radially symmetric nonuniform aquifers, Water Resour. Res., 26(2), 291–306.

[22] Carlier, E., 2008. Analytical solutions of the advection-dispersion equation for transient groundwater flow. A numerical validation, Hydrol. Process., 22, 3500–3506.

[23] Charbeneau R. J., 2006. Groundwater hydraulics and pollutant transport. Long Grove: Waveland Press, Inc.

[24] Chen, C.-S., 1985. Analytical and approximate solutions to radial dispersion from an injection well to a geological unit with simultaneous diffusion into adjacent strata, Water Resour. Res., 21, 1069–1076.

[25] Chen, C.-S., 1986. Solutions for radionuclide transport from an injection well into a single fracture in a porous formation, Water Resour. Res., 22, 508–518.

[26] Chen, C.-S., 1987. Analytical solutions for radial dispersion with Cauchy boundary at injection well, Water Resour. Res., 23, 1217–1224.

[27] Chen, C.-S., and G.D. Woodside, 1988. Analytical solution for aquifer decontamination by pumping, Water Resour. Res., 24, 1329–1338.

[28] Chen J. S., Wu C. L., and Liu C. W., 2010. Analysis of contaminant transport towards a partially penetrating extraction well in an anisotropic aquifer. Hydrol. Process., 24(15), 2125–2136.

[29] Cheng A.H.D., Halhal D., Naji A., and Ouazar D., 2000. Pumping optimization in saltwater-intruded coastal aquifers. Water Resour. Res., 36(8), 2155–2165.

[30] Coats, K.H., and B.D. Smith, 1964. Dead-end pore volume and dispersion in porous media, Soc. Pet. Eng. J., 4, 73–81.

[31] Corless, R.M., G.H. Gonnet, D.E.G. Hare, D. J. Jeffrey, and D. E. Knuth, 1996. On the Lambert W Function, Adv. Comp. Math., 5, 329–359.

[32] Croucher A. E., and O'Sullivan M. J., 1995. The Henry problem for saltwater intrusion. Water Resour. Res., 31(7), 1809–1814.

[33] Culkin S. L., Singha K., and Day-Lewis F. D., 2008. Implications of rate-limited mass transfer for aquifer storage and recovery. Ground Water, 46(4), 591–605.

[34] Dagan, G., and Zeitoun D.G., 1998. Seawater-freshwater interface in a stratified aquifer of random permeability distribution. J. Contam. Hydrol., 29(3), 185–203.

[35] de Hoog, F. R., J. H. Knight, and A. N. Stokes, 1982. An improved method for numerical inversion of Laplace transforms, SIAM J. Sci. Stat. Comput., 3, 357–366.

[36] Dhar A., and Datta B., 2009. Saltwater intrusion management of coastal aquifers. I: Linked simulation-optimization. J. Hydrol. Eng., 14(12), 1263–1272.

[37] Diersch H. J. G., and Kolditz O., 2002. Variable-density flow and transport media: Approach and challenges. Adv. Water Resour., 25, 899–944.

[38] Dror I., Berkowitz B., and Gorelick S. M., 2004. Effects of air injection on flow through porous media: observations and analyses of laboratory-scale processes. Water Resour. Res., 40(9), W09203.

[39] Eastwood J. C., and Stanfield P. J., 2001. Key success factors in an ASR scheme. Q. J. Eng. Geol. Hydrogeol., 34, 399–409.

[40] Esmail O. J. and Kimbler O. K., 1967. Investigation of the technical feasibility of storing fresh water in saline aquifers. Water Resour. Res., 3(3), 683–695.

[41] Faybishenko B. A., Javandel I., and Witherspoon P. A., 1995. Hydrodynamics of the capture zone of a partially penetrating well in a confined aquifer. Water Resour. Res., 31(4), 859–866.

[42] Fienen M. N., Luo J., and Kitanidis P. K., 2006. A Bayesian geostatistical transfer function approach to tracer test analysis. Water Resour. Res., 42, W07426.

[43] Galeati G., Gambolati G., and Neuman S. P., 1992. Coupled and partially coupled Eulerian-Lagrangian model of freshwater seawater mixing zone. Water Resour. Res., 28(1), 149–165.

[44] Gaus I., Shand P., Gale I. N., Williams A. T., and Eastwood J. C., 2002. Geochemical modeling of fluoride concentration changes during Aquifer Storage and Recovery (ASR) in the Chalk aquifer in Wessex, England. Q. J. Eng. Geol. Hydrogeol., 35, 203–208.

[45] Goltz, M.N., and Oxley M.E., 1991. Analytical modeling of aquifer decontamination by pumping when transport is affected by rate-limited sorption, Water Resour. Res., 27, 547–556.

[46] Goyal V., Jhorar B. S., Malik R. S., and Streck T., 2008. Performance evaluation of aquifer storage recovery wells for conjunctive water management as influenced by buffer storage volume and storage volume and storage time. Curr. Sci., 94(4), 465–472.

[47] Grove D. B. and Konikow L. F., 1976. Modeling cyclic storage of water in aquifers. Trans. Am. Geophys. Union, 57(12), 916–917.

[48] Haitjema H. M., and Kraemer S. R., 1988. A new analytic function for modeling partially penetrating wells, Water Resour. Res., 24(5), 683–690.

[49] Hantush M.S., 1961. Drawdown around a partially penetrating well. J. Hydrol. Div., Proc. Am. Soc. Civil Eng. 87(4), 83–98.

[50] Harmsen E. W., Converse J. C., Anderson M.P., and Hoopes J. A., 1991. A model for evaluating the three-dimensional groundwater dividing pathline between a contaminant source and a partially penetrating water-supply well. J. Contam. Hydrol., 8(1), 71–90.

[51] Harvey, C.F., Haggerty R., and Gorelick S.M., 1994. Aquifer remediation: a method for estimating mass transfer rate coefficients and evaluation of pulsed pumping, Water Resour. Res., 30, 1979–1991.

[52] Henry H. R., 1964. Effects of dispersion on salt encroachment in coastal aquifers, U.S. Geol. Survey Water-Supply Paper 1613-C, C70–C82.

[53] Hoopes, J. A., and D. R. F. Harleman, 1967. Dispersion in radial flow from a recharge well, J. Geophys. Res., 72, 3595–3607.

[54] Hsieh, P. A., 1986. A new formula for the analytical solution of the radial dispersion problem, Water Resour. Res., 22, 1597–1605.

[55] Huang, J., Christ J.A., and Goltz M.N., 2010. Analytical solutions for efficient interpretation of single-well push-pull tracer tests, Water Resour. Res., 46, W08538.

[56] Huang, J., and Goltz M.N., 2006. Analytical solutions for solute transport in a spherically symmetric divergent flow field, Trans. Porous Media, 63, 305–321.

[57] Hutson S. S., Barber N. L., Kenny J.F., Linsey K. S., Lumia D. S., and Maupin M. A., 2004. Estimated Use of Water in the United States in 2000. Ciucular 1268. U. S. Geological Survey, Reston, Virginia.

[58] Hvilshoj S., Jensen K. H., Barlebo, H. C., and Madsen B., 1999. Analysis of pumping tests of partially penetrating wells in an unconfined aquifer using inverse numerical optimization. Hydrogeol. J., 7(4), 365–379.

[59] Indelman, P., Dagan, G., 1999. Solute transport in divergent radial flow through heterogeneous porous media, J. Fluid. Mech., 384, 159–182.

[60] Izbicki J. A., Petersen C. E., Glotzbach K. J., Metzger L. F., Christensen A. H., Smith G. A., O'Leary D., Fram M. S., Joseph T. and Shannon H., 2010. Aquifer Storage Recovery (ASR) of chlorinated municipal drinking water in a confined aquifer. Appl. Geochem., 25(8), 1133–1152.

[61] Javadi A. A., Abd-Elhamid H. F., and Farmani R., 2012. A simulation-optimization model to control seawater intrusion in coastal aquifers using abstraction/recharge wells. Int. J. Numer. Anal. Methods Geomech., 36(16), 1757–1779.

[62] Javandel I., and Witherspoon P. A., 1983. Analytical solution of a partially penetrating well in a two-layer aquifer, Water Resour. Res., 19(2), 567–578.

[63] Johnson G. S., Frederick D. B., and Cosgrove D. M., 2002. Evaluation of a pumping test of the Snake River Plain aquifer using axial-flow numerical modeling. Hydrogeol. J., 10(3), 428–437.

[64] Johnson T., 2007. Battling seawater intrusion in the central & west coast basins. WRD Technical Bulletin, 13.

[65] Kacimov A.R., and Sherif M. M., 2006. Sharp interface, one-dimensional seawater intrusion into a confined aquifer with controlled pumping: Analytical solution. Water Resour.Res., 42, W06501.

[66] Kacimov A. R., and Obnosov Y. V., 2001. Analytical solution for a sharp interface problem in sea water intrusion into a coastal aquifer. Proc. R. Soc. A, 457(2016), 3032–3038.

[67] Kim J. M., Parizek R. R., 2005. Numerical simulation of the Rhade effect in layered aquifer systems due to groundwater pumping shutoff. Adv. Water Resour., 28(6), 627–642.

[68] Kimbler O. K., Kazmann R. G., and Whitehead W. R., 1975. Cyclic Storage of Fresh Water in Saline Aquifers. 78 pp., Louisiana Water Resour. Res. Inst. Bulletin 10, Baton Rouge, LA.

[69] Konikow L. F., August L. L., and Voss C. I., 2001. Effects of clay dispersion on aquifer storage and recovery in coastal aquifers. Transport porous med., 43(1), 45–64.

[70] Kourakos G., and Mantoglou A., 2009. Pumping optimization of coastal aquifers based on evolutionary algorithms and surrogate modular neural network models. Adv. Water Resour., 32(4), 507–521.

[71] Kumar A., and Kimbler O. K., 1970. Effect of dispersion, gravitational segregation, and formation stratification on the recovery of freshwater stored in saline aquifers. Water Resour. Res., 6(6), 1689–1700.

[72] Langevin C. D., 2008. Modeling axisymmetric flow and transport, Ground Water, 46(4), 579–590.

[73] Langevin C. D., and Guo W., 2006. MODFLOW/MT3DMS-based simulation of variable-density ground water flow and transport. Ground Water, 44(3), 339–351.

[74] Langevin C.D., Shoemaker W.B., and Guo W., 2003. MODFLOW-2000, the U.S. Geological Survey modular groundwater model-Documentation of the SEAWAT-2000 version with the variable-density flow process (VDF) and the integrated MT3DMS transport process (IMT). USGS Open-File Report 03-426. Reston, Virginia: USGS.

[75] Lowry C. S., and Anderson M. P., 2006. An assessment of aquifer storage recovery using ground water flow models. Ground Water, 44(5), 661–667.

[76] Lu C. H., Chen Y. M., and Luo J., 2012. Boundary condition effects on maximum groundwater withdrawal in coastal aquifers. Ground Water, 50(3), 386–393.

[77] Lu C. H., Du P. F., Chen Y. M., and Luo J., 2011. Recovery efficiency of aquifer storage and recovery (ASR) with mass transfer limitation. Water Resour. Res., 47, W08529.

[78] Lu, C.H., Kitanidis P.K., and Luo J., 2009. Effects of kinetic mass transfer and transient flow conditions on widening mixing zones in coastal aquifers, Water Resour. Res., 45, W12402, doi:10.1029/2008WR007643.

[79] Luo, J., O.A. Cirpka, M.N. Fienen, W.-M. Wu, T.L. Mehlhorn, J. Carley, P.M. Jardine, C.S. Criddle, and P.K. Kitanidis, 2006. A parametric transfer function

methodology for analyzing reactive transport in nonuniform flow, J. Contam. Hydrol., 83, 27–41.

[80] Luther K., and Haitjema H.M., 1999. An analytic element solution to unconfined flow near partially penetrating wells. J. Hydrol., 226, 197–203.

[81] Luyun R., Momii K., and Nakagawa K., 2011. Effects of recharge wells and flow barriers on seawater intrusion. Ground Water, 49(2), 239–249.

[82] Maliva R. G., Guo W. X., and Missimer T. M., 2006. Aquifer storage and recovery: Recent hydrogeological advances and system performance. Water Environ. Res., 78(13), 2428–2435.

[83] Mantoglou A., 2003. Pumping management of coastal aquifers using analytical models of saltwater intrusion. Water Resour. Res., 39(12), 1335.

[84] Mantoglou A., and Papantoniou M., 2008. Optimal design of pumping networks in coastal aquifers using sharp interface models. J. Hydrol., 361, 52–63.

[85] Merritt M. L., 1985. Subsurface storage of freshwater in South Florida: A digital model analysis of recoverability. U.S. Geol. Survey Water-Supply Paper 2261.

[86] Merritt M.L., 1986. Recovering fresh-water stored in saline limestone aquifers. Ground Water, 24(4), 516–529.

[87] Minsley B. J., Ajo-Franklin J., Mukhopadhyay A., and Morgan F. D., 2011. Hydrogeophysical methods for analyzing aquifer storage and recovery systems. Ground Water, 49(2), 250–269.

[88] Miotlinski K., Dillon P. J., Pavelic P., Cook P. G., Page D. W., and Levett K., 2011. Recovery of injected freshwater to differentiate fracture flow in a low-permeability brackish aquifer. J. Hydrol., 409, 273–282.

[89] Mirecki J. E., Campbell B. G., Conlon K. J., and Petkewich M. D., 1998. Solute changes during aquifer storage recovery testing in a limestone clastic aquifer. Ground Water, 36(3), 394–403.

[90] Mishra P. K., Vesselinov V. V., and Neuman S. P., 2012. Radial flow to a partially penetrating well with storage in an anisotropic confined aquifer. J. Hydrol., 448, 255–259.

[91] Missimer T. M., Drewes J. E., Amy G., Maliva R. G., and Keller S., 2012. Restoration of Wadi aquifers by artificial recharge with treated waste water. Ground Water, 50(4), 514–527.

[92] Missimer T. M., Guo W., Walker C. W., and Maliva R. G., 2002. Hydraulic and density considerations in the design of aquifer storage and recovery systems. Florida Water Res. J. (February), 31–35.

[93] Moench, A.F., 1995. Convergent radial dispersion in a double-porosity aquifer with fracture skin: Analytical solution and application to a field experiment in fractured chalk, Water Resour. Res., 31, 1823–1835.

[94] Moench, A.F., 1989. Convergent radial dispersion: A Laplace transform solution for aquifer tracer testing, Water Resour. Res., 25, 439–447.

[95] Moench, A, F., and A. Ogata, 1981. A numerical inversion of the Laplace transform solution to radial dispersion in a porous medium, Water Resour. Res., 17, 250–252.

[96] Moulder E. A., 1970. Freshwater bubbles: A possibility for using saline aquifers to store water. Water Resour. Res., 6(5), 1528–1531.

[97] Muskat M., 1937. The Flow of Homogeneous Fluids Through Porous Media, McGraw-Hill, New York.

[98] Naji, A., Cheng A.H.D., and Ouazar D., 1998. Analytical stochastic solutions of saltwater/freshwater interface in coastal aquifers. Stoch. Hydrol. Hydraul., 12(6), 413–430.

[99] Neuman S.P., 1972. Theory of flow in unconfined aquifers considering delayed response of the water table. Water Resour. Res., 8, 1031–1045.

[100] Neuman S.P., 1974. Effect of partial penetration on flow in unconfined aquifers considering delayed gravity response, Water Resour. Res., 10(2), 303–312.

[101] Neuweiler I, Attinger S, Kinzelbach W, 2001. Macrodispersion in a radially diverging flow field with finite Peclet numbers 1. Perturbation theory approach, Water Resour. Res., 37, 481–493.

[102] Nicklow J., Reed P., Savic D., Dessalegne T., Harrell L., Chan-Hilton A., Karamouz M., Minsker B., Ostfeld A., Singh A. and Zechman E., 2010. State of the art for genetic algorithm and beyond in water resources planning and management. J. Water Resour. Plan Manage., 136(4), 412–432.

[103] Novakowski, K.S., 1992. The analysis of tracer experiments conducted in divergent radial flow fields, Water Resour. Res., 28, 3215–3225.

[104] Ozturk, Y.F., 1970. Seawater intrusion length in stratified estuaries. Water Res., 4(7), 477–484.

[105] Park C. H., and Aral M. M., 2004. Multi-objective optimization of pumping rates and well placement in coastal aquifers. J. Hydrol., 290, 80–99.

[106] Pavelic P., Dillon P.J., and Simmons C.T., 2002. Lumped parameter estimation of initial recovery efficiency during aquifer storage and recovery. In: Dillon P.J. (Ed.), Management of Aquifer Recharge for Sustainability, Proceedings of the 4th International Symposium on Artificial Recharge (ISAR4), Adelaide, September 22-26, 2002. Swets & Zeitlinger, Lisse, ISBN 90 5809 527 4, 285–290.

[107] Pavelic P., Dillon P. J., Barry K. E., and Gerges N. Z., 2006(a). Hydraulic evaluation of aquifer storage and recovery (ASR) with urban stormwater in a brackish limestone aquifer. Hydrogeol. J., 14(8), 1544–1555.

[108] Pavelic P., Dillon P. J., and Simmons C. T., 2006(b). Multiscale characterization of a heterogeneous aquifer using an ASR operation. Ground Water, 44(2), 155–164.

[109] Perina T., and Lee T.C., 2006. General well function for pumping from a confined, leaky, or unconfined aquifer. J. Hydrol., 317, 239–260.

[110] Peters J. H., 1983. The movement of fresh water injected in saline aquifers. Geologia. Appl. Idroge, 18, 144–155.

[111] Pool M., and Carrera J., 2010. Dynamics of negative hydraulic barriers to prevent seawater intrusion. Hydrogeol. J., 18(1), 95–105.

[112] Pool M., and Carrera J., 2011. A correction factor to account for mixing in Ghyben-Herzberg and critical pumping rate approximations of seawater intrusion in coastal aquifers. Water Resour. Res., 47, W05506.

[113] Pyne, R. D. C., 2005. Aquifer Storage and Recovery Issues and Concepts, St. Johns River Water Management District Special Publication SJ2005-SP12; St. Johns River Water Management District: Jacksonville, Florida.

[114] Pyne R. D. G., 1995. Groundwater Recharge and Wells: A Guide to Aquifer Storage Recovery, CRC Press, Boca Raton, FL.

[115] Pyne R. D. G., and Howard J. B., 2004. Desalination/Aquifer storage recovery (DASR): a cost-effective combination for Corpus Christi, Texas, Desalination, 165, 363–367.

[116] Qahman K., Larabi A., Quazar D., Naji A., and Cheng A. H. D., 2005. Optimal and sustainable extraction of groundwater in coastal aquifers. Stoch. Env. Res. Risk A., 19(2), 99–110.

[117] Shackelford, C.D., 1995. Cumulative mass approach for column testing, J. Geotech. Engr.-ASCE, 121, 696–703.

[118] Shammas, M.I., 2008. The effectiveness of artificial recharge in combating seawater intrusion in Salalah coastal aquifer, Oman. Environ. Geol., 55, 191–204.

[119] Sheng, Z., 2005. An aquifer storage and recovery system with reclaimed wastewater to preserve native groundwater resources in El Paso, Texas, J. Environ. Manage., 75, 367–377.

[120] Simmons C. T., 2005. Variable density groundwater flow: From current challenges to further possibilities. Hydrogeol. J., 13(1), 116–119.

[121] Simpson M. J., and Clement T. P., 2003. Theoretical analysis of the worthiness of Henry and Elder problems as benchmarks of density-dependent groundwater flow models. Adv. Water Resour., 26(1), 17–31.

[122] Singh, S.K., 2002. Well loss estimation: Variable pumping replacing step drawdown test, J. Hydraul. Engr.-ASCE, 128, 343–348.

[123] Sreekanth J., and Datta B., 2010. Multi-objective management of saltwater intrusion in coastal aquifers using genetic programming and modular neural network based surrogate models. J. Hydrol., 393, 245–256.

[124] Strack O.D.L., 1976. A single-potential solution for regional interface problem in coastal aquifers. Water Resour. Res., 12(6), 1165–1174.

[125] Strack O.D.L., 1984. Three-dimensional streamlines in Dupuit–Forchheimer models. Water Resour. Res., 20(7), 812–822.

[126] Sugio S., Nakada K., and Urish D. W., 1987. Subsurface seawater intrusion barriers analysis. J. Hydraul. Eng., 113(6), 767–779.

[127] Tang, D. H., and D. K. Babu, 1979. Analytical solution of a velocity dependent dispersion problem, Water Resour. Res., 15, 1471–1478.

[128] Tiedeman C., and S. M. Gorelick, 1993. Analysis of uncertainty in optimal groundwater contaminant capture design. Water Resour. Res., 29(7), 2139–2153.

[129] Todd D., 1980. Groundwater hydrology, chap. 14. Wiley, Chichester, UK.

[130] Tomasko, D., G.P. Williams, and K. Smith, 2001. An analytical model for simulating step-function injection in a radial geometry, Math. Geol., 33, 155–165.

[131] USWRC, 1979. The Nation's Water Resources, 1975-2000, Vol. 1-4. Second National Water Assessment, Washington, DC: U.S. Water Resources Council.

[132] Vandenbohede, A., Van Houtte E., and Lebbe L., 2008. Study of the feasibility of an aquifer storage and recovery system in a deep aquifer in Belgium, Hydrolog. Sci. J., 53, 844–856.

[133] Van Genuchten, M.T., and Wierenga P.J., 1976. Mass-transfer studies in sorbing porous-media: 1. Analytical solution, Soil Sci. Soc. Am. J., 40, 473–480.

[134] Voss C. I., and Souza W. R., 1987. Variable density flow and solute transport simulation of regional aquifers containing a narrow freshwater-seawater mixing zone. Water Resour. Res., 23(10), 1851–1866.

[135] Ward J. D., Simmons C. T., and Dillon P. J., 2007. A theoretical analysis of mixed convection in aquifer storage and recovery: How important are density effects? J. Hydrol., 343, 169–186.

[136] Ward J. D., Simmons C. T., and Dillon P. J., 2008. Variable-density modeling of multiple-cycle aquifer storage and recovery (ASR): Importance of anisotropy and layered heterogeneity in brackish aquifers. J. Hydrol., 356, 93–105.

[137] Ward J. D., Simmons C. T., Dillon P. J., and Pavelic P., 2009. Integrated assessment of lateral flow, density effects and dispersion in aquifer storage and recovery. J. Hydrol., 370, 83–99.

[138] Werner A. D., Bakker M., Post V. E. A., Vandenbohede A., Lu C. H., Ataie-Ashtiani B., Simmons C. T., and Barry D. A., 2013. Seawater intrusion processes, investigation and management: Recent advances and future challenges. Adv. Water Resour., 51, 3–26.

[139] Yang S. Y., and Yeh H. D., 2012. A general semi-analytical solution for three types of well tests in confined aquifers with a partially penetrating well. Terr. Atmos. Ocean. Sci., 23(5), 577–584.

[140] Yang Y. J., Restivo A., Jun Y-S., Schupp D. A., Mash H., and Krishnan E. R., 2010. Aquifer storage and recovery as a viable climate change adaptation technique: sustainable development under the current regulatory framework. EWRI 2010: challenges of change, 154–163.

[141] Yeh H. D., Chen Y. J., and Yang S. Y., 2008. Semi-analytical solution for a slug test in partially penetrating wells including the effect of finite-thickness skin. Hydrol. Process., 22(18), 3741–3748.

[142] Zlotnik V. A., 1997. Effects of anisotropy on the capture zone of a partially penetrating well, Ground Water, 35(5), 842–847.

[143] Zlotnik V.A., Chen X., and Sun B., 1998. Semi analytical evaluation of three-dimensional velocity near a partially penetrating well in an unconfined aquifer. Ground Water, 36(3), 514–519.